Ab Initio Studies of Strained Ring Molecules

A thesis

submitted in partial fulfilment

of the requirements for the degree

of

Doctor of Philosophy in Chemistry

in the

University of Canterbury

by

Aaron. J. Thorpe

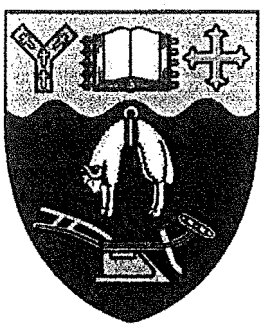

University of Canterbury

1999

Contents

Abstract:

The work reported in this thesis concerns the acid catalysed rearrangement of epoxides in the presence and absence of intramolecular nucleophiles. The potential energy surface (MP2/6-31G*//MP2/6-31G* and B3LYP/6-31G*) for rearrangement of protonated propene oxide to protonated propanal has been established. The rearrangement exhibits a 2 kcal/mol preference for rotation of oxygen away from the more hindered face of the oxirane plane containing the methyl. The rearrangement pathway involves two distinct steps; first, rupture of the oxirane and second, hydride migration. The latter does not commence until rupture of the C-O bond is complete. The combination of these two steps defines a concerted asynchronous rearrangement pathway and exhibits a 20 : 1 preference for migration of the proton *trans* to the methyl over the *cis*.

Kinetic isotope effects of the acid and BF_3-catalysed rearrangement of methylpropene oxide to methylpropanal are consistent with a 1,2 hydride shift to a carbocation intermediate (B3LYP/6-31G*). Inverse secondary kinetic isotope effects for hydride migration reflect changes in C1-H(D) stretching and out of plane bending frequencies. A calculated correction applied to the experimentally observed migration of hydrogen/deuterium (M_H/M_D = 1.92) results in a primary kinetic isotope effect for the reaction (k_H/k_D = 1.557) close to the theoretically calculated value (k_H/k_D = 1.677).

The inversion and retention transition structures for intramolecular reaction of protonated *cis*- and *trans*-3,4-epoxypentan-1-ol which give

protonated *cis*- and *trans*-2-methylfuran-3-ols have been determined at the *ab initio* MP2/6-31G* and hybrid density functional B3LYP/6-31G* levels of theory. Intrinsic reaction coordinate calculations for the lower energy inversion pathways for formation of the 2-methylfuran-3-ols show that intramolecular attack occurs in concert with ring opening. A complex of the 5-membered transition structure from the *trans*-epoxide with the Houk theozyme 3.5 kcal/mol lower in energy than the complex previously reported as a model for the antibody IgG26D9 catalysed intramolecular cyclisation of *trans*-4,5-epoxyhexan-1-ol reverses the preference of that theozyme to favour furan formation. This negates the theozyme as a model for the antibody reaction. A new theozyme is reported which favours pyran formation over furan formation consistent with the antibody result.

The potential energy surface for the acid and BF_3 catalysed rearrangement of *cis*- and *trans*-4,5-epoxyhexan-1-ol involving inversion and retention of configuration at the reaction centre at the HF/6-31G* and B3LYP/6-31G* levels are reported. The preference for furan formation over pyran is attributed to the more favourable O-C_{ep}-O bond angles at the transition structures for furan formation.

Chapter 1

Ab initio methods.

Introduction.

The investigation of chemical problems by electronic structure methods (*ab initio*) theory has gained wide spread use over recent years and has provided a valuable link with experimental results. *Ab initio* theory is based upon the laws of quantum mechanics, the science which relates the motion and interactions of electrons and nuclei to molecular properties. In order to calculate the energy and many properties of a stationary state of a molecule using a quantum mechanics approach, the Schrödinger wave equation (SWE) must be solved. In shortened form, the time-independent SWE is expressed as:

$$H\Psi = E\Psi \qquad (1.0)$$

In the SWE, H is the Hamiltonian of the particle, and E is the total energy of the particular state assessed. The wavefunction, Ψ, can be thought of as a probability distribution which depends on the cartesian coordinates of all particles and on the spin coordinates (corresponding to spin angular momentum components in a defined direction). The probability distribution of the constituent particles within a molecule is given by the square of the wavefunction, Ψ^2 (or $|\Psi|^2$ if Ψ is complex). There are many possible solutions to the SWE, each corresponding to the different stationary states of the molecule. Normally, the lowest energy ground state is sought after. The Schrödinger equation is a

differential equation which describes the wavefunction of a molecule. Its origin can be traced back to classical particle physics. Equations describing the motion of a particle or group of particles are expressed by a function which incorporates the momenta and coordinates of the system. Analogous to the energy in classical mechanics, the Hamiltonian operator, H, is the sum of the kinetic and potential energy operators in time-independent systems.

$$\hat{H} = \hat{T} + \hat{V} \qquad (1.1)$$

The kinetic operator $\hat{T}$ is a sum of the differential operators over all particles *i* (nuclei + electrons)

$$\hat{T} = \frac{-h^2}{8\pi^2} \sum_i \frac{1}{m_i} \left(\frac{\partial^2}{\partial x_i^2} + \frac{\partial^2}{\partial y_i^2} + \frac{\partial^2}{\partial z_i^2} \right) \qquad (1.2)$$

where h is Planck's constant and m_i is the mass of the particle *i*. The potential energy operator $\hat{V}$ represents the Coulomb interaction between each pair of charged particles (*i*,*j*)

$$\hat{V} = \frac{1}{4\pi\varepsilon_0} \sum_{i<j} \sum \left(\frac{e_i e_j}{r_{ij}} \right) \qquad (1.3)$$

with electric charges e_i, e_j separated by a distance r_{ij}. The electronic charge for an electron is –e while for a nucleus the charge is +Ze where Z represents the nuclear charge for that atom. By considering the terms corresponding to electron-nuclear

attraction, electron-electron repulsion and nuclear-nuclear repulsion, the potential energy $\hat{V}$ can be expressed as:

$$\hat{V} = \frac{1}{4\pi\varepsilon_0}\left[-\sum_{i}^{elec}\sum_{s}^{nucl}\left(\frac{Z_s e^2}{r_{is}}\right) + \sum_{i<j}^{electrons}\sum\left(\frac{e^2}{r_{ij}}\right) + \sum_{s<t}^{nuclei}\sum\left(\frac{Z_s Z_t e^2}{r_{st}}\right)\right] \quad (1.4)$$

The molecular system can be expressed as the full Hamiltonian:

$$H = T^{elec}(\vec{r}) + T^{nucl}(\vec{R}) + V^{nucl\text{-}elec}(\vec{R},\vec{r}) + V^{elec}(\vec{r}) + V^{nucl}(\vec{R}) \quad (1.5)$$

where $\vec{r}$ and $\vec{R}$ are the set of component vectors describing the position of each particle within the molecule. *Ab initio* theory utilizes the Born-Oppenheimer approximation which separates nuclear and electronic motions to simplify the SWE. This approximation is possible since typical nuclear masses are much greater than those of electrons. Consequently electronic motion is rapid in relation to nuclear motion and it is reasonable to assume that electronic distribution depends only on the instantaneous positions of the nuclei and not on their velocities. Within the framework of the Born-Oppenheimer approximation the kinetic energy term $T^{nucl}(\vec{R})$ can be omitted from (1.5).

Model quantum chemical methods for *ab initio* calculations are usually characterised by a combination of the theoretical procedure and basis set applied. A number of *ab initio* procedures corresponding to different approximation methods are available *via* standard program packages. These are commonly

referred to as *levels of theory*. Some commonly used approximations are listed in Table 1.

Table 1

Model	Method	Availability
HF	Hartree-Fock	Geometry optimisation
B3LYP	Becke-style-3-Parameter Density Functional Theory (using the Lee-Yang-Parr correlational functional.	Geometry optimisation
MP2	2^{nd} Order Møller-Plesset Perturbation Theory.	Geometry optimisation
MP4	4^{th} Order Møller-Plesset Perturbation Theory.	Single point energies

Hartree-Fock theory (HF) is a good starting point and useful for providing initial predictions for a variety of molecular systems. The Hartree-Fock model takes electron-electron repulsion into account through the use of the *self consistent field* (SCF) method. This is based on the interaction between an electron in a given orbital and the mean field of the other electrons in the molecule. Of the models presented in Table 1, the HF model demands the least CPU time for a given calculation. However a major weakness is that electron correlation is not taken into account. The B3LYP model is based on Density Functional Theory (DFT) which has gained steady popularity in recent years. DFT methods, which take electron correlation into account, achieve significantly greater accuracy than Hartree-Fock theory at only a modest increase in computational cost. For medium to large sized molecular systems DFT methods require less CPU time than the MP2 model. The MP2 model, referred to as second order Møller-Plesset

perturbation theory, also provides an improvement of the Hartree-Fock model by taking electron correlation into account but at a substantial computational cost. The CPU requirements scale higher than the fourth power of the number of basis functions (if the number of electrons stay the same) for the higher order MPn methods (n = 3,4 or 5) limiting computational investigations to small molecules.

Basis sets.

A basis set is used as a mathematical approximation for the "exact" molecular orbitals within a molecule. Standard basis sets assign a group of basis functions to build the orbitals. Such basis functions are usually composed of a linear combination of Gaussian functions which are assigned to each atom within a molecule to approximate its orbitals. Component Gaussian functions are known as 'primitives'. A basis function can be termed 'contracted' or 'uncontracted' depending on whether it contains a single primitive gaussian function, or a linear combination of fixed Gaussian functions respectively.

Basis sets are classified according to their description of the molecular orbitals and a wide range is currently available. Split valence basis sets are constructed such that the atomic orbitals are split into two parts, an inner compact orbital and an outer, more diffuse one. Split valence orbitals allow orbitals to change size but not shape. A widely used split valence basis set is the 3-21G basis set. This is comprised of two sizes of basis functions for each valence orbital. The nomenclature implies the use of 3 Gaussian functions for the inner core orbital and 2 and 1 Gaussian functions respectively for the inner and outer valence orbitals.

Polarized basis sets offer an improvement from split valence basis sets through the addition of d-orbitals for all heavy (nonhydrogen) atoms. Polarization allows for displacement of electronic charge away from the nuclear centres. By considering the interaction of a p-orbital with a d-orbital, mixing results in a deformation of the resulting orbital (Figure 1).

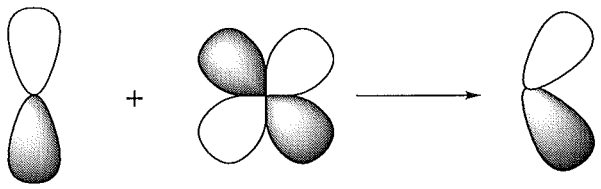

Figure 1. Polarization of a *p*-orbital by mixing with a *d*-function.

A commonly used polarised basis set is the 6-31G* basis set. It is comprised of 6 primitive Gaussians for the core orbitals while the inner and outer components of the s- and p- valence orbitals are made up of 3 and 1 Gaussian functions respectively. The asterisk denotes a single set of d-functions equivalent to five d- and one s-orbital.

Reaction path following.

A reaction path connecting reactants and products *via* a transition structure can be studied in detail through the use of an intrinsic reaction coordinate calculation (IRC) available with standard program packages. IRC calculations require initial force constants of the transition structure and step along the reaction path a fixed number or times in each direction, (with a default step of 0.1 $amu^{1/2}$.bohr) toward the two minima that it connects. The IRC calculations employed throughout the following chapters compute the reaction path in mass-weighted internal coordinates.

Chapter 2.

Rearrangement of protonated propene oxide to protonated propanal.

Summary.

Calculations at the MP2/6-31G* level show there are concerted asynchronous pathways connecting protonated propene oxide and protonated propanal. With cleavage of the C-O bond of protonated propene oxide, the preference for rotation of oxygen away from the more hindered face of the oxirane plane containing the methyl group is quantified as 2 kcal/mol. This pathway involves two distinct steps; first, rupture of the oxirane and second, hydride migration. The latter does not commence until rupture of the C-O bond is complete. The combination of these two steps defines a concerted asynchronous rearrangement pathway. The reaction is predicted to show a 20 : 1 preference for migration of the proton *trans* to the methyl over the *cis*.

Introduction.

The rearrangement of oxiranes to carbonyl compounds, like nucleophilic substitution at a saturated carbon, is representative of a reaction of fundamental importance in organic synthesis. Rearrangement can be catalysed by proton or Lewis acid[1] inducing a hydrogen, alkyl or aryl atom to migrate between adjacent carbons in the carbonyl-forming step. Many arene oxides react in aqueous solution by both spontaneous and acid-catalysed pathways to give diols and phenols.[2] In this latter reaction the 1,2-hydride migration leading to an intermediate cyclohexadienone is referred to as an "NIH-shift."[3] This occurs in nature, for example, in the biosynthesis of tyrosine.[4] Oxiranes sufficiently activated by substituent aryl and vinyl groups also yield carbonyl products in aqueous solution by the spontaneous reaction pathway.

Acid-induced rearrangement of epoxides by alkyl, aryl or hydrogen migration was for many years considered to be a concerted process. However, for epimeric pairs of exocyclic tertiary substituted epoxides, acid catalysed rearrangement resulted in similar mixtures of epimeric aldehydes[5] consistent with a stepwise rearrangement involving the intermediacy of carbocations (Figure 1).

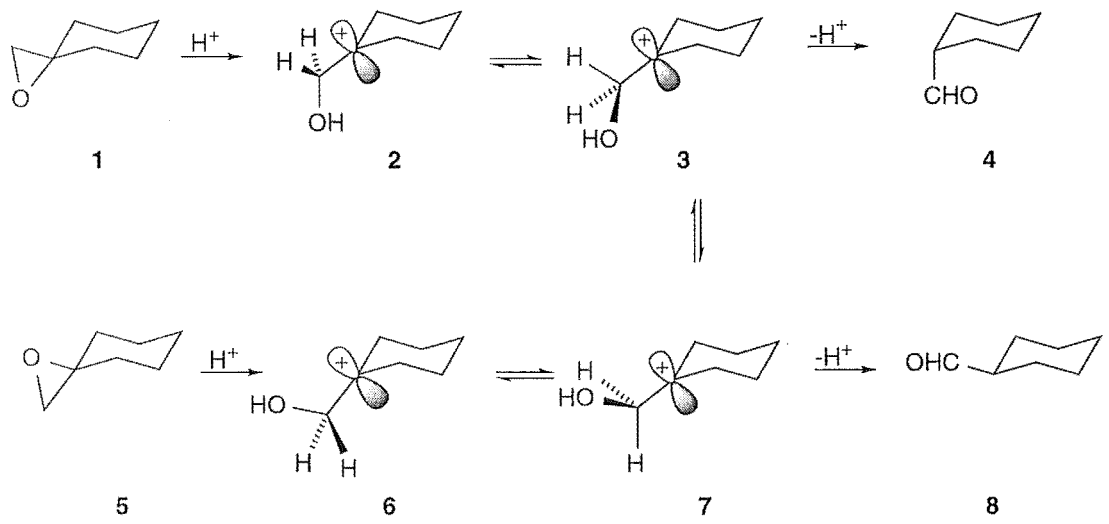

Figure 1. Schematic representation of epoxide rearrangement. (Configuration defined *e.g.* by a 4-*t*-Bu group).

For each epimeric epoxide, where conformation is defined, for example, by a 4*t*-butyl group or by fusion to a second ring, a marginal preference for the aldehyde resulting from inversion is observed i.e. **4** from **1** and **8** from **5**. The formation, however, of aldehyde **4** along with **8** from **5** is evidence for the intermediacy of a carbocation. A concerted hydride migration from **5** would give only **8**. The fact that **4** is also formed is consistent with the reaction proceeding at least in part *via* a carbocation. On cleavage of the more substituted C-O bond, rotation about the C^+–CH_2O bond in either direction places a hydrogen *anti* to the original C-O in a geometry favourable for hydrogen migration. This necessarily occurs before further rotation places a hydrogen *syn* to the original C-O bond. For example epoxide **5** opens to **6** and rotation to **7** (or the mirror image) occurs before formation of **3** (or the mirror image). Provided that the rate of bond rotation converting **7** to **3** is not rapid relative to hydride migration a preference for formation of **8** from **5** will be observed.

By the same argument, reaction of **1** would be expected to give a higher yield of **4** than **8**. The extent of bias for the product of inversion at C2 contains information about the relative rate of rotation and hydride migration. For example, if rotation is fast relative to hydride migration then both epimeric epoxides should give an identical ratio of epimeric aldehydes, which is not observed.[6]

Ab initio calculations of the acid-catalysed rearrangement of ethylene oxide to acetaldehyde in the gas phase show protonated epoxide **9** to be an energy minimum on the potential energy surface.[7] These early studies of the $C_2H_5O^+$ potential energy surface at the MP3/6-31G**//RHF/4-31G level[8] suggested carbocation **11** to be an intermediate to protonated acetaldehyde **13**. A transition structure **10** between **9** and **11** was identified along with a small activation barrier from **11** to a transition structure for rearrangement to **13**. With the inclusion of polarization functions in the basis set and incorporation of electron correlation the energy of **12** falls below that of the intermediate **11**. Thus although cation **11** is predicted to be stable with respect to cyclisation to **9** and with respect to a 1,2-proton shift to protonated vinyl alcohol Radom et al.[7] suggested it was unlikely to be an observable species because of facile rearrangement by means of a 1,2-hydride shift to **13**.

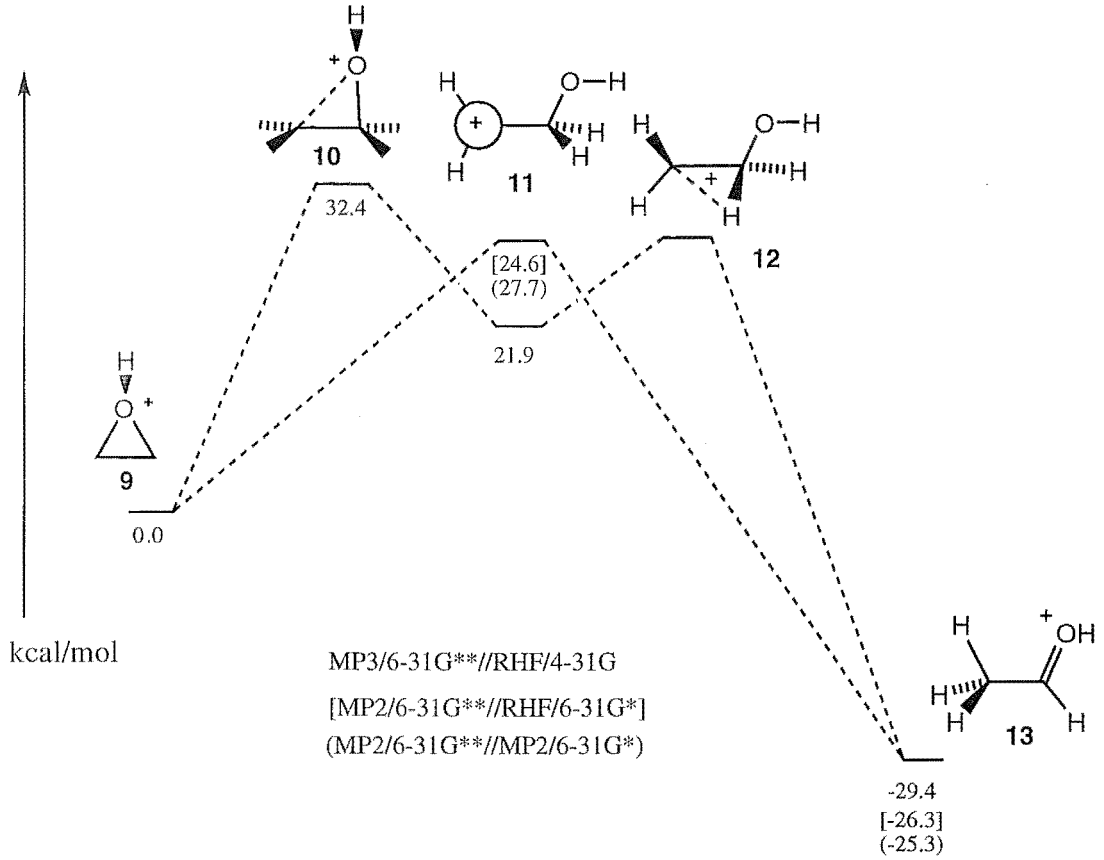

Figure 2. Acid catalysed rearrangement of oxirane.

Later calculations at the MP2/6-31G**//HF/6-31G*[9] and MP2/6-31G**//MP2/6-31G*[10] levels predict gas-phase unimolecular ring opening of protonated oxirane **9** to lead to protonated acetaldehyde **13** *via* an activation barrier of 24.6 and 27.7 kcal/mol respectively with no intervening minima. A transition structure **11** was established with the C2 cation *p*-orbital orthogonal to the C2-C1-O plane. The imaginary vibration exhibited a twist of the hydrogens on C2 and rotation of a hydrogen on C1 into the plane of the *p*-orbital of the cation.[8] The migrating hydrogens of **9** in the rearrangement to **13** are diastereotopic with respect to the proton on oxygen. However, the symmetry of the cation **11** precludes differentiation in hydrogens in the migration. In contrast, rearrangement of protonated fluorooxirane was calculated (MP2/6-31G*//MP2/6-31G*)[9] to open to protonated aldehyde by two stereospecific pathways involving carbocation intermediates.

In contrast to the calculations for acid catalysed rearrangement of ethylene oxide, acid-catalysed opening of benzene oxide, styrene oxide and analogous substituted epoxides in the gas phase are calculated by *ab initio* methods to give carbocations as energy minima.[11] The rearrangement of these epoxides is therefore considered stepwise. For the rearrangement of benzene oxide (**14**) to phenol (**18**), calculations[12] at the MP2/6-31G*//RHF/6-31G* level of theory show the hydroxycyclohexadienyl cation **16** to be an intermediate 13 kcal/mol lower in energy than the protonated oxirane **15**. The protonated dienone **17** resulting from ring opening of **15** followed by a NIH shift is calculated to be 42 kcal/mol lower in energy than **15**. The oxonium ion **15** was considered to be the transition state for the interconversion of the two otherwise identical carbocation structures in which the HO group is located at adjacent carbons. Carbocation **16** could collapse to phenol by proton loss from C1 or undergo a NIH shift, the latter being favoured (Figure 3). From studies of deuterium-labelled substrates, it was shown that the NIH pathway is energetically favoured.

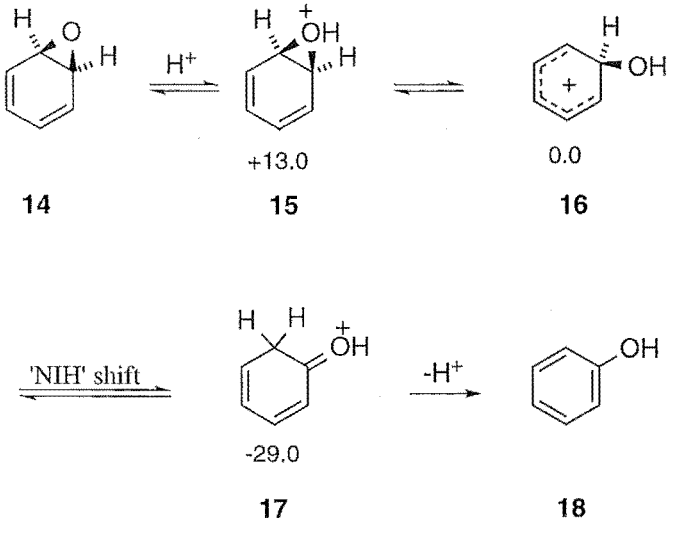

Figure 3. Arene oxide rearrangement.

Carbocations rather than oxonium ions have been similarly calculated to be intermediates in the rearrangement of monohydroxy, amino and vinyl oxiranes at the RHF/6-31G*//RHF/6-31G* level of theory.[10] For oxirane and the fluoro, methyl, cyano, formyl and formaldimino derivatives, both *anti* and the *syn* oxonium ions, which differ in energy by less than 2 kcal/mol, are calculated to be more stable than the corresponding carbocations. In previous work, *syn* and *anti* oxonium ions have been referred to as invertomers.[10] The corresponding carbocations are intermediates but are consistently higher in energy than the protonated epoxides. Calculations are now reported on the proton catalysed rearrangement of propene oxide in order to define in detail the potential energy surface for the more important regions of the rearrangement process.

Computational methods.

Exploratory calculations were carried out at semi-empirical (AM1) and Hartree-Fock (3-21G* and 6-31G*) levels. All results reported here, including optimised structures, vibrational frequencies, and intrinsic reaction coordinate (IRC)[13] paths, were derived from MP2/6-31G* calculations using the GAUSSIAN 94[14] suite of programs. The absolute and relative energies of the optimised transition structures and minima, including scaled zero point vibrational energies are presented in Table 1 (Appendix A).

Results and Discussion.

The acid catalysed rearrangement of propene oxide to propanal requires ring opening and hydrogen migration (Figure 4). The extent to which the hydrogen is aligned with the developing carbocation centre for migration is a matter for investigation and related to the nature of the potential energy surface defining a concerted synchronous, concerted asynchronous or stepwise rearrangement. This investigation addresses this question and the location and importance of the structures

enclosed in brackets in the simplified scheme (Figure 4) on the potential energy surface are assessed by *ab initio* calculations.

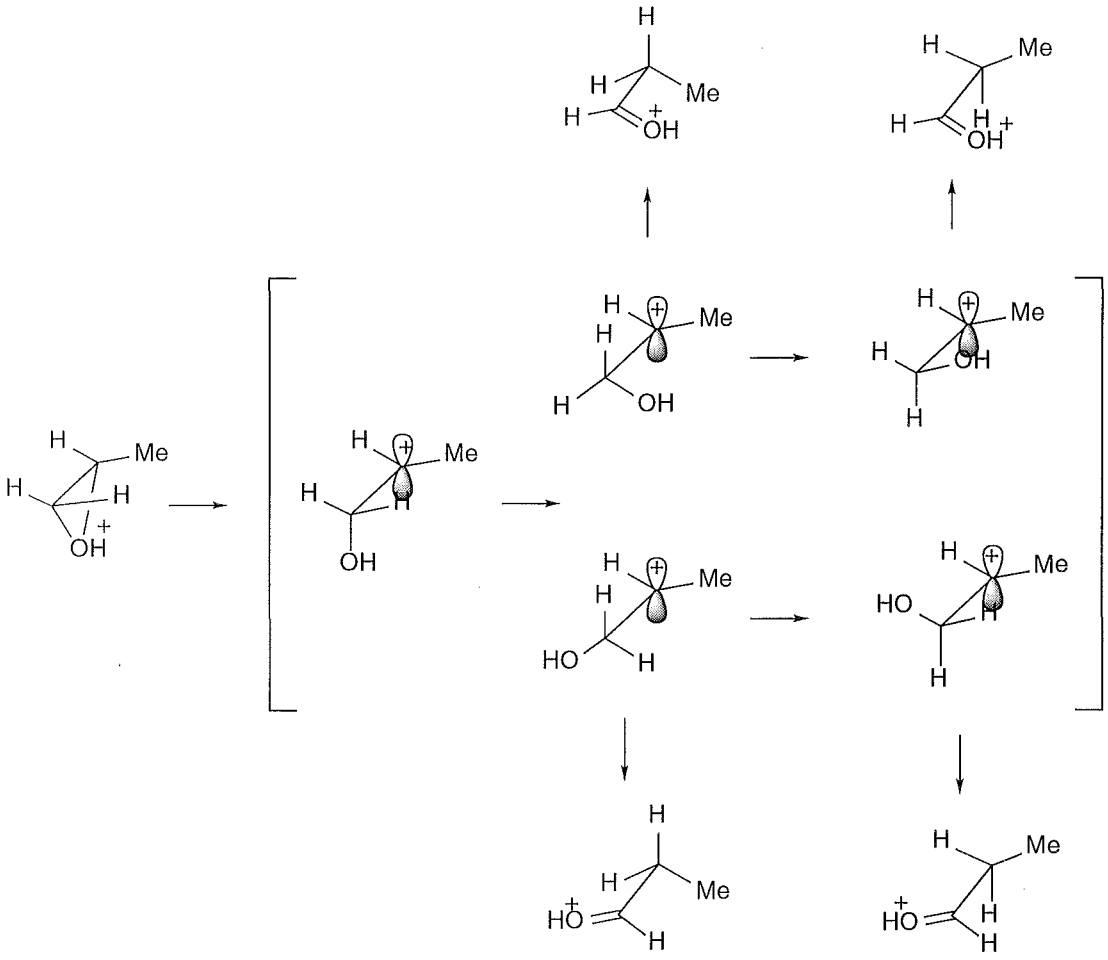

Figure 4. Schematic representation of acid-catalysed rearrangement of propene oxide.

Protonation of propene oxide can occur on either face of the oxirane ring, to give the stereoisomeric *syn* and *anti* oxonium ions **19** and **21**. At all levels of theory the *syn* co-ordinated oxonium ion **19** was found to be marginally higher in energy than the *anti* oxonium ion **21** - at the MP2/6-31G* level of theory by 0.2 kcal/mol.[15] Protonation of propene oxide is expected to be reversible and the diastereomers most likely interconvert in this way. However an intramolecular transition structure **20** has been established 16.9 kcal/mol higher in energy than **21**.

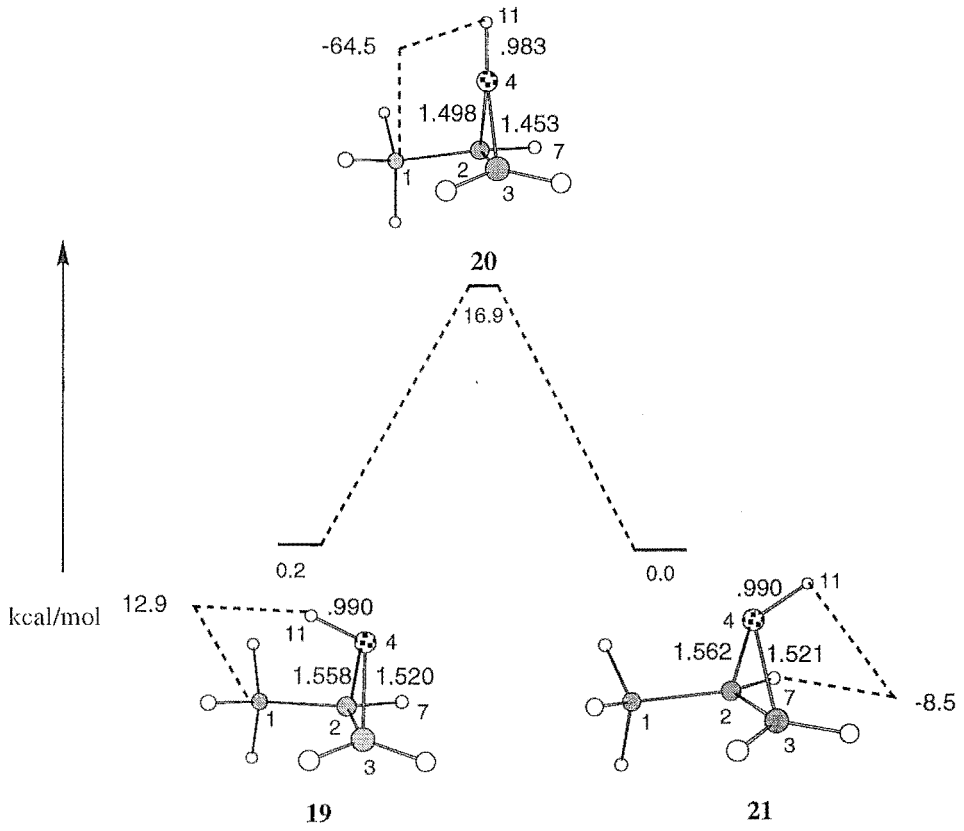

Figure 5. Intramolecular interconversion of stereoisomeric protonated propene oxides. (Dashed lines refer to dihedral angles C1-C2-O4-H11 for **19** and **20** and H7-C2-O4-H11 for **21**).

Four transition structures involving ring cleavage of **19** and **21** have been established, each involving rupture of the more substituted C-O oxirane bond and rotation about the C^{+}–CH_2-O bond. The energies of these transition structures are within 3 kcal/mol. Importantly the calculations quantify the preference for oxygen to rotate away from the methyl and relieve the skew oxabutane interaction. Such rotation is favoured by ca 2 kcal/mol (Figure 6).[16]

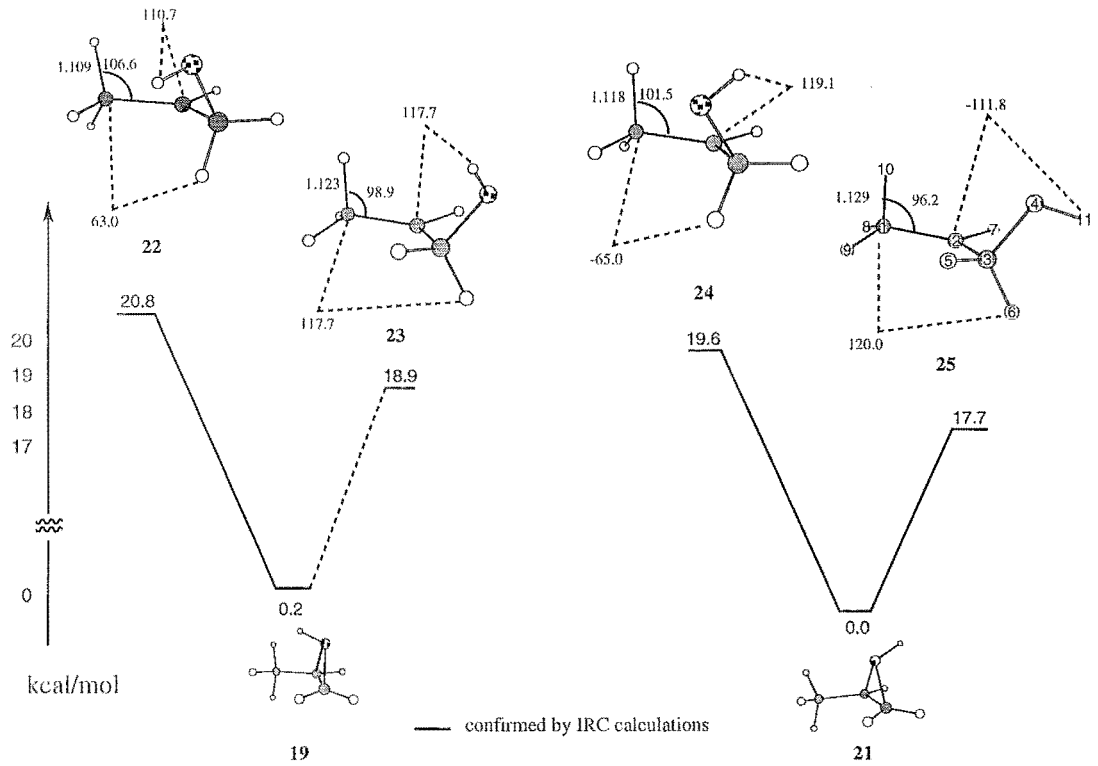

Figure 6. Transition structures involved in the potential energy surface for ring cleavage of protonated propene oxide. (Dashed lines refer to dihedral angles C1-C2-C3-H5 for **22** and **24** and C1-C2-C3-H6 for **23** and **25**).

Three features of the structures are of particular note. The first is the importance at the transition structure of CH hyperconjugation from the methyl hydrogen in the plane of the carbocation *p*-orbital. This CH is bent towards the carbocation and the H10-C1-C2 angle in **25** is 96°. Furthermore the CH bond is extended in length (1.129Å). Similar but less marked effects are observed in the other three higher energy transition structures. The second feature of note is that at the transition structures the optimised bond angles (C2-C3-H6 angles are 109-110° and the C1-C2-C3 angles 122-126° respectively) suggest that C2 and C3 are essentially sp^2 and sp^3 hybridised.[17] Finally of note is that C3H6 has not started to migrate at the transition structures nor is the C3H6 bond aligned with the carbocation *p*-orbital, the C1-C2-C3-H6 dihedral angles being some 25 to 30° from the plane of the carbocation *p*-orbital.

In view of the large structural differences between transition structures, reactants and products, IRC paths were determined to establish connectivities. The most favoured pathway for ring cleavage involves transition structure **25**. It seemed pertinent to study this pathway in some detail. An intrinsic reaction coordinate calculation (IRC) was performed at the MP2/6-31G* level and showed the transition structure to collapse to protonated epoxide **21** and protonated aldehyde in conformation **26** (Figure 7).

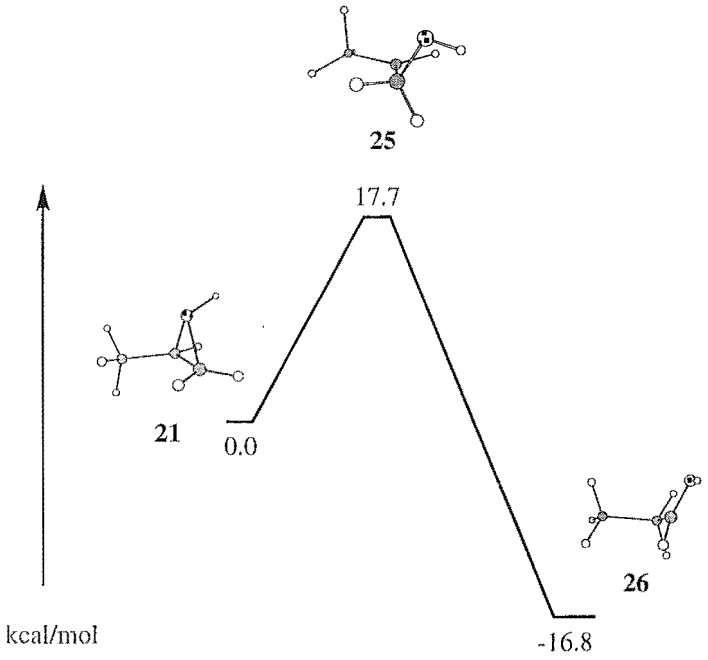

Figure 7. Intrinsic reaction coordinate relating **21** and **26**.

Analysis of the reaction trajectory reveals two major distinct and interdependent processes: first, rupture of the oxirane and second, hydride migration. The overall reaction profile *via* this transition structure is consistent with an asynchronous concerted rearrangement elaborated in some detail below.

The variation of the C1-H10 bond length, H10-C1-C2 bond angle, and the H10-C1-C2-C3 torsional angle with reaction coordinate are shown in Figure 8. In the very early stages of reaction, before any other changes are observed, the methyl begins to

rotate to bring the C1-H10 bond into alignment with the developing carbocation center at C2 as shown by the variation in the torsional angle H10-C1-C2-C3 with reaction coordinate. This dihedral angle reaches a minimum of 96° at the transition structure. The importance of hyperconjugation by a methyl hydrogen in stabilising the transition structure is shown by the H10-C1 bond length which is longest and the H10-C1-C2 bond angle which is most compressed at the transition structure. The demand for hyperconjugation at the transition structure is consistent with the charge development at C2 being greatest at this point in the reaction coordinate.

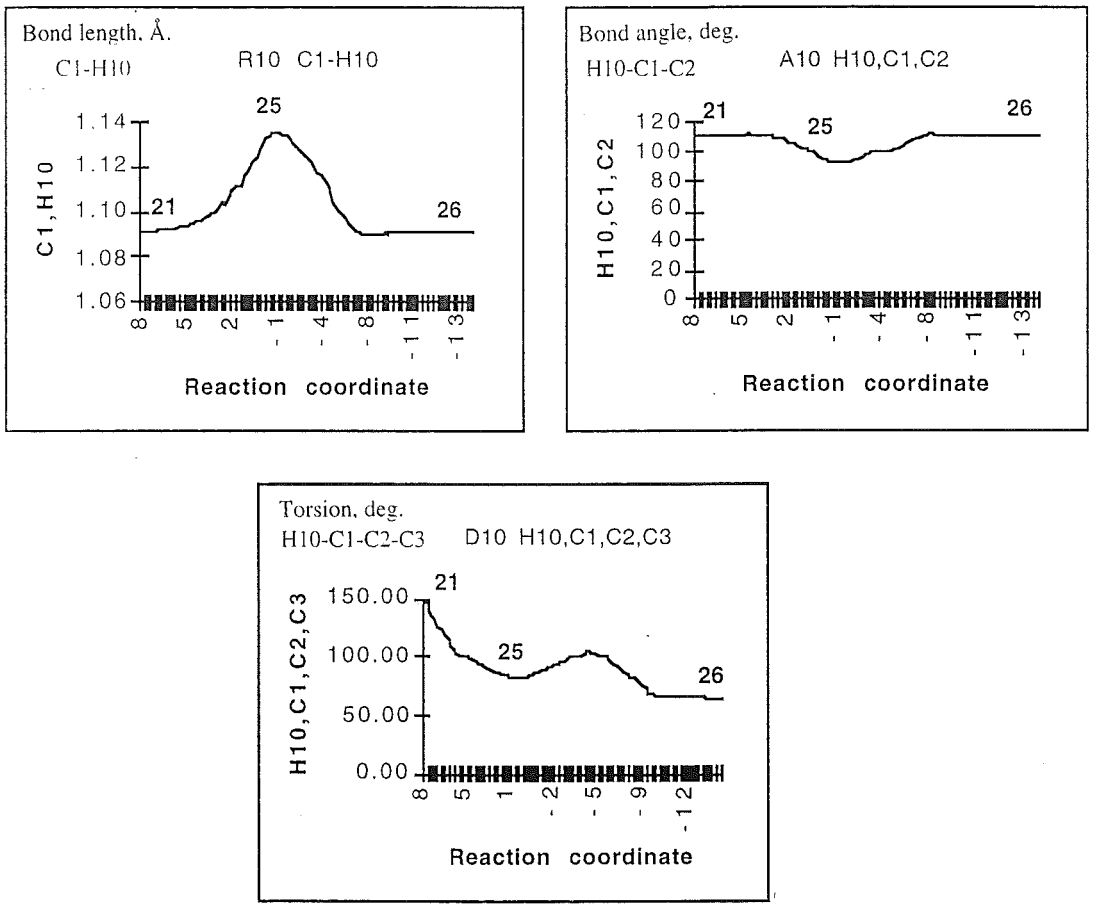

Figure 8. The importance of hyperconjugation. Reaction coordinate in units of $amu^{1/2}$.bohr.

At the transition structure the oxirane ring has opened such that C2 and C3 are essentially sp^2 and sp^3 hybridised respectively according to the optimised C2-C3-H6 and C1-C2-C3 bond angles. With rupture of the epoxide the O-C3-C2 angle increases

so that at the transition structure this angle is 102°, just short of tetrahedral, and thereafter increases to that for sp^2 hybridisation as in protonated aldehyde (Figure 9). Concomitant with C2-O bond rupture is rehybridization at C3 to tetrahedral. A notable feature apparent in the plot of the C3-O bond distance with reaction coordinate is that the double bond character of the protonated carbonyl is formed late in the reaction coordinate, in a second step of the reaction profile.

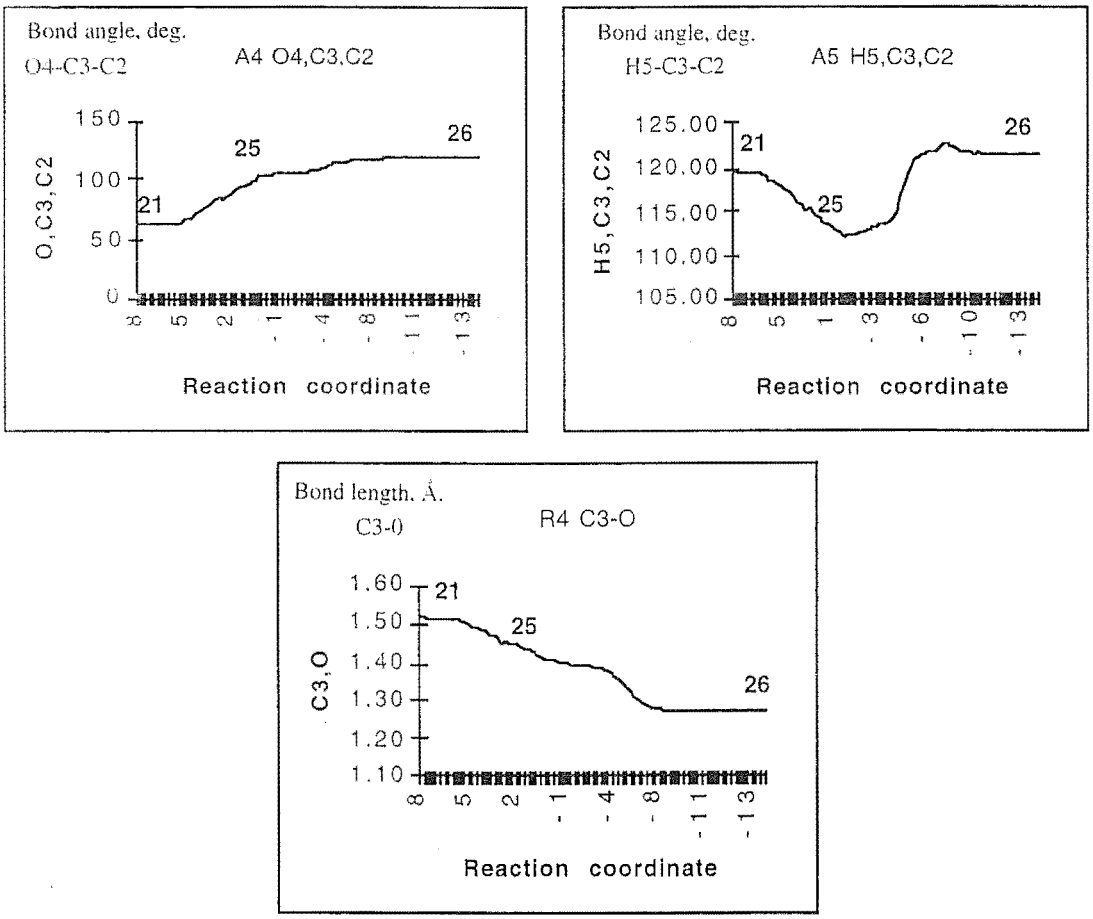

Figure 9. Oxirane ring rupture. Reaction coordinate in units of $amu^{1/2}$.bohr.

The migration of hydride is late in the reaction coordinate with the C3-H6 distance remaining constant well past the stage where the oxirane ring has ruptured. The transfer of hydride coincides with a change in the hybridisation at C2 from sp^2 to sp^3, which is reflected by the C3-C2-C1 and H6-C3-C2 angles (Figure 10).

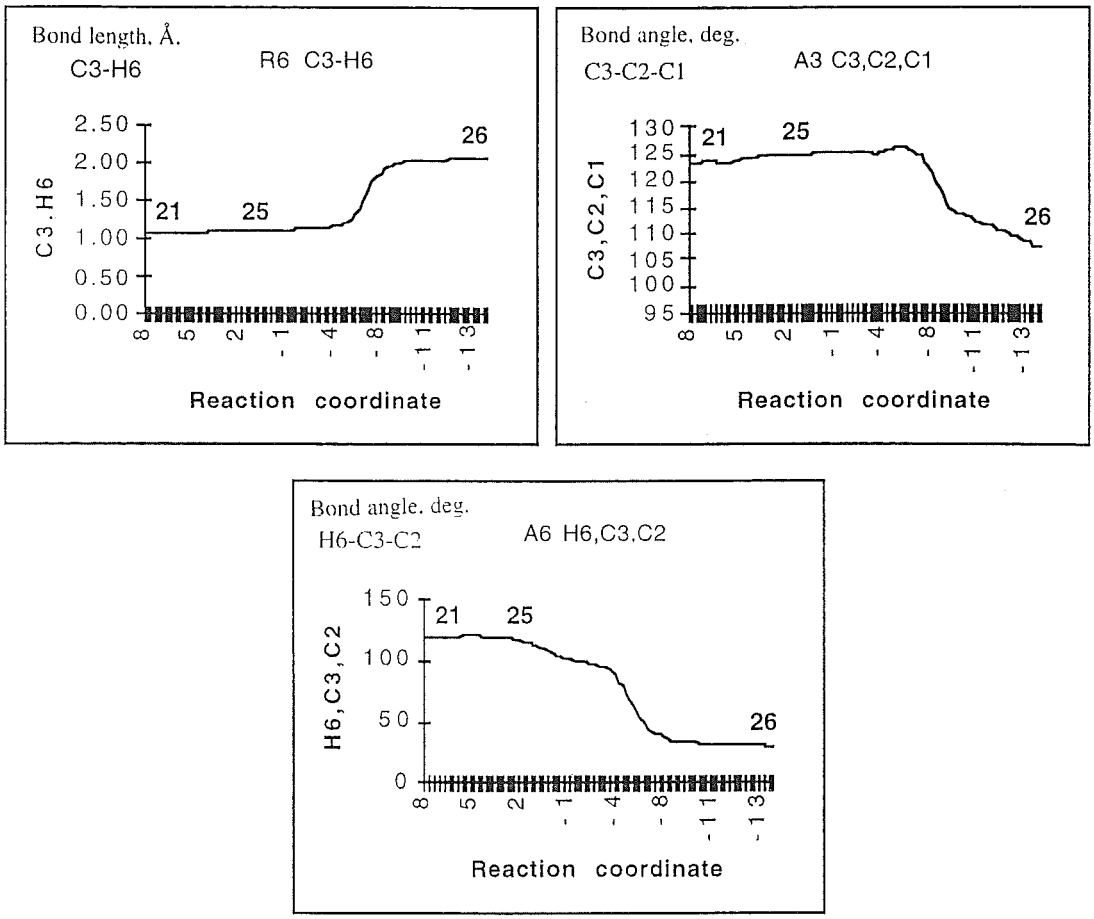

Figure 10. Hydride migration. Reaction coordinate in units of amu$^{1/2}$.bohr.

Two other stationary points **28** and **29** were established on the reaction surface (Figure 11). For both these structures C1-C2-C3-OH is planar. Structure **29** is flanked by minima where the eclipsing of the C-O with the adjacent CH is relieved by a change in the torsional angle of 2°. Surprisingly **29** is computed at the MP2/6-31G* level to be higher in energy than **28** where the oxygen is *cis* to the methyl. An IRC calculation shows the connection of **19** *via* transition structure **22** to **28**. A surface between **28** and aldehyde has not been established. The importance of **29** on the reaction surface was also difficult to elaborate but the structure optimised to **26**, shown by a dotted line in Figure 11.

An IRC calculation of transition structure **24** shows it to be linked to aldehyde **27** and protonated epoxide **21**. The calculation failed before reaching the aldehyde and protonated epoxide but had progressed sufficiently in each direction to establish

this concerted asynchronous pathway between **21** and **27**. The broken lines represent extrapolations based on the last geometry reached. At each of the break points in Figure 11, the IRC algorithm suddenly failed to optimize to the IRC path and terminated abruptly with a bizarre extrapolation of the geometry. The failure is speculated to be due to a bifurcation point, *i.e.*, a point where a zero force constant for a normal mode perpendicular to the IRC is encountered. Conformation **27** of the protonated aldehyde is computed to be 0.5 kcal/mol lower in energy that conformation **26**, consistent with the known preference of a carbonyl to eclipse with a C-C bond in preference to a C-H bond.

An IRC calculation for transition structure **23** showed it going to **26** but the surface on the other side of the transition structure was difficult to define because methyl rotation resulted in a minimum close to transition structure **23** despite the fact that the trajectory of **23** along the normal mode of the imaginary frequency gave no evidence for this motion.

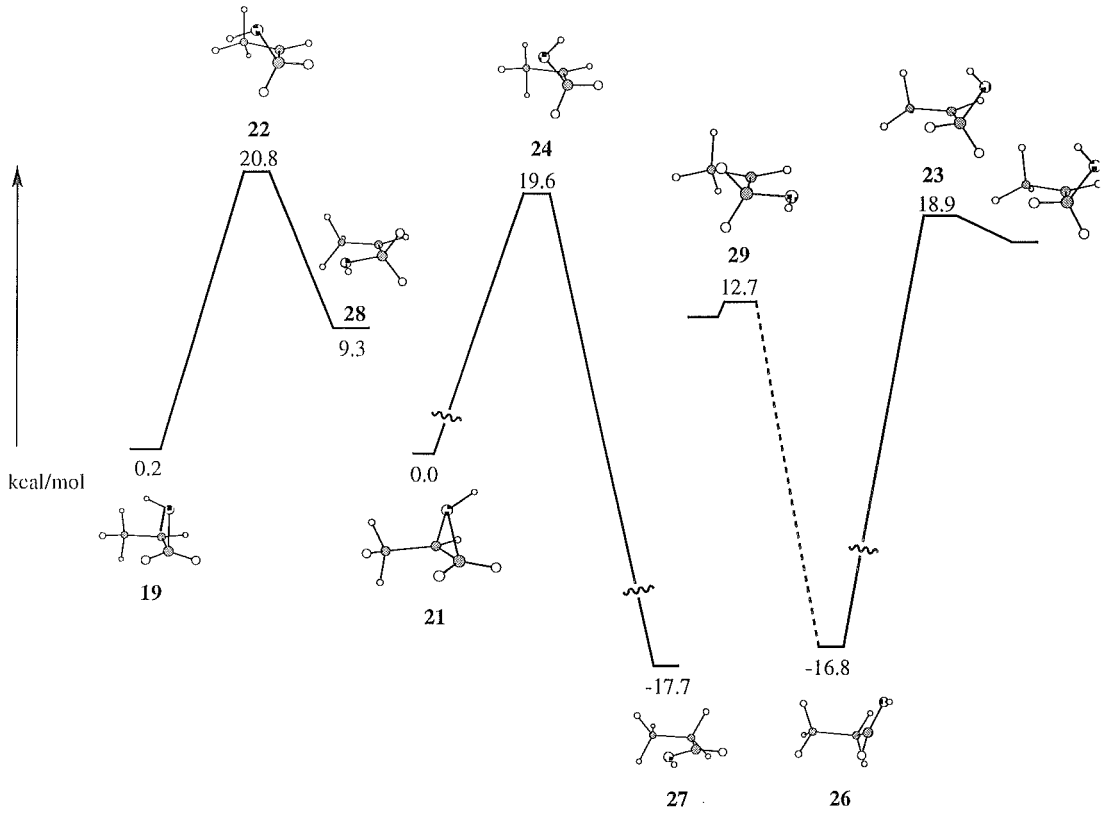

Figure 11. Reaction surface connecting protonated propene oxides and aldehydes.

The lowest energy concerted reaction coordinate diagram connecting **21** and **26** *via* transition structure **25** summarises an asynchronous but concerted reaction surface for the acid-catalysed rearrangement of propene oxide (Figure 12).

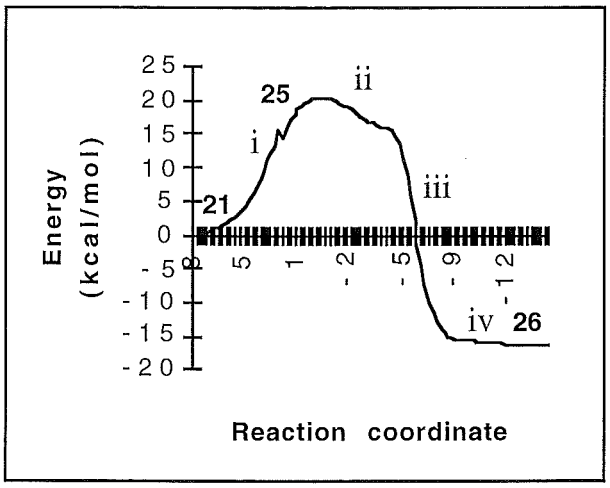

Figure 12. Lowest energy reaction coordinate diagram connecting **21** and **26** *via* transition structure **25**: (i) ring opening, (ii) preparation for hydride transfer, (iii) hydride transfer, (vi) approach to a low energy conformation of protonated aldehyde.

The reaction surface is characterised by (i) methyl rotation and ring opening which leads directly to the transition structure **25**, (ii) preparation for hydride transfer stage (i.e. the plateau), (iii) hydride transfer itself at the rapid drop from the plateau, (iv) a flat approach to a low energy conformation of protonated aldehyde. Unlike a tertiary epoxide (Figure 1) the calculations show a potential energy surface for rearrangement of protonated propene oxide which does not require a discrete carbocation intermediate. Any diastereoselectivity in the rearrangement will reflect the relative preference for the transition structures **25** and **23** versus **24** and **22** (Figure 6). The calculations, using a Boltzmann distribution, predict a 20 : 1 preference for migration of the proton *trans* to the methyl over the *cis*.

Conclusion.

Ab initio calculations show that concerted asynchronous pathways exist between protonated propene oxide and protonated propanal. The preferred pathway connects **21** *via* **25** to **26** (Figures 7 and 12). In the cleavage of the C-O bond the preference for rotation of oxygen away from the more hindered face of the oxirane plane containing the methyl is quantified as 2 kcal/mol. The reaction is predicted to show a 20 : 1 preference for migration of the proton *trans* to the methyl over the *cis*, The lowest energy pathway involves two distinct steps. The first step, rupture of the oxirane ring, is followed a second step, hydride migration, a process not commenced until breaking of the C-O bond is complete. The combination of these two steps defines a concerted asynchronous pathway. Of special interest is the fact that carbocation **28** with the methyl and hydroxy groups *cis* is calculated to be 3 kcal/mol more stable than the corresponding *trans* isomer. Yet rearrangement of the protonated propene oxide to protonated propanal by ring opening in the direction of the less stable *trans* carbocation is calculated to be the favoured pathway for isomerisation.

References.

1 Norman, R.O.C.; Coxon, J. M. Principles of Organic Synthesis, 3rd Ed., Blackie, Chapman and Hall, London, **1993**, p.590.

2 Islam, N. B.; Gupta, S. C.; Yagi, H.; Jerina, D. M.; Whalen, D. L. *J. Am. Chem. Soc.* **1990**, *112*, 6363. Nashaat, N. T.; Balani, S. K.; Loncharich, R. J.; Shipley, D. Y.; Mohan, R. S.; Whalen, D. L.; Jerina, D. M. *J. Am. Chem. Soc.* **1991**, *113*, 3910.

3 Jerina, D.; Daly, J.; Witkop, B.; Zaltaman-Nirenberg, P.; Underfriend, S. Arch. Biochem. Biophys. **1969**, *128*, 176. Jerina, D. M.; Daly, J. W.; Witkop, B.; Zaltaman-Nirenberg, P.; Underfriend, S. *Biochemistry*, **1970**, *9*, 147. Jerina, D. M.; Daly, J. W.; Witkop, B.; Zaltaman-Nirenberg, P.; Underfriend, S. *J. Am.*

Chem. Soc. **1968**, *90*, 6523, 6525. Boyd, D. R.; Jerina, D. M.; Daly, J. *J. Org. Chem.* **1970**, *35*, 3170. Boyland, E.; Sims, P. *Biochem. J.* **1965**, *95*, 788.

4 Dipple, A.; Moschel, R. C.; Bigger, A. H. Chemical. Carcinogens, 2nd Ed., Searle, C. E., Ed., Vol. 1, ACS Monograph, 182, American Chemical Society, Washington, D. C., **1984**, p. 41. Polycyclic. Hydrocarbons. and. Carcinogenesis, Harvey, R. G., Ed., ACS Symposium Series 283, American Chemical Society, Washington, D. C., **1985**. Polycyclic. Hydrocarbons. and. Cancer, Gelboin, H. V.; Tso, P. O. P., Eds.; Vol. 1, Academic Press: New York, **1978**.

5 Blackett, B. N.; Coxon, J. M.;Hartshorn, M. P.; Jackson, B. L.J .; Muir, C. N. *Tetrahedron,* **1969**, *25*, 1479.

6 Blackett, B. N.; Coxon, J. M.; Hartshorn, M. P.; Richards. K. E. *Aust. J. Chem.* **1970**, *23*, 839. Blackett, B. N.; Coxon, J. M.; Hartshorn, M. P.; Richards, K. E. *J. Am. Chem. Soc.* **1970**, *92*, 2574. Blackett, B. N.; Coxon, J. M.; Hartshorn, M. P. Richards, K. E. *Aust. J. Chem.* **1970**, *23*, 2077. Coxon, J. M.; Chom-Ey Lim. *Aust. J. Chem.* **1977**, *30*, 1137. Coxon, J. M.; McDonald, D. Q. *Tetrahedron Letters.* **1988**, *29*, 2575.

7 Nobes, R. H.; Rodwell, W. R.; Bouma, W. J.; Radom, L. *J. Am. Chem. Soc.* **1981**, *103,* 1913.

8 The MP3 results are estimated.[7]

9 Ford, G. P.; Smith, C. T. *J. Am. Chem. Soc.* **1987**, *109*, 1325

10 Bock, C. W.; George, P.; Glusker, J. P. *J. Org. Chem.* **1993**, *58*, 5816.

11 George, P.; Bock, C. W.; Glusker, J. P. *J. Phys. Chem.* **1992**, *96* 7302

12 George, P.; Bock, C. W.; Glusker, J. P. *J. Phys. Chem.* **1990**, *94*, 8161

13 Gaussian 94, Revision B.1, Frisch, M. J.; Trucks, G. W.; Schlegel, H. B.; Gill, P. M.W.; Johnson, B. G.; Robb, M. A.; Cheeseman, J. R.; Keith, T.; Petersson, G. A.; Montgomery, J. A.; Raghavachari, K.; Al-Laham, M. A.; Zakrzewski, V. G.; Ortiz, J. V.; Foresman, J. B.; Cioslowski, J.; Stefanov, B. B.; Nanayakkara, A.; Challacombe, M.; Peng, C. Y.; Ayala, P. Y.; Chen, W.; Wong, M. W.;

Andres, J. L.; Replogle, E. S.; Gomperts, R.; Martin, R. L.; Fox, D. J.; Binkley, J. S.; Defrees, D. J.; Baker, J.; Stewart, J. P.; Head-Gordon, M.; Gonzalez, C.; Pople, J. A. Gaussian, Inc., Pittsburgh PA, **1995**.

15 Similar results have been noted by George[10,11] who reported that the inclusion of electron correlation at the MP2/6-31G*//RHF/6-31G* level does not change these small energy differences to any appreciable extent.

16 The energy difference is greater than between **19** and **21** which reflects the hydrogen atom configuration in the two diastereomers.

17 However the size of the C2-C3-H6 and C1-C2-C3 angles may very well be an artifact of the difference in mass and vdw between H and C.

Chapter 3.

The potential energy surface for the acid and BF_3 catalysed rearrangement of methylpropene oxide.

Summary.

The acid and BF_3-catalysed rearrangement of methylpropene oxide to methylpropanal has been investigated by *ab initio* molecular orbital methods. Kinetic isotope effects are consistent with the reaction occurring by 1,2 hydride shift from a carbocation intermediate. Inverse secondary kinetic isotope effects for the hydride migration step were calculated and shown to reflect a combination of changes in C1-H(D) stretching and out of plane bending frequencies which reflect tighter force constants and stronger H-C1 bonds at the transition structure than in the reactant. Gas phase B3LYP/6-31G* level calculations favour the intermediacy of a cation in a conformation with the BF_3 below the plane. B3LYP/6-31G*(SCI-PCM) single point solvation calculations favour a conformer with BF_3 in the plane of the cation. From this latter conformation hydride migration is equally disposed to occur with inversion or retention of configuration. The transition structure for hydride (deuteride) migrating is early. A calculated correction applied to the experimentally observed migration of hydrogen/deuterium (M_H/M_D = 1.92) results in a primary kinetic isotope effect for the reaction (k_H/k_D = 1.557) close to the theoretically calculated value (k_H/k_D = 1.677).

Introduction.

Kinetic isotope effects (KIEs), which reflect changes in reaction rate as a result of isotopic substitution related to structural changes in reactant and transition structure, can be used to provide mechanistic information.[1] Isotope effects primarily reflect

changes in the vibrational frequencies between the reactant and transition structure which are related to the force constants and atomic masses of the isotopes and depend largely on the nature of the bonds being formed or broken. The vibrational modes where there is a significant change between the reactant and transition structure contribute most to a KIE.

Kinetic isotope effects, expressed as the ratio k_H/k_D are termed 'normal' if k_H/k_D >1 and inverse when k_H/k_D <1. When the bond to an isotope is broken during the course of a reaction, a primary kinetic isotope effect (PKIE) is observed for that step in the reaction process and its magnitude is determined largely from changes in stretching vibrations. Secondary kinetic isotope effects (SKIEs) arise when the bond to the isotope is at the reaction centre but not broken during the course of a reaction. The isotope influences nearby vibrations. The connection between (SKIEs) and hybridisation changes at an isotopically substituted reaction centre was first investigated by Streitweiser.[2] He established that changes in the C_α-H(D) out of plane bending frequencies are the most important in effecting the SKIE. For an S_N2 reaction, a hybridisation change from sp^3 to sp^2 at the centre undergoing reaction gives rise to a normal SKIE >1 when deuterium is substituted at the reaction centre while an inverse SKIE <1 occurs for a hybridisation change from sp^2 to sp^3. Recent work has demonstrated that changes in stretching as well as bending vibrations can be important in SKIEs.[3]

From absolute rate theory and statistical mechanics, the total energy of a molecule can be expressed as the sum of individual partition functions, Q, representing translational, rotational, vibrational and electronic energy levels:

$$Q = Q_{trans}.Q_{rot}.Q_{vib}.Q_{elec} \qquad (2.10)$$

where Q is expressed as $Q = \sum p_i e_i^{-e_i/kT}$ and is the summation over all energy states.

Isotopic substitution has little influence on the reduced mass of a molecule and so Q_{elec} can be ignored since the potential energy surface and electronic levels remain

essentially unchanged. The translational and rotational partition functions can also be ignored since in most cases the molecular masses and moments of inertia give no appreciable contribution to the isotope effect. An expression for the equilibrium constant involving the partition functions Q for the reactant and $Q^{\dagger}$ representing the transition structure is defined as:

$$K^{\dagger} = [Q^{\dagger}/Q(\text{reactant})].e^{-E_a/kT} \qquad (2.11)$$

and a kinetic isotope effect is expressed as:

$$\frac{k_H}{k_D} = \frac{K_H^{\dagger}}{K_D^{\dagger}} = \frac{Q_H^{\dagger}}{Q_D^{\dagger}} \cdot \frac{Q_D\,(\text{reactants})}{Q_H\,(\text{reactants})} \qquad (2.12)$$

Bigeleisen and Mayer derived equation[4] 2.13 which, in the absence of symmetry number effects, contains terms for all vibrations of the reactant and transition structure.

$$\left(\frac{S_2}{S_1}\right) f_{react} = \prod_{i}^{3N-6} \frac{u_{2i}}{u_{1i}} \frac{[1-e^{-u_{1i}}]}{[1-e^{-u_{2i}}]} \exp\left[\sum_{i}^{3N-6} \frac{(u_{1i} - u_{2i})}{2}\right]$$

$$\left(\frac{S_2}{S_1}\right) f_{TS} = \frac{V_{1L}^{\dagger}}{V_{2L}^{\dagger}} \prod_{i}^{3N-7} \frac{u_{2i}}{u_{1i}} \frac{[1-e^{-u_{1i}}]}{[1-e^{-u_{2i}}]} \exp\left[\sum_{i}^{3N-7} \frac{(u_{1i} - u_{2i})}{2}\right]$$

$$\frac{k_H}{k_D} = \frac{(s_2 / s_1) f_{react}}{(s_2 / s_1) f_{TS}} \qquad (2.13)$$

$$u_i = h\nu_i / kT = 1.4387\nu_i / T$$

The subscripts 1 and 2 refer to the atomic masses of hydrogen and deuterium respectively and u_i is defined by the parameters ν_i, a normal-mode harmonic frequency, Boltzmann's constant k and the absolute temperature, T. The reactant molecule is represented by 3N-6 normal vibrational modes where N is the number of atoms in the

molecule. For transition structures there are 3N-7 normal vibrational modes since the imaginary frequency is not treated as a proper vibrational mode and any movement away from the saddle point results in decomposition along the reaction coordinate. The kinetic isotope effect is expressed as the ratio of the reduced isotopic partition function of the reactant $(S_2/S_1)f_{react}$ divided by the reduced isotopic partition function of the transition structure $(S_2/S_1)f_{TS}$, and includes a term ($V_{1L}\dagger$ /$V_{2L}\dagger$) representing the ratio of imaginary frequencies of the nondeuterated and deuterated transition structures. Standard *ab inito* molecular orbital programs calculate reactant and transition structure geometries and their associated normal-mode vibrational frequencies.

An alternative equation 2.14 for calculating kinetic isotope effects utilises the difference in Gibbs free energy between the nondeuterated and deuterated reactant and transition structure, a methodology also based on statistical mechanics and transition state theory.

$$k_H/k_D = \exp^{-(\Delta G_H - \Delta G_D)/RT} \qquad (2.14)$$

where $\Delta G = G^{\dagger} - G^{r}$

$\dagger$ = transition structure, r = reactant.

These values are also contained in the output of *ab initio* frequency calculations. The use of equation 2.13 requires more data than equation 2.14, but allows the frequencies which contribute most to the KIE to be determined. Both methods are used in the present study.

The rearrangement of methylpropene oxide with BF_3 gives methylpropanal which is trapped by further reaction with epoxide as dioxolanes.[5] Previous work[6,7] on the BF_3 catalysed rearrangement of 1-deutero-2-methyl-1,2-epoxypropane in carbon tetrachloride showed the formation of the deuterated-methylpropanals (17%) **3** and **4**, along with a mixture of dioxolones (79%) **5** and **6** and 1,4-dioxan (4%) **7** (Figure 1).

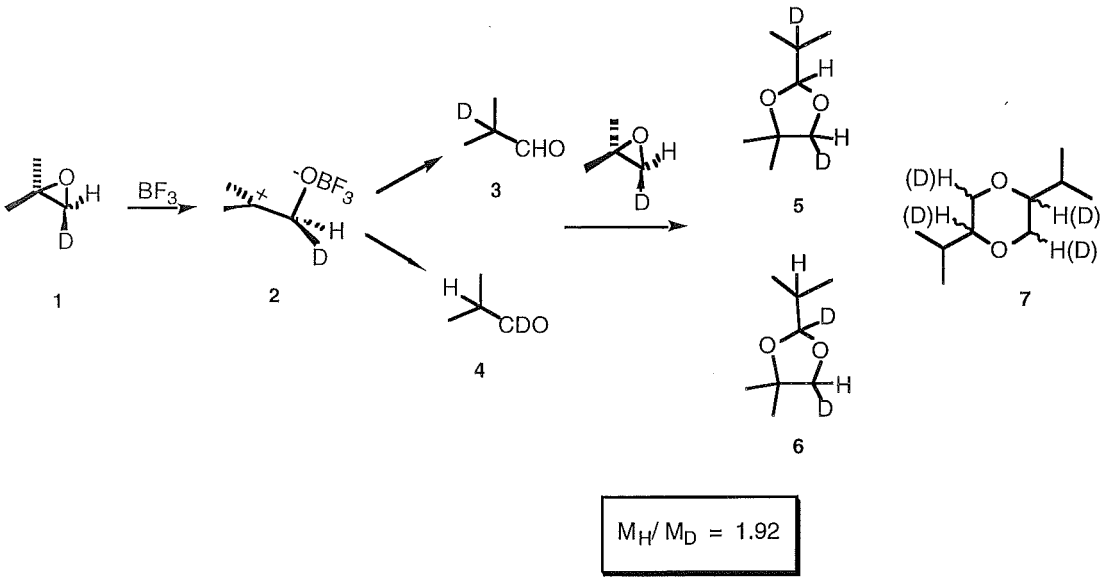

Figure 1. The rearrangement of **1** with BF_3, *via* intermediate **2** to aldehydes **3** and **4**, dioxolones **5** and **6** and 1,4-dioxan **7**.

The mechanism for formation of the aldehydes **3** and **4** from epoxide **1** was considered to occur by ring opening of epoxide coordinated to Lewis acid to give a carbocation **2**, followed by a 1,2-hydride shift to Lewis acid coordinated aldehyde. No deuterium was lost in the rearrangement, thereby excluding an enol intermediate in the reaction and also showing the aldehyde was not enolised under the reaction conditions. The results are therefore consistent with the rearrangement involving a hydride migration. A primary deuterium isotope effect is observed in the reaction which was considered a result of preferential selection of a hydride *vs* deuteride to migrate in **2** resulting in formation of aldehydes **3** and **4**. Comparison of the relative yields **3** and **4** therefore allows an estimate of the primary isotope effect k_H/k_D for the hydride (deuteride) shift. However since the aldehydes are somewhat unstable the ratio of hydride/deuteride migration M_H/M_D =1.92 (standard deviation 0.04) was established from detailed integration of the nmr spectrum of the dioxolans **6** and **7** mixture.

The primary isotope effect k_H/k_D for the hydride (deuteride) shift could be derived from the M_H/M_D ratio assuming no isotope effect in the reaction of aldehyde with epoxide and if the secondary isotope effect implicit in all the internal H/D-competitive reactions to aldehyde were allowed for. Furthermore since the aldehyde is

not completely converted into dioxolane, a small secondary isotope effect arising from reaction of aldehyde with epoxide must be included. The effect of this correction would allow k_H/k_D to be established and result in a minor change from the experimental value $M_H/M_D = 1.92$.

The present study seeks to investigate, by *ab initio* molecular orbital calculations, the key stationary points on the potential energy surface for the rearrangement of **1** to **3** and from **1** to **4** with acid and BF_3. Appropriate primary and secondary kinetic isotope effects for the stationary points directly involved with the hydride shift to aldehyde are calculated and compared with experiment. A further aim is to address whether hydride migration occurs *via* a concerted or a non-concerted process. Stationary point structures and calculated kinetic isotope effects are now reported for the protonated and BF_3 catalysed rearrangement of methylpropene oxide to methylpropanal at the B3LYP/6-31G* and B3LYP/6-31G*/SCI-PCM levels of theory.

Computational methods.

Exploratory calculations were carried out at the semi-empirical AM1[8] level followed by *ab initio* calculations at the Hartree Fock level with the 3-21G* and 6-31G* basis sets. Electron correlation was accounted for through the use of the gradient-corrected hybrid density functional B3LYP/6-31G*[9] theory. Intrinsic reaction coordinate (IRC) calculations at the B3LYP/6-31G* level were employed to determine the relevance of the transition structures on the potential energy surface. Theoretical primary and secondary kinetic isotope effects were calculated from equations 2.13 and 2.14 using vibrational frequencies and the Gibbs free energy data from frequency calculations using the *Gaussian*94[10] program. Vibrational frequencies were computed at 298.15K and scaled[11] by 0.961 and 0.893 for the B3LYP/6-31G* and HF/6-31G* levels accordingly. Single point solvation calculations were performed at the B3LYP/6-31G* level in conjunction with the self-consistent isodensity polarized continuum model[12] (SCI-PCM) within *Gaussian*94 and with a dielectric constant of 2.23.[13]

Results and discussion.

The potential energy surface for the rearrangement of protonated propene oxide to propanal has previously been reported at the MP2(full)/6-31G* level.[14] Since this study was reported, density functional methods have been shown to be more cost effective so for comparison the B3LYP/6-31G* geometries and energies of the stationary points on the surface (Figure 2) have been computed. This study is important as a comparison with the present investigation on methylpropene oxide.

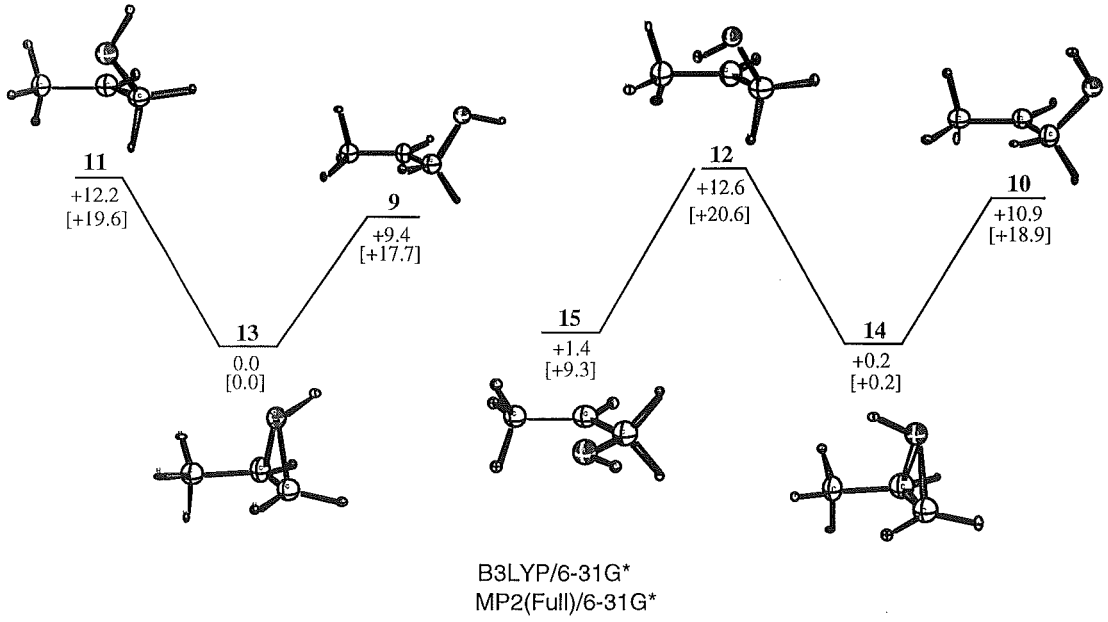

Figure 2. Optimised transition structures for the rearrangement of protonated propene oxide at the B3LYP/6-31G* and MP2(Full)/6-31G* levels of theory. Energies are in kcal/mol.

A total of four transition structures (**9-12**) were established (MP2/6-31G*) from the rearrangement of the two protonated epoxide invertomers[15] **13** and **14** (Figure 2). Intrinsic reaction coordinate calculations (MP2/6-31G*) for each of the transition structures (**9-12**) lead to the appropriate protonated epoxides (**13** and **14**). In the other direction the three lowest energy transition structures (**9-11**) gave aldehydes with each IRC showing a rearrangement by 1,2 hydride shift in a concerted asymmetric reaction pathway.[16] The highest energy transition structure **12** lead to a symmetrical carbocation

intermediate **15** where both C1 protons are equally positioned to migrate *via* a 1,2-hydride shift.

Rearrangement of protonated methylpropene oxide to methylpropanal.

The stationary points for the rearrangement of protonated methylpropene oxide to protonated methylpropanal are shown in Figure 3. Addition of a proton to methylpropene oxide produces an oxonium cation **16** activated for ring opening. The C2-O bond of **16** is lengthened (1.691Å) relative to the C1-O bond (1.495Å) reflecting the preference of the epoxide to open at the more stable tertiary $C2^+$ centre. Ring opening occurs with rotation about the C1-C2 bond to give transition structures **17** and **18**.

Rotation of the $C1H_2OH$ about C1-C2, as defined by the C3-C2-C1-O torsional angle in **17** (63.2^0) and in **18** (119.7^0), brings a C1-H proton into alignment with the p orbital of the $C2^+$ centre. The C1 hydrogen most aligned to the carbocation p-orbital is the C1-H_a proton (H_a-C1-C2-C3 = 59.0^0) in transition structure **17** and the C1-H_b proton (H_b-C1-C2-C4 = 58.1^0) in transition structure **18**. At the transition structure these C1-H bonds are not lengthened and the H-C1-$C2^+$ bond angles are tetrahedral (**17**, H_a-C1 = 1.100Å and H_a-C1-$C2^+$ = 109.6^0, **18**, H_b-C1 = 1.099Å and H_b-C1-$C2^+$ = 109.6^0). Transition structure **17** is the lowest in energy (0.3 kcal/mol) exhibiting an activation barrier of 2.7 kcal/mol (B3LYP/6-31G*). The activation barriers for ring opening are substantially lower compared to those calculated for the ring opening of protonated propene oxide (E_a for the lowest energy pathway being 9.4 kcal/mol (B3LYP/6-31G*), 17.7 kcal/mol (MP2(Full)/6-31G*)). For transition structure **17**, hyperconjugative stabilisation of the carbocation at C2 occurs with a hydrogen on both methyls (H-C4-$C2^+$ = 105.1^0, C4-H = 1.111Å and H-C3-$C2^+$ = 106.3^0, C3-H = 1.107Å) and similarly for transition structure **18** (H-C4-$C2^+$ = 103.8^0, C4-H = 1.112Å and H-C3-$C2^+$ = 111.6^0, C3-H = 1.100Å).

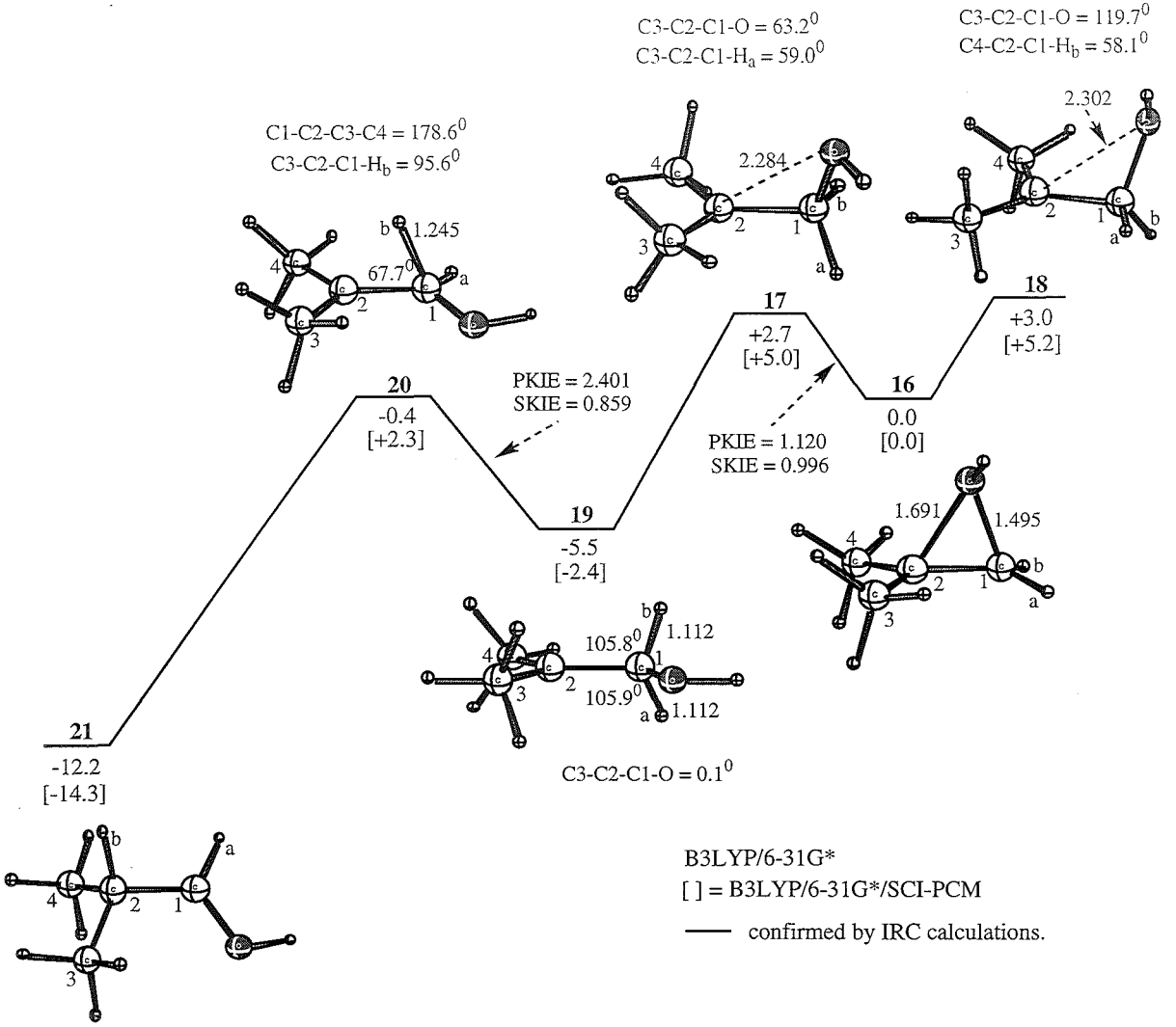

Figure 3. The rearrangement of protonated methylpropene oxide **16** to methyl propanal **21**. Energies in kcal/mol relative to **16** include a ZPVE correction. Bond lengths (Å).

An IRC calculation from transition structure **17** gave protonated epoxide **16** in one direction along the reaction coordinate and in the other direction, a planar carbocation intermediate **19** (C1-C2-C3-C4 dihedral (0.1^0)). Both C1 protons (H_a and H_b) exhibit hyperconjugation with the $C2^+$ centre and H_a and H_b are equally disposed to migrate (C1-H_b =1.112, C1-H_a = 1.112Å and H_b-C1-C2 = 105.8^0 and H_a-C1-C2 = 105.9^0). A transition structure **20** for 1,2-hydride migration from **19** to aldehyde **21** was identified and the connection between the three structures was confirmed by an IRC calculation. The 1,2-hydride shift is well advanced in transition structure **20** with a C1-C2-H_b angle of 67.7^o showing H_b to be almost equally positioned between C1 and C2. The H_b proton is almost aligned with the p-orbital of the near planar C2 cation (C3-C2-C1-H_b = 95.6^0, C1-C2-C3-C4 = 178.6^0) and is substantially lengthened (C1-H_b = 1.245Å) in comparison with the analogous bond length in **19** (1.112Å).

Analysis of the calculated theoretical kinetic isotope effects.

The primary and secondary isotope effects calculated in this study are presented in Table 3 along with geometrical parameters representative of the transition structures. The KIEs calculated by using equations 2.13 and 2.14 are identical in value.[17]

Table 3. Primary and secondary kinetic isotope effects for hydride migration.

		Geometric parameters		Isotope effects	
process	ΔE (TS-Min) (kcal/mol)[a,b]	H_{mig}-C1 Bond length[a]	H_{mig}-C1-C2 Bond angle[a]	PKIE[c] k_H/k_D	SKIE[c] k_H/k_D
H^+					
16 → TS17	+2.7[a]/+4.6[b]	1.100Å	109.6^0	1.120	0.996
19 → TS20	+5.1[a]/+5.0[b]	1.245Å	67.7^0	2.401	0.859
BF_3					
22 → TS25	+27.6[a]/+23.5[b]	1.111Å	105.4^0	1.202	1.022
27 → TS28	+1.4[a]/+0.4[b]	1.167Å	83.7^0	1.995	0.892
27 → TS29	+1.9[a]/+1.6[b]	1.211Å	73.7^0	2.092	0.902
31 → TS28	-1.8[a]/+1.2[b]	1.167Å	83.7^0	1.677	0.811
31 → TS29	-1.3[a]/+2.4[b]	1.211Å	73.7^0	1.898	0.760

[a] B3LYP/6-31G*. [b] B3LYP/6-31G*/(SCI-PCM) calculated at 298.15K with ε=2.23 (CCl_4)
[c] KIEs calculated with B3LYP/6-31G* optimised geometries and frequencies.

The magnitude of a primary kinetic isotope effect is determined by two aspects of the transition structure geometry. For a 3-centre transition structure model, a maximum isotope effect is observed when the C-H-X is linear and the hydrogen positioned "*midway*" between the C and X atoms. An asymmetric transition structure can be ascribed as 'early' or 'late.'

C····H·····X	C·····H·····X	C·····H···X
'*early*' TS	'*symmetrical*' TS	'*late*' TS

The position of the transition structure along the reaction coordinate reflects the force constants for the forming/breaking bonds. A 1,2-hydride shift requires bending of C2-C1-H from near tetrahedral in intermediate **19** to 67.7^0 in transition structure **20**. As a consequence, differences in bending modes are important in the kinetic isotope effect. Experimentally determined deuterium isotope effects for 1,2-hydride shifts lie in the range of 1.2-3.0.[18]

Quantum mechanical tunneling affects KIEs and a number of procedures have been developed[19] to calculate tunneling which has a more pronounced effect on PKIEs than on SKIEs and is more important the larger the activation barrier. Equation 2.15 proposed by Bell[20] was used for the present study to establish the importance or otherwise of tunneling.

$$\left(\frac{k_H}{k_D}\right)_{corr} = \frac{Q_t(H)}{Q_t(D)} \cdot \frac{k_H}{k_D} \qquad \text{with} \quad Q_t = \frac{0.5\, u_i^{\dagger}}{\sin(0.5\, u_i^{\dagger})} \qquad (2.15)$$

The tunneling effects, calculated using equation 2.15 are minute and result in no change to the KIEs presented in Table 3. This is consistent with the very low activation barriers for the 1,2-hydride shift. Although the transformation from **16** to **18** *via* transition structure **17** is the rate determining step on the potential energy surface (Figure 3), the process does not involve hydride migration though there is some C1-H hyperconjugation with the $C2^+$ centre at the transition structure.

Primary and secondary isotope effects were determined by replacing H_a and H_b respectively with deuterium. The calculated primary isotope effect for H_a, the proton most aligned with the developing cation is small (k_H/k_D = 1.120). The secondary isotope effect of H_b, the bystander proton (deuteron) (k_H/k_D = 0.996) with H_b almost in the nodal plane of the carbocation (H_b-C1-C2$^+$-C4 = 5.2^0), is close to unity which suggests that any change in hybridisation at the C1 centre between **16** and **17** is minimal.

The symmetry (excluding the methyl orientations) of intermediate **19** determines that migration of H_a and H_b is equally favoured. The primary and secondary kinetic isotope effects for hydride migration were determined for **19** → **20** by replacing H_a and H_b respectively with deuterium. The calculated primary isotope effect for hydride/deuteride migration is k_H/k_D = 2.401 and is nearer the higher end of the PKIE values (1.2-3.0) observed experimentally for 1,2-hydride shifts. A large inverse kinetic secondary isotope effect was calculated k_H/k_D = 0.859 for the hydride/deuteride shift between **19** → **20**. This is surprising when one considers the hybridisation in **19** which is sp^3 hybridised but modified by H_a and H_b hyperconjugation with C2$^+$. For transition structure **20**, the migrating proton is positioned close to midway between C1 and C2 with C1-C2-H *'cyclopropane-like'* and the hybridisation between sp and sp^2 character. Isotopically sensitive vibrational modes that increase in frequency in proceeding from reactant to transition structure are responsible for inverse SKIEs. Inverse α-deuterium SKIEs are not uncommon for sp^3 → sp^2 processes and bimolecular S_N2 reactions at methyl have been reported to be as low as 0.87.[21] The vibrational frequencies responsible for the SKIE between the nondeuterated and deuterated transition structure **20** and intermediate **19** are presented in Table 4.

Table 4 Harmonic vibrational frequencies (cm^{-1}) for the SKIE between 19 → 20

	Transition structure		Intermediate	
Mode	TS20 C1-Hα	TS20 C1-Dα	Min19 C1-Hα	Min19 C1-Dα
1	3729	3729	3754	3754
2	3186	3186	3195	3195
3	3166	3166	3171	3171
4	3150	3130	3055	3055
5	3130	3122	3023	3023
6	3122	3050	3018	3018
7	3050	3036	2999	2999
8	3036	2329	2930	2925
9	2151	2148	2924	2146
10	1611	1588	1529	1522
11	1525	1522	1513	1511
12	1495	1494	1478	1461
13	1488	1481	1461	1452
14	1467	1467	1429	1428
15	1431	1431	1391	1378
16	1422	1416	1383	1353
17	1399	1338	1353	1334
18	1322	1301	1334	1271
19	1295	1250	1270	1251
20	1262	1201	1240	1199
21	1192	1119	1197	1154
22	1166	1070	1159	1088
23	1079	1014	1096	1002
24	1031	983	1002	959
25	1005	939	950	918
26	902	900	819	819
27	811	792	795	783
28	584	580	711	667
29	509	488	538	535
30	429	425	390	382
31	380	377	383	369
32	299	286	309	308
33	273	270	274	273
34	191	191	200	193
35	127	127	143	141
36	638i	619i	97	94

The C-H stretching modes for transition structure **20** and intermediate **19** show the greatest variation upon isotopic substitution. In each case they reduce in frequency. These frequencies are characterised as C1-H = 3036 cm^{-1} and C1-D = 2329 cm^{-1} in **20** and C1-H = 2924 cm^{-1} and C1-D = 2146 cm^{-1} in **19**. The frequencies for **20** are 112–185 cm^{-1} greater than in the latter. These larger frequencies in **20** are consistent with the transition structure H-C(sp^2) bonds being stronger than the reactant **19** H-C(sp^3) bonds. The difference between the C-H and C-D stretching frequencies in **19** is

larger (880 cm^{-1}) than for **20** (707 cm^{-1}) and this would give a normal contribution to the overall SKIE.

The out of plane bending frequencies at C1 for **20** and **19** also show a decrease with isotopic substitution but less than for the C1-H(D) stretching modes. The nondeuterated and deuterated out of plane bending frequencies at C1 are characterised at 1166 cm^{-1} and 1070 cm^{-1} for **20** and at 1096 cm^{-1} and 1002 cm^{-1} for **19** respectively (Table 4). These along with the other mid to low range bending frequencies between 1399-938 cm^{-1} collectively make a more significant multiplicative contribution to the reduced isotopic partition function of transition structure **20** $[(S_2/S_1)f_{TS}]$ than for the intermediate **19** $[(S_2/S_1)f_{react}]$ and are responsible for the inverse SKIE. This implies that the bending motion of the C1-α-hydrogen/deuterium is more constrained for the sp^2 hybridised transition structure **20** than in the sp^3 hybridised intermediate **19**.

BF_3 catalysed rearrangement of methylpropene oxide to methylpropanal.

A study of the potential energy surface of the reaction of BF_3 and methylpropene oxide shows a low energy pathway from **22** *via* transition structure **23** to **24** (Figure 4) with the stationary points optimised at the B3LYP/6-31G* level. The barrier to addition is higher (+22.4 kcal/mol) than that for ring opening of the epoxide with acid (+2.7 kcal/mol, Figure 3). Ring opening to transition structure **23** is accompanied by rotation about the C1-C2 bond which positions a fluorine of the BF_3 (C2-F = 2.416Å) to allow an intramolecular reaction with $C2^+$ with retention of configuration to occur. Neither C1 hydrogens are positioned to migrate (O-C1-C2-C4 = 69.3^0).

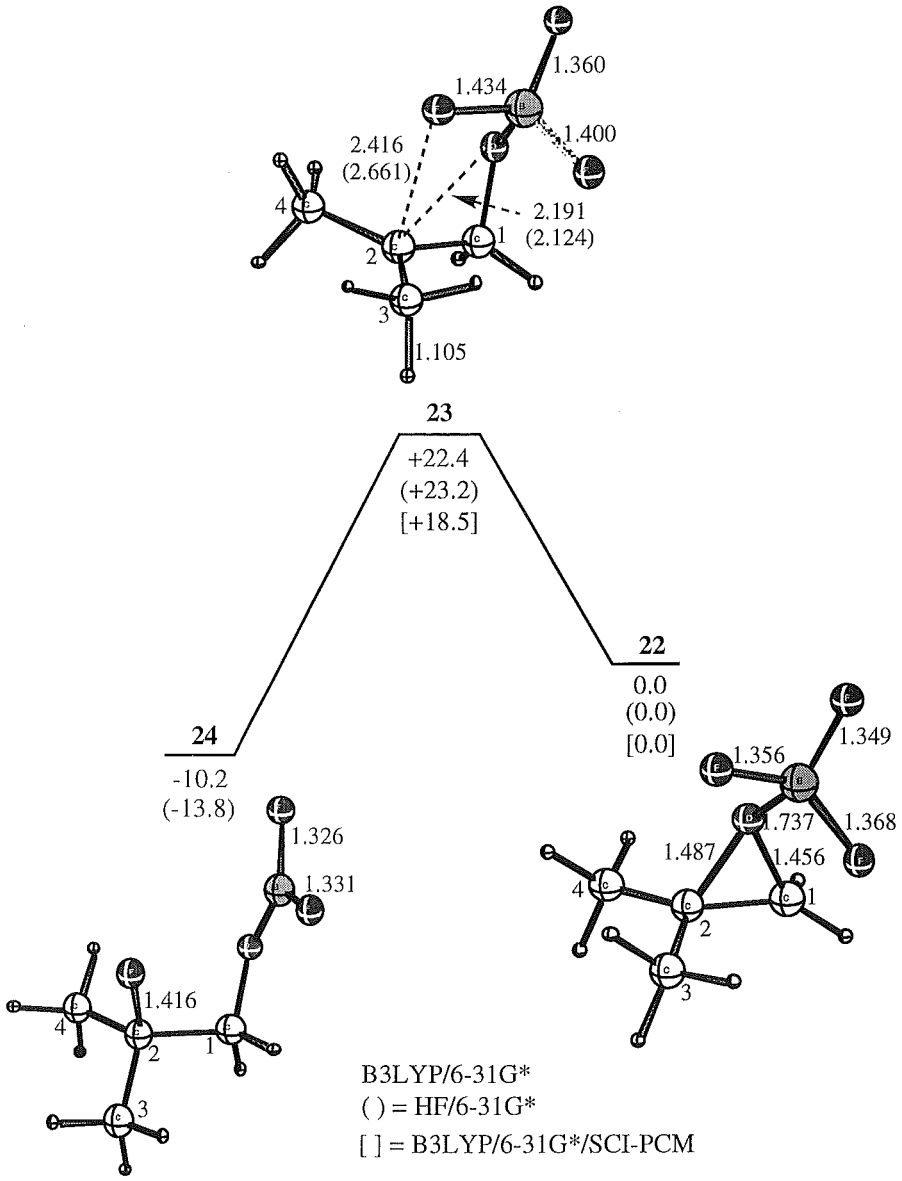

Figure 4. The lowest energy pathway for the addition reaction of epoxide with BF_3 **22** to **24** *via* transition structure **23**. All stationary points are optimised at the B3LYP/6-31G* level. Bond lengths in Å with energies relative to **22** in kcal/mol.

An IRC calculation on transition structure **23** lead to **22** and **24**, the latter involving migration of fluorine from the BF_3 group to C2. Fluorohydrin, which would be the product of work up of such a reaction is not observed in the experiment.[22] Structure **24** is a weaker Lewis acid than BF_3, and in the absence of more than one mole equivalent of BF_3 rearrangement to aldehyde would not be expected since **24** is unlikely to act as a Lewis acid catalyst for the removal of the C2-F. The reaction **22** →

24 is exothermic and is not expected to be reversible. Therefore the fluoro compound **24** does not appear to be on the potential energy surface to aldehyde.

Two further transition structures **25** and **26** on the potential energy surface were established (Figure 5) with activation barriers **22** → **25** (+27.6 kcal/mol) and **22** → **26** (+28.0 kcal/mol) higher than for **22** → **23** (+22.4 kcal/mol). These transition structures are favourable for hydride migration since rotation about C1-C2 positions C1-H_a to overlap with the p orbital at $C2^+$ (**25**: C3-C2-C1-H_a = 74.4^0, **26**: C3-C2-C1-H_a = 75.6^0). Hyperconjugation is observed in **25** (C2-C1-H_a = 105.4^0) but not in **26**. The methyls in the lower energy transition structure **25** have rotated relative to their positions in **22** such that a C4-H exhibits hyperconjugation with $C2^+$ and is anti to H_a which also exhibits hyperconjugation with the cation centre. A C3-H forms an intramolecular H-F bond with the BF_3 group (C3H-F = 1.892Å, C3H-F = 2.300Å).

An IRC calculation performed on transition structure **25** lead to **22** but failed to converge to a minima in the other direction. The last structure from the IRC calculation (before convergence failure) was optimised by recalculating the force constants. The optimisation ran a number of steps with no change in energy and with converged maximum and rms force constants to give structure **27**. A frequency calculation revealed the presence of a very small imaginary frequency (5i cm^{-1}). In **27** (Figure 5) a boron – fluorine bond of the BF_3 group is lengthened (1.435Å) and involved in an intramolecular H-F bond with a C3-H proton (1.918Å). The C3-H proton exhibits hyperconjugation with the $C2^+$ centre (H-C3-$C2^+$ = 102.6^0 and C3-H = 1.116Å). The other methyl has rotated from its conformation in **25** to position a C4-H to hyperconjugate (H-C4-C2+ = 107.8^0) with the $C2^+$ centre also. The O-C1-C2-C3 torsion in **27** is near planar (3.6^0) and H_b is in a more favourable position to hyperconjugate with the $C2^+$ centre than H_a (H_b-C1-$C2^+$ = 102.5^0, C4-C2-C1-H_b = 60.9^0 and H_a-C1-$C2^+$ = 107.2^0, C4-$C2^+$-C1-H_a = 46.3^0).

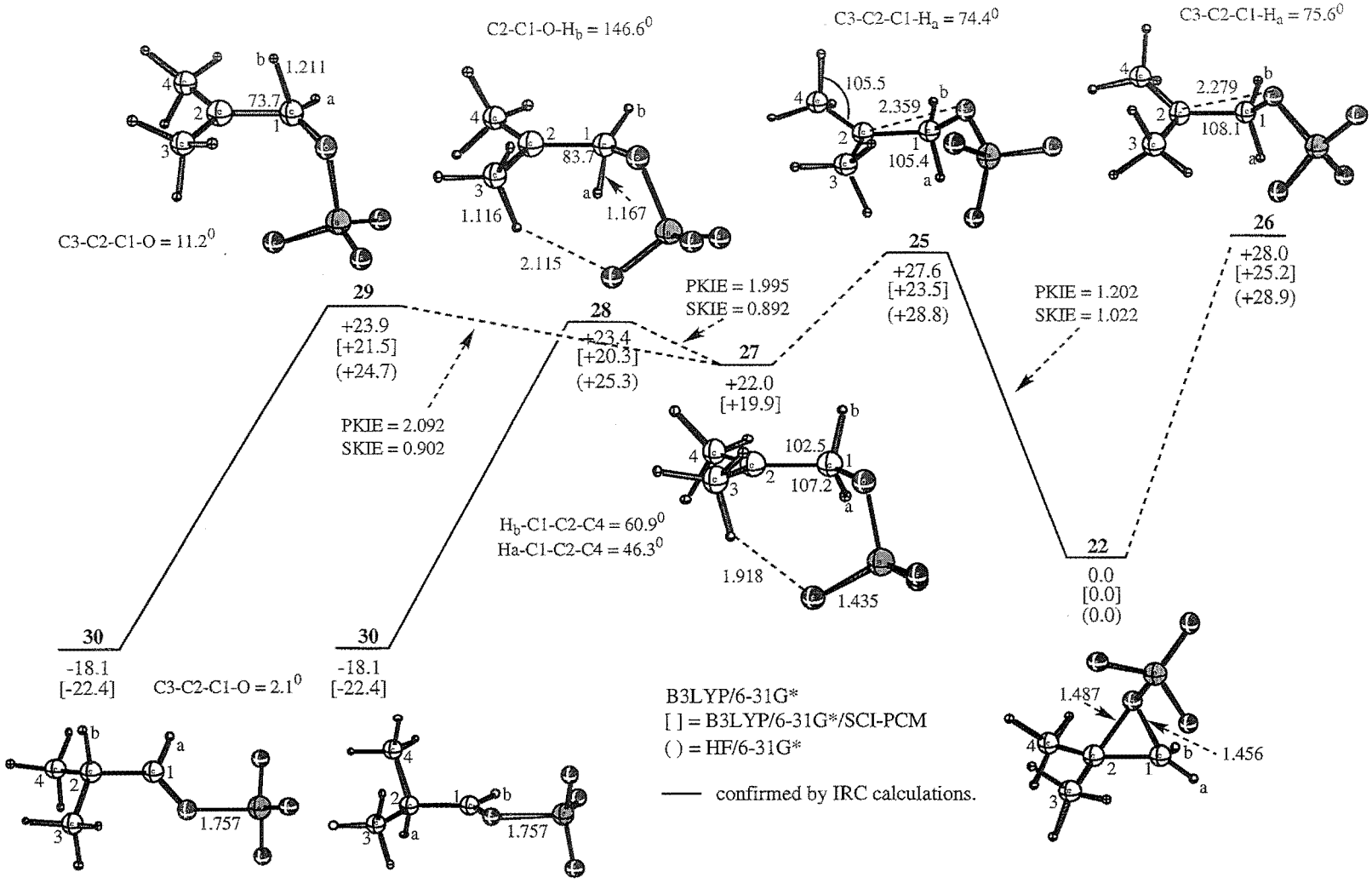

Figure 5. The rearrangement of BF_3 coordinated methylpropene oxide **22** to BF_3 coordinated methyl propanal **30**. Energies in kcal/mol relative to **22** include a ZPVE correction. Bond lengths (Å).

Two transition structures **28** and **29** for hydride migration (from **27**) were identified (Figure 5). For these structures the OBF_3 has rotated about C1-O, (**28**: C2-C1-O-B = 103.2^0, **29**: 85.5^0) in opposite directions relative to its position in **27** (C2-C1-O-B = 91.0^0). While H_b is more favourably positioned to migrate than H_a in **27**, the pathway involving migration of H_a *via* transition structure **28** is 0.5 kcal/mol lower in energy than the pathway involving H_b *via* transition structure **29**. At the HF/6-31G* level **29** is calculated to be 0.6 kcal/mol lower in energy than **28** demonstrating the effect of inclusion of electron correlation. For B3LYP/6-31G* optimised **28**, the H_a-C1-C2 bond angle (83.7^0) is reduced and C1-H_a (1.167Å) lengthened compared with **27** (107.2^0 and 1.115Å). Hydride migration is not well advanced in **28** and in accord with the Hammond principle,[23] the geometry of **28** is closer to intermediate **27** than to product **30**.

Interaction of a C3-H proton with a fluorine is maintained in **28** although weaker with the C3-H-F bond (2.115Å) longer than in **27** (1.918Å). Hydride migration in transition structure **29** is more advanced than in **28** as evidenced by the $C2^+$-C1-H_a bond angle (73.7^0) and the C1-H_a bond length (1.211Å). The small activation barrier (1.9 kcal/mol) from **27** to **29** is consistent with an early transition structure. There is less interaction between the BF_3 group and the C3 methyl hydrogen in **29** as a result of rotation of the methyl from it's conformation in **27**. Hyperconjugation of the C3-H (H-C3-$C2^+$ = 105.0^0) and C4-H (H-C4-$C2^+$ = 105.9^0) protons with $C2^+$ occurs anti to the migrating H_b.

A carbocation structure **31**, akin to the planar protonated carbocation intermediate **19** (Figure 3), was isolated (Figure 6).

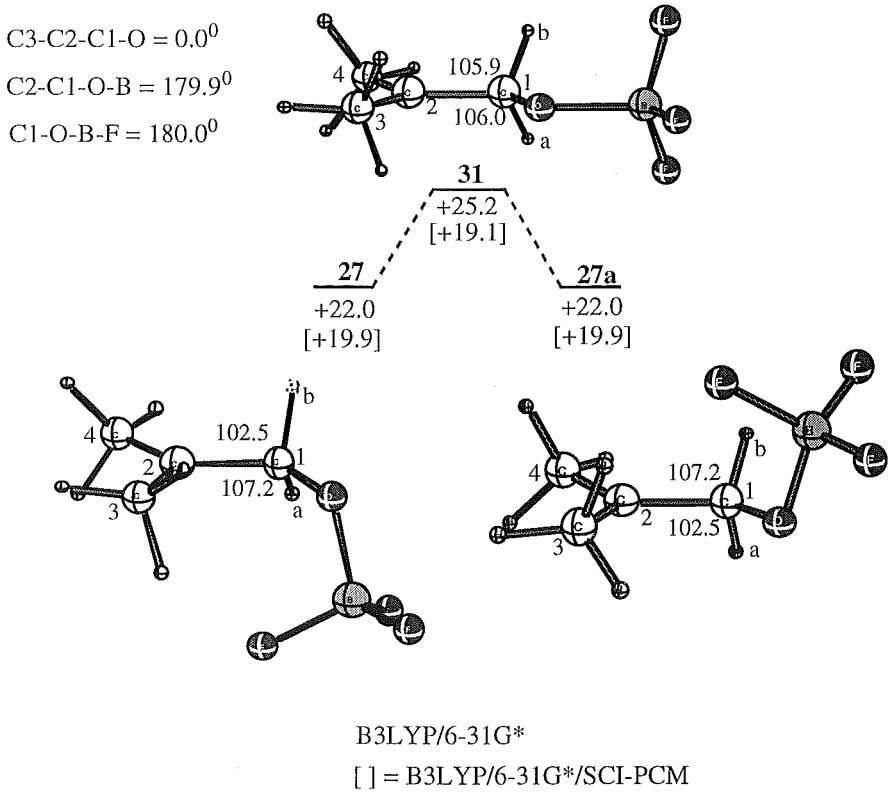

Figure 6. The interconversion of **27** to **27a** *via* transition structure **31**. Energies (kcal/mol) are relative to BF_3 coordinated epoxide **22**. Bond angles are in degrees.

Vibrational frequency analysis confirms **31** as a transition structure due to the presence of a small single imaginary frequency (55i cm^{-1}) and animation of this frequency shows a "wagging" motion of the O-BF_3 group about the O-C1-C2-C3 plane. Structure **31** is planar throughout the C3-C2-C1-O (0.0^0), C2-C1-O-B (179.9^0) and C1-O-B-F (180.0^0) torsional angles and is thought to be the transition structure between **27** and it's mirror image **27a**. An IRC calculation on **31** did not proceed more than one step along the reaction coordinate in either downhill direction. Although the barrier for interconversion between **27** and **27a** *via* **31** is small (3.2 kcal/mol, B3LYP/6-31G*), the activation barrier is higher than the barriers for migration of H_a or H_b from **27** *via* transition structures **28** and **29** (1.4 and 1.9 kcal/mol) respectively.

Single point SCRF(SCI-PCM) calculations were performed on all the B3LYP/6-31G* optimised geometries in Figures 5 and 6 and the relative energies are shown in Table 1 (Appendix B1). A dielectric constant of 2.23 was used for CCl_4 at 298.15K. The activation barriers leading to the transition structures **25**, **26**, **28** and **29** are lowered by 2-4 kcal/mol in solvent. While the highest energy gas phase transition structures **25** and **26** are lowered by the greatest amount in solvent they still remain the rate determining step in the rearrangement of **22**. Of notable interest is the lowering in energy of transition structure **31** (Figure 6) from +25.1 kcal/mol in the gas phase to +19.1 kcal/mol in solvent relative to **22** which places it lower in energy than the intermediate **27** (+19.9 kcal/mol). Although CCl_4 has a low dielectric constant (2.23), the geometry of **31** would favour more charge stabilisation at the cationic $C2^+$ centre by solvent since there is less steric hindrance from the OBF_3 group than is present in **27**.

Kinetic Isotope Effects.

Kinetic isotope effects were determined for the gas phase B3LYP/6-31G* optimised stationary points in Figure 5 by replacing the C1-H_a and C1-H_b protons respectively with deuterium. For transition structure **25**, a concerted mechanism for aldehyde formation *via* a 1,2-hydride shift cannot be excluded since an IRC calculation failed to locate a minima other than **22**. Consequently a PKIE and a SKIE was investigated for the rate determining step from **22** → **25**. The calculated PKIE k_H/k_D = 1.202 for H_a is larger than the PKIE k_H/k_D = 1.120 for the rate determining step **16** → **17** (Table 3) for protonated methylpropene oxide, consistent with the nearer alignment and hyperconjugation of the H_a proton with the $C2^+$ centre in **25** (C3-C2-C1-H_a (74.4^0) and C2-C1-H_a (105.4^0)) relative to **17** (Figure 3, C3-C2-C1-H_a (59.0^0) and C2-C1-H_a (109.6^0). A small SKIE was calculated k_H/k_D = 1.022 between **22** → **25** which reflects a modest change in hybridisation at C1.

The two competing processes for hydride migration involving the C1-H_a and C1-H_b protons of the non-symmetrical intermediate **27** were investigated. A PKIE k_H/k_D = 1.995 was calculated for the migration of C1-$\mathbf{H_a}$ from intermediate **27** *via* transition structure **28**. This value is smaller than the PKIE k_H/k_D = 2.401 calculated for the 1,2-hydride shift between protonated **19** → **20** (Figure 3) showing that hydride migration is less advanced in **28** (H_a-C1-C2 = 83.7^0 and H_a-C1 = 1.167Å, Table 3). An inverse SKIE was calculated (k_H/k_D = 0.892) at the C1 centre for the process **27** → **28**. The C1-H_b proton exhibits hyperconjugation with the $C2^+$ centre in **27** which weakens the bond resulting in a distortion from sp^3 hybridisation. For **28**, the C1 centre shows less sp^3 character than in **27** but is not fully sp^2 hybridised as evidenced by the C2-C1-O-H_b torsional angle of 146.6^0. The vibrational frequencies responsible for the SKIE between the nondeuterated and deuterated transition structure **28** and intermediate **27** are presented in Table 5.

The vibrational modes of particular interest are the C1-H(D) stretching and out of plane bending frequencies. For transition structure **28**, isotopic substitution lowers the C1-H stretching frequency from 3003 cm^{-1} to 2475 cm^{-1} and both of these values are higher than for intermediate **27** (2833 cm^{-1} and 2073 cm^{-1}) respectively. However the greater difference between the C1-H frequencies in **27** (760 cm^{-1}) than for **28** (528 cm^{-1}) results in a normal contribution to the overall KIE. A large inverse contribution to the overall SKIE is provided by a stretching frequency of C1-H_a in **28** which decreases from 2475 cm^{-1} with H_b adjacent to C1 to 2208 cm^{-1} with D_b adjacent to C1. The nondeuterated and deuterated out of plane bending frequencies are higher in **28** (1271 cm^{-1} and 1158 cm^{-1}) than in **27** (1218 cm^{-1} and 1104 cm^{-1}) reflecting tighter bonding at the C1 centre in the former. The greater collective multiplicative contribution of the mid to low range bending frequencies for the transition structure **28** than for the intermediate **27** also provides an inverse contribution to the SKIE. Tunneling effects do not change the value of the PKIEs and SKIEs for the hydride migration between **27** → **28**, consistent with the very low activation barrier of 1.4 kcal/mol.

Table 5 Harmonic vibrational frequencies (cm^{-1}) for the SKIEs between 27 → 28 and 31 → 28

	Transition structure		Intermediate		Intermediate	
Mode	TS28 C1-Hα	TS28 C1-Dα	Min27 C1-Hα	Min27 C1-Dα	Min31 C1-Hα	Min31 C1-Dα
1	3175	3175	3184	3184	3178	3178
2	3154	3154	3155	3155	3154	3154
3	3101	3101	3088	3088	3078	3078
4	3059	3059	3059	3059	3038	3038
5	3034	3034	3033	3033	3032	3032
6	3008	3008	2890	2889	3012	3012
7	3003	2475	2866	2866	2809	2795
8	2475	2208	2833	2073	2782	2043
9	1527	1521	1521	1519	1529	1528
10	1516	1513	1512	1511	1507	1506
11	1492	1491	1482	1481	1481	1481
12	1461	1457	1432	1423	1451	1444
13	1455	1437	1421	1409	1444	1444
14	1418	1417	1398	1392	1409	1408
15	1398	1391	1359	1344	1369	1369
16	1364	1322	1347	1328	1330	1318
17	1301	1284	1317	1278	1286	1274
18	1286	1268	1274	1241	1272	1249
19	1271	1158	1246	1227	1248	1199
20	1234	1137	1231	1189	1183	1149
21	1136	1100	1218	1104	1176	1116
22	1119	1069	1103	1084	1123	1074
23	1090	1017	1084	1014	1072	1006
24	1019	1011	1014	982	1006	981
25	1006	952	951	948	976	907
26	890	889	892	871	905	881
27	878	874	809	806	866	866
28	819	795	798	790	827	799
29	736	729	742	721	761	756
30	613	610	677	646	610	609
31	565	561	600	596	607	590
32	503	501	541	534	532	528
33	478	472	505	502	507	506
34	461	460	465	463	437	436
35	386	383	388	387	387	384
36	358	355	368	367	365	362
37	305	304	344	332	301	291
38	286	280	316	312	290	289
39	252	252	302	300	222	218
40	241	236	246	227	219	210
41	195	194	219	215	180	179
42	108	107	171	170	113	106
43	105	105	142	141	107	103
44	26	26	59	58	40	40
45	333i	307i	6i	6i	56i	56i

The vibrational frequencies for the SKIE between the nondeuterated and deuterated transition structure **29** and the intermediate **27** are shown in Table 6.

Table 6 Harmonic vibrational frequencies (cm^{-1}) for the SKIEs between 27 → 29 and 31 → 29

	Transition structure		Intermediate		Intermediate	
Mode	TS29 C1-Hα	TS29 C1-Dα	Min27 C1-Hα	Min27 C1-Dα	Min31 C1-Hα	Min31 C1-Dα
1	3173	3173	3184	3184	3178	3178
2	3154	3154	3155	3155	3154	3154
3	3122	3122	3088	3088	3078	3078
4	3111	3111	3059	3059	3038	3038
5	3051	3051	3033	3033	3032	3032
6	3042	3042	2890	2868	3012	3012
7	3027	2264	2866	2832	2809	2793
8	2257	2222	2833	2115	2782	2045
9	1546	1534	1521	1519	1529	1528
10	1520	1517	1512	1510	1507	1506
11	1494	1492	1482	1482	1481	1481
12	1481	1471	1432	1422	1451	1444
13	1464	1460	1421	1410	1444	1444
14	1427	1427	1398	1395	1409	1408
15	1417	1412	1359	1344	1369	1369
16	1378	1344	1347	1321	1330	1317
17	1313	1289	1317	1275	1286	1274
18	1292	1284	1274	1245	1272	1249
19	1287	1181	1246	1231	1248	1199
20	1235	1156	1231	1182	1183	1149
21	1156	1102	1218	1101	1176	1116
22	1149	1092	1103	1076	1123	1073
23	1090	1018	1084	1014	1072	1006
24	1030	1002	1014	969	1006	981
25	1010	954	951	923	976	907
26	892	891	892	890	905	881
27	859	853	809	798	866	866
28	818	795	798	777	827	799
29	700	697	742	740	761	756
30	624	618	677	661	610	609
31	549	540	600	592	607	590
32	498	497	541	535	532	528
33	468	465	505	504	507	506
34	449	434	465	464	437	436
35	391	388	388	386	387	384
36	360	358	368	364	365	362
37	325	315	344	334	301	291
38	288	286	316	314	290	289
39	235	234	302	298	222	218
40	200	200	246	226	219	210
41	182	181	219	218	180	179
42	97	96	171	170	113	106
43	84	83	142	140	107	103
44	30	31	59	58	40	40
45	615i	594i	6i	6i	56i	55i

The 1,2-hydride shift between **27** and transition structure **29** involves the C1-H_b which is more aligned with the $C2^+$ p-orbital (H_b-C1-C2-C4 = 60.9^0) than the C1-H_a (H_a-C1-C2-C4 = 46.3^0) in **27**. A PKIE for C1-H_b migration was calculated to be k_H/k_D = 2.092 and larger than the PKIE between **27** → **28** k_H/k_D = 1.995, a consequence of hydride migration being more advanced in the former process. This is illustrated by the smaller C2-C1-H_b bond angle (73.7^0) and lengthened C1-H_b bond (1.211Å) in **29** than in **28** (C2-C1-H_a = 83.7^0 and C1-H_a =1.167Å). An inverse SKIE (k_H/k_D = 0.902) was calculated for hydrogen/deuterium placed at the C1-H_a position in **27** and **29**. The C1-H stretching frequencies for the non deuterated (3027 cm^{-1}) and deuterated (2264 cm^{-1}) transition structure **29** (Table 6) are higher than the corresponding modes in intermediate **27** (2833 cm^{-1} and 2115 cm^{-1}). The difference between these frequencies is larger for **29** (763 cm^{-1}) than for **27** (718 cm^{-1}) and results in an inverse contribution to the overall SKIE. The out of plane bending mode frequencies for **29** (1287 cm^{-1} and 1181 cm^{-1}) are also higher than the corresponding frequencies in **27** (1218 cm^{-1} and 1101 cm^{-1}) and the net effect is only a 1% normal contribution to the SKIE.

B3LYP/6-31G*/SCI-PCM solvent calculations predict transition structure **31** to be lower in energy (+19.1 kcal/mol) than intermediate **27** (+19.9 kcal/mol) relative to **22**. On the assumption **31** is a "stable" minimum in solvent, KIEs have been investigated for hydride migration *via* transition structures **28** and **29** using the frequency data from the gas phase optimised geometries of **28**, **29** and **31** (Figure 7). Although the gas phase frequency data for **31** show a small imaginary frequency 55i cm^{-1}, it results in no significant contribution to the overall KIE and it can essentially be ignored. H_a and H_b in **31** hyperconjugate with the $C2^+$ centre and are equally positioned to migrate to give aldehyde *via* a process involving either inversion or retention of configuration. A PKIE for hydride/deuteride placed at the C1-H_a position in **31** and in **28** was calculated to be k_H/k_D = 1.677, a result considerably smaller than the PKIE k_H/k_D = 1.995 for the **27** → **28** process.

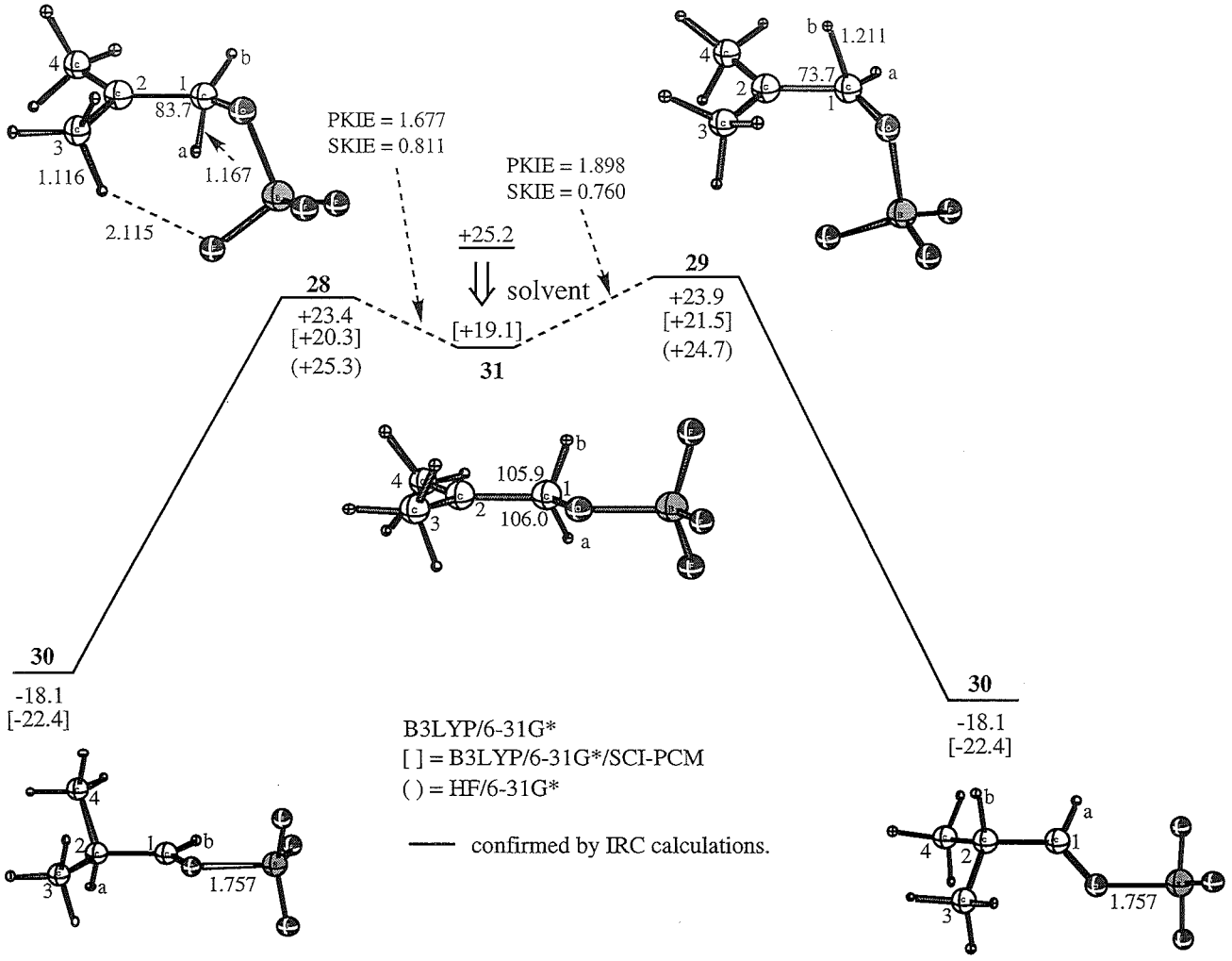

Figure 7. Hydride migration from intermediate **31** *via* transition structures **28** and **29**.
Energies in kcal/mol relative to **22** include a ZPVE correction. Bond lengths (Å), bond angles in deg.

A large inverse SKIE was calculated k_H/k_D = 0.811 between **31** → **28**, (cf. SKIE k_H/k_D = 0.892 calculated between **27** → **28**). This result is a consequence of the different vibrational modes associated with **31** which are displayed in Table 5. The nondeuterated and deuterated C1-H_b and C1-D_b stretching frequencies for **31** (2782 cm^{-1} and 2043 cm^{-1}) are lower than the corresponding frequencies in **27** (2833 cm^{-1} and 2073 cm^{-1}) respectively. The smaller difference between the C1-H_b and C1-D_b frequencies in **31** (739 cm^{-1}) than in **27** (760 cm^{-1}) reduces the normal contribution to the overall SKIE from **31** relative to **27**. This is outweighed by the large inverse contribution from the C1-$H_a(D_a)$ stretching frequencies in transition structure **28**.

For the 1,2-hydride shift between **31** → **29**, a PKIE was calculated k_H/k_D = 1.898 for migration of H_b, a value smaller than the PKIE calculated (k_H/k_D = 2.092) between **27** → **29**. A large inverse SKIE was calculated (k_H/k_D = 0.760) between **31** → **29**, greater than the SKIE calculated between **27** → **29** (k_H/k_D = 0.906). The greater inverse SKIE is primarily a result of the smaller differences between the nondeuterated and deuterated mid to low range bending frequencies between 1286 cm^{-1} and 1006 cm^{-1} in **31** relative to the analogous frequencies in **27** (Table 6). As a result, the contribution to the overall reduced isotopic partition function $(S_2/S_1)f_{react}$ from these bending frequencies is smaller in **31** than in **27**, therefore resulting in a greater inverse SKIE for **31** → **29** than for **27** → **29**.

The true k_H/k_D ratio reflecting the 1,2-hydride shift between **2** → **3** and **2** → **4** (Figure 1), requires a correction for the secondary isotope effect introduced by the formation of **4** to be applied to the experimentally determined ratio (M_H/M_D = 1.92). The correction is presented in the following expressions and it can be shown that the ratio (M_H/M_D = 1.92) is required to be multiplied by an appropriate SKIE (equation (2.19)).

$$M_H/M_D = \frac{k^{H_{mig}}_{D_{adj}}}{k^{D_{mig}}_{H_{adj}}} = 1.92 \quad (2.16) \qquad \text{where the true PKIE is : PKIE} = \frac{k^{H_{mig}}_{H_{adj}}}{k^{D_{mig}}_{H_{adj}}} \quad (2.17)$$

$$\text{An expression for a SKIE is:} \quad \text{SKIE} = \frac{k^{H_{mig}}_{H_{adj}}}{k^{H_{mig}}_{D_{adj}}} \quad (2.18)$$

Substituting (2.18) into (2.16) gives (2.19) :

$$1.92 = \frac{\frac{k^{H_{mig}}_{H_{adj}}}{\text{SKIE}}}{k^{D_{mig}}_{H_{adj}}} \quad \text{and} \quad \frac{k^{H_{mig}}_{H_{adj}}}{k^{D_{mig}}_{H_{adj}}} = (1.92).(\text{SKIE}) \qquad (2.19)$$

The subscripts *mig* and *adj* in equations (2.16) → (2.19) refer to the hydrogen (deuterium) migrating *via* a 1,2 shift and to the hydrogen (deuterium) adjacent to the reaction centre respectively. From Table 3 and Figure 7, the PKIE and SKIE most representative of the true experimental PKIE is that for the process **31** → **28** where a PKIE of k_H/k_D = 1.677 and a SKIE of k_H/k_D = 0.811 is calculated. Multiplying the latter SKIE with the experimental ratio (M_H/M_D = 1.92) gives the corrected experimental PKIE of k_H/k_D = 1.557. This value is close to the calculated PKIE k_H/k_D = 1.677 and its low magnitude indicates that hydride (deuteride) migration is not fully advanced in the transition structure leading to aldehyde formation.

Conclusion.

The present study has established the origins of kinetic isotope effects for a 1,2 hydride (deuteride) shift through analysis of the vibrational frequencies of reactant and transition structure. The primary kinetic isotope effects primarily result from differences between the C1-H(D) stretching frequencies between reactant and transition structure

which decrease upon isotopic substitution. Inverse secondary kinetic isotope effects were calculated and are attributed to a combination of changes in C1-H(D) stretching and out of plane bending frequencies and the importance of each varies between the substrates. In all cases these frequencies are lower in the reactant than the transition structure reflecting tighter force constants and stronger H-C1(sp^2) bonds at the transition structure than the H-C1(sp^3) bonds in the reactant. The calculations support a 1,2 hydride shift from an intermediate **31** (Figure 7) where hydride migration is equally favoured to occur with inversion or retention of configuration *via* an 'early' transition structure **28** where the migrating hydride (deuteride) is not equally positioned between C1 and C2. A calculated correction applied to the experimentally observed result (M_H/M_D = 1.92) results in a primary kinetic isotope effect for the reaction (k_H/k_D = 1.557) close to the theoretically calculated value (k_H/k_D = 1.677).

References

[1] Lars Melander, *Isotope Effects on Reaction Rates*, The Ronald Press Company, New York, **1960**.

[2] Streitweiser. A.. Jr.; Jagow, R. H.; Fahey, R. C.; Suzuki, S. *J. Am. Chem. Soc.* **1958**. *80*. 2326-2332.

[3] (a) X. G. Zhao, S. C. Tucker and D. G. Truhlar, *J. Am. Chem. Soc.*, **1991**, *113*, 826-832; (b) X. G. Zhao, D.-H. Lu, Y.-P. Liu, D. G. Lynch and D. G. Truhlar, *J. Chem. Phys.*, **1992**,*97*, 6369.

[4] (a) Bigeleisen, J.; Mayer, M. G. *J. Chem. Phys.* **1947**, *15*, 261-67. (b) Bigeleisen, J. *J. Chem. Phys.* **1949**, *17*, 675. (c) Bigeleisen, J.; Wolfsberg, M. *Adv. Chem. Phys.* **1958**, *1*, 15.

[5] Yandovskii, Y.N.; Temnikova, T.*L J. Org. Chem.* **1968**, *4*, 1695. Blackett, B.N.; Coxon, J.M.; Hartshorn.; Lewis, A.J.; Little,; G.R.; Wright, G.J. *Tetrahedron*, **1970**, *26*, 1311. O^{18} studies show the mechanism of dioxolane formation involves attack of a carbonyl (the aldehyde) on the epoxide, not the reverse. Coxon, J.M.; Hartshorn, M.P.; Sutherland, B.L.S. *Aust J. Chem*, **1974**, 27. The epimeric 6-t-

butyl-1-oxaspior[2,5]octanes react with O^{18} labeled acetone to give epimeric mixtures of dioxolanes with the O^{18} attached to the cyclohexyl ring, consistent with a preference for axial attack an intermediate tertiary cation coupled with a preference of acetone attack with inversion.

[6] Coxon, J. M.; Hartshorn, M. P.; Swallow, W. H. *Aust. J. Chem.* **1973**, *26*, 2521-2526.

[7] Blackett, B.N.; Coxon, J.M.; Hartshorn, M.P.; Richards, K.E. *Aust J. Chem*, **1970**, *23*, 839.

[8] Dewar, M. J. S.; Zoebisch, E. G.; Healy, E. F.; Stewart, J. J. P. *J. Am. Chem. Soc.* **1985**, *107*, 3902.

[9] Becke, A. D. Phys. Rev. A **1988**, *38*, 3098. Becke, A. D. *J. Chem. Phys.* **1993**, *98*, 1372. Lee, C.; Yang, W.; Parr, R. G. *Phys. Rev.* B **1988**, *37*, 785.

[10] Gaussian 94, Revision D.2. Frisch, M. J.; Trucks, G. W.; Schlegel, H. B.; Gill, P. M. W.; Johnson, B. G.; Robb, M. A.; Cheeseman, J. R.; Keith, T.; Petersson, G. A.; Montgomery, J. A.; Raghavachari, K.; Al-Laham, M. A.; Zakrzewski, V. G.; Ortiz, J. V.; Foresman, J. B.; Cioslowski, J.; Stefanov, B. B.; Nanayakkara, A.; Challacombe, M.; Peng, C. Y.; Ayala, P. Y.; Chen, W.; Wong, M. W.; Andres, J. L.; Replogle, E. S.; Gomperts, R.; Martin, R. L.; Fox, D. J.; Binkley, J. S.; Defrees, D. J.; Baker, J.; Stewart, J. P.; Head-Gordon, M.; Gonzalez, C.; Pople, J. A. Gaussian, Inc., Pittsburgh PA, **1995**.

[11] Exploring Chemistry with Electronic Structure Methods. 2nd Edition. James B. Foresman and Aeleen Frisch. Chapter 4, pg 62.

[12] Foresman, J. B.; Keith, T. A.; Wiberg, K. B.; Snoonian, J.; Frisch, M. J. *J. Phys. Chem.* **1996**, *100*, 16098-16104.

[13] *Handbook of Chemistry and Physics*, 60th ed.; Weast, R. C., Ed.; CRC Press: Boca Raton, FL, **1980**; p E55.

[14] Coxon, J. M.; Maclagan, R. G. A. R.; Rauk, A.; Thorpe, A. J.; Whalen, D. *J. Am. Chem. Soc.* **1997**, *119*, 4712-4718.

[15] The term "invertomer" has been coined to describe the diastereomers resulting from positioning of a proton on either face of an epoxide. George, P.; Bock, C. W.; Glusker, J. P. *J. Phys. Chem.* **1990**, *94*, 8161-8168.

[16] See supplementary material (ref 14).

[17] It has been noted that if a scale factor of 1.0 is not specified in the *Gaussian* program input file for an isotope calculation, the program automatically assigns a scale factor of 0.8929. If the original frequency data (from which the checkpoint file is used for an isotope calculation) is not scaled and is used in conjunction with the isotope calculation frequency data then this can lead to erroneous isotope effects.

[18] (a) Myhre, P. C.; Brown, K. S. *J. Am. Chem. Soc.* **1969**, *91,* 5639-5641. (b) Myhre, P. C.; Evans, E. *J. Am. Chem. Soc.* **1969**, *91,* 5641-5644. (c) Karabatsos, G. J.; Hsi, N.; Meyerson, S. *J. Am. Chem. Soc.* **1970**, *92,* 621-626. (d) Karabatsos, G. J.; Mount, R. A.; Rickter, D. O.; Meyerson, S. *J. Am. Chem. Soc.* **1970**, *92,* 1248-1253.

[19] (a) D. G. Truhlar, A. D. Isaacson and B. C. Garrett, in *The Theory of Chemical Reaction Dynamics*, ed. M. Baer, CRC Press; Boca Raton, FL; 1985, **4**, ch. 2; (b) A. Gonzalez-Lafont, T. N. Truong and D. G. Truhlar, *J. Chem. Phys.*, **1991**, *95*, 8875. (c) D. G. Truhlar, R. Steckler and M. S. Gordan, *Chem. Rev.*, **1987**, *87*, 217; (d) G. C. Schatz, *Chem. Rev.*, **1987**, *87*, 81.

[20] Bell, R. P. *The Tunnel Effect in Chemistry*; Chapman and Hall: New York, **1980**; pp61.

[21] Llewellyn, J. A.; Robertson, R. E.; Scott, J. W. M. *Can. J. Chem.* **1960**, *38*, 222.

[22] Fluorohydrins have been reported for reaction of epoxides with BF_3 in ether and are known to rearrange on further reaction with BF_3. Coxon, J. M.; Hartshorn, M. P.; Lewis, A. J.; Richards, K. E.; Swallow, W. H. *Tetrahedron.* **1969**, *25*, 4445-8. Blackett, B. N.; Coxon, J. M.; Hartshorn, M. P.; Richards, K. E. *Tetrahedron.* **1969**, *25*, 4999-5005. Coxon, J. M.; Lawrey, M. G. *Chem and Ind.* **1969**, 1558.

[23] Hammond, G. S. *J. Am. Chem. Soc.* **1955**, *77*, 334.

Chapter 4.

Molecular orbital studies of the intramolecular reaction of protonated *cis*- and *trans*- 3,4-epoxypentan-1-ol.

Summary.

The transition structures for the intramolecular reaction of protonated *cis*- and *trans*- 3,4-epoxypentan-1-ol (**13**) and (**16**), which result in the formation of protonated *cis*- and *trans*-2-methylfuran-3-ols (**14**) and (**18**) with inversion and retention, have been determined at the *ab initio* MP2/6-31G* and hybrid density functional B3LYP/6-31G* levels of theory. Intrinsic reaction coordinate calculations for the lower energy inversion pathways for formation of the 2-methylfuran-3-ols show that intramolecular attack occurs in concert with ring opening. The reaction pathways are far from optimum for best orbital overlap, reflecting the strained bicyclic nature of the transition structures.

Introduction.

Empirical rules elaborated by Baldwin[1] for predicting the regiochemistry of ring closure reactions are used as a guide in planning the synthesis of cyclic molecules. For example a reaction that forms a strainless or near strainless five- or six-membered ring generally occurs readily, however ring closure is disfavored when it involves reaction at a trigonal carbon atom that forms a double bond to an atom inside the incipient ring (the 5-*endo-trig* system). In contrast 5-*exo-trig* reactions are

successful when reaction is at a double bond that is *outside* the incipient ring (Figure 1).

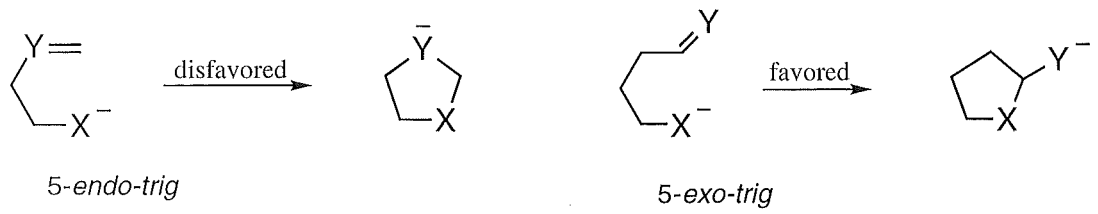

Figure 1. 5-*endo* and *exo-trig* cyclisation.

Ring opening of epoxides with a proton or Lewis acid is an important method of initiating intramolecular ring closure. For example *trans*-5,6-epoxyheptan-1-ol (**1b**) (n=4) reacts with BF_3 to give (1SR,2'RS)-1-(tetrahydropyran-2'-yl)ethanol (**2**) (>95%) in preference to formation of *trans*-2-methyloxepan-3-ol (**3**) (3%) (Figure 2).[2] Both products are the result of reaction occurring with inversion of configuration at the site of nucleophilic attack. For *trans*-4,5-epoxyhexan-1-ol (**1a**) (n=3), five-membered ring formation to give (1SR,2'RS)-1-(tetrahydrofuran-2'-yl)ethanol (**4**) competes with formation of *trans*-2-methyltetrahydropyran-3-ol (**5**) (4:1) (Figure 2) with both products a result of inversion of configuration at the site of nucleophilic attack.

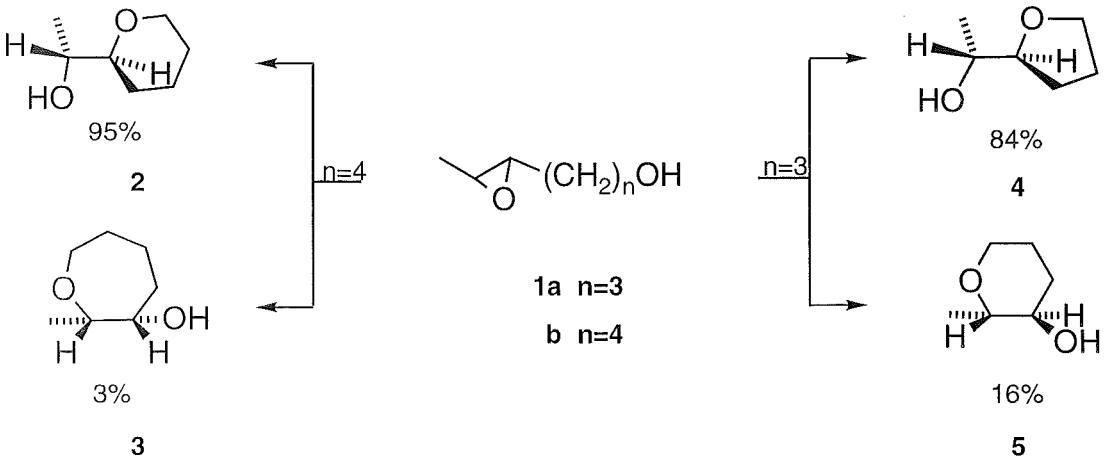

Figure 2. Acid catalyzed rearrangement of *trans*-5,6-epoxyheptan-1-ol and *trans*-4,5-epoxyhexan-1-ol.

Recently Janda and Lerner[3] developed a catalytic antibody to overcome the stereoelectronic preference for five- over six-membered ring formation and catalyze the rearrangement of *trans*-7-aryl-4,5-epoxyheptan-1-ol **6** to the 6-*endo-tet* product **8** rather than give the tetrahydropyran **7**, the major product in the absence of the catalytic antibody (see Figure 3).[4]

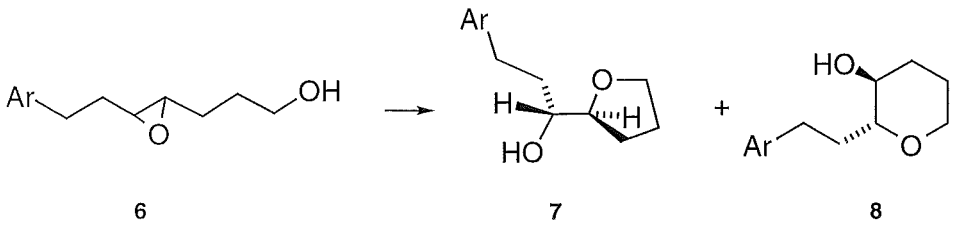

6 7 8

Figure 3. Intramolecular rearrangement of *trans*-7-aryl-4,5-epoxyheptan-1-ol **6** to 6-*endo-tet* product **8** and tetrahydropyran **7**.

Houk has carried out calculations at the MP2 level, for a model system *trans*-4,5-epoxyhexan-1-ol (**1a**) lacking the aryl group (Figure 2). Specifically the barrier that needs to be overcome by the catalytic antibody was calculated. The 5-*exo* process is calculated to be favored by 1.9 kcal/mol. Assuming a negligible entropic difference in the two transition structures this translates to a 96:4 product ratio at 25 ^{o}C[4] "To favor the 6-*endo* product **5** to a similar amount, the catalytic antibody must lower the 6-*endo* activation energy 3.6 kcal/mol more than it lowers the 5-*exo* activation barrier." Furthermore, some imaginative calculations have been used to show the effect of a proximate acid source and counterion in influencing transition state structure thereby mimicking the regiochemistry dictated by the catalytic antibody.[5]

The boron trifluoride catalyzed reaction of *trans*- and *cis*-3,4-epoxypentan-1-ol **9** and **10** in diethyl ether results in the formation of *trans*- and *cis*-2-methylfuran-3-ols **11** and **12** (Figure 4). There is no evidence in either reaction for the formation of the more strained four-membered ring ether. The *trans*-isomer **9** gives predominantly, and in high yield, *trans*-2-methylfuran-3-ol (**11**) the product resulting from inversion of configuration at the reaction centre. The mechanism for formation of the lesser *cis*-isomer **12** is in doubt. It could be formed *via* an intermediate fluorohydrin or by nucleophilic attack with retention of configuration.

The *cis*- epoxide **10** is unusual in that it gives a predominance of the same *trans*-2-methylfuran-3-ol (**11**), a product, in this case at least formally, of retention of configuration at the reaction center.[2] It is again not known if the predominance of this product is the result of a mechanism involving retention of configuration at the site of nucleophilic attack, or if the reaction involves a fluorohydrin and two sequential inversion reactions.

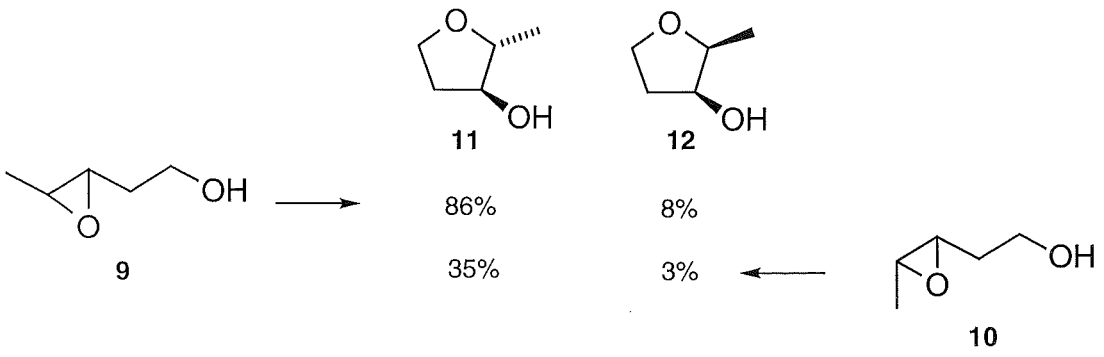

Figure 4. Acid catalyzed rearrangement of **9** and **10**.

The reaction of the protonated form of **9** and **10** has been investigated using *ab initio* and density functional methods to determine stationary points in an effort to quantify electronic and steric factors and further examine the pathway for ring formation *via* intrinsic reaction coordinate calculations.[6]

Computational methods.

Exploratory calculations were carried out at semi-empirical AM1[7] and Hartree-Fock 3-21G* and 6-31G* levels. The results reported here, including optimized structures, vibrational frequencies and intrinsic reaction coordinate (IRC), were obtained at the ab initio MP2/6-31G*(Full) and the gradient-corrected hybrid density functional B3LYP/6-31G*[8] levels of theory. Stationary points were examined at both levels of theory to validate the appropriateness of the less expensive B3LYP method.[9] All stationary points were identified for the number of imaginary frequencies by vibrational frequency analysis. Zero-point corrections (ZPC) are included in any relative energies with B3LYP/6-31G* and MP2/6-31G* zero point vibrational energies scaled by 0.961 and 0.95 respectively. The GAUSSIAN 94[10] suite of programs was used throughout the present work.

Results and Discussion.

The results of *ab initio* and density functional calculations of the transition structures for the intramolecular rearrangement of the protonated form of *trans*- and *cis*- 3,4-epoxypentan-1-ol (**9**) and (**10**) involving *inversion* of configuration at the site of intramolecular nucleophilic attack which result in formation of the protonated form of *trans*- and *cis*-2-methylfuran-3-ols (**11**) and (**12**) and the corresponding 1-

(oxacyclobutan-2'-yl)ethanols are now reported. Transition structures for formation of **11** and **12** with *retention* of configuration are also presented.

Acid catalyzed rearrangement and addition to epoxides is considered to occur *via* the intermediacy of the protonated or Lewis acid coordinated epoxide oxygen.[11] Protonation can occur from either face of the epoxide ring to give the stereoisomeric *syn* and *anti* oxonium ions.[11] Calculations carried out on the proton catalyzed rearrangement of propene oxide[12] show the *syn* protonated oxonium ion is marginally higher in energy than the *anti* diastereomer. Therefore if hydrogen bonding effects are neglected, protonation of *cis*-3,4-epoxypentan-1-ol (**10**) would be expected to be favored on the less hindered face of the epoxide (i.e. **13**) while for the *trans*-3,4-epoxypentan-1-ol (**9**) the faces are hindered more equally.

The potential energy surface for rearrangement of protonated *cis*-3,4-epoxypentan-1-ol (13).

Conformations of protonated *cis*-3,4-epoxypentan-1-ol (13), protonated *cis*-2-methylfuran-3-ol (14) and protonated 1-(oxacyclobutan-2'-yl)ethanol (15).

The lowest energy conformation of the reactant, *anti*-protonated *cis*-3,4-epoxypentan-1-ol **13**, is shown in Figure 5. The corresponding *syn*-diastereomer 17 is lower in energy (ca. 11 kcal/mol both at the MP2/6-31G* and the B3LYP/6-31G* level) (Figure 6)[13] as a result of hydrogen bonding between $OH10^{+}$ of the protonated epoxy group and the alcohol oxygen. Protonated *cis*-2-methylfuran-3-ol **14**[14] and protonated 1-(oxacyclobutan-2'-yl)ethanol **15** are the two possible products of intramolecular rearrangement of **13** with inversion (Figure 5).

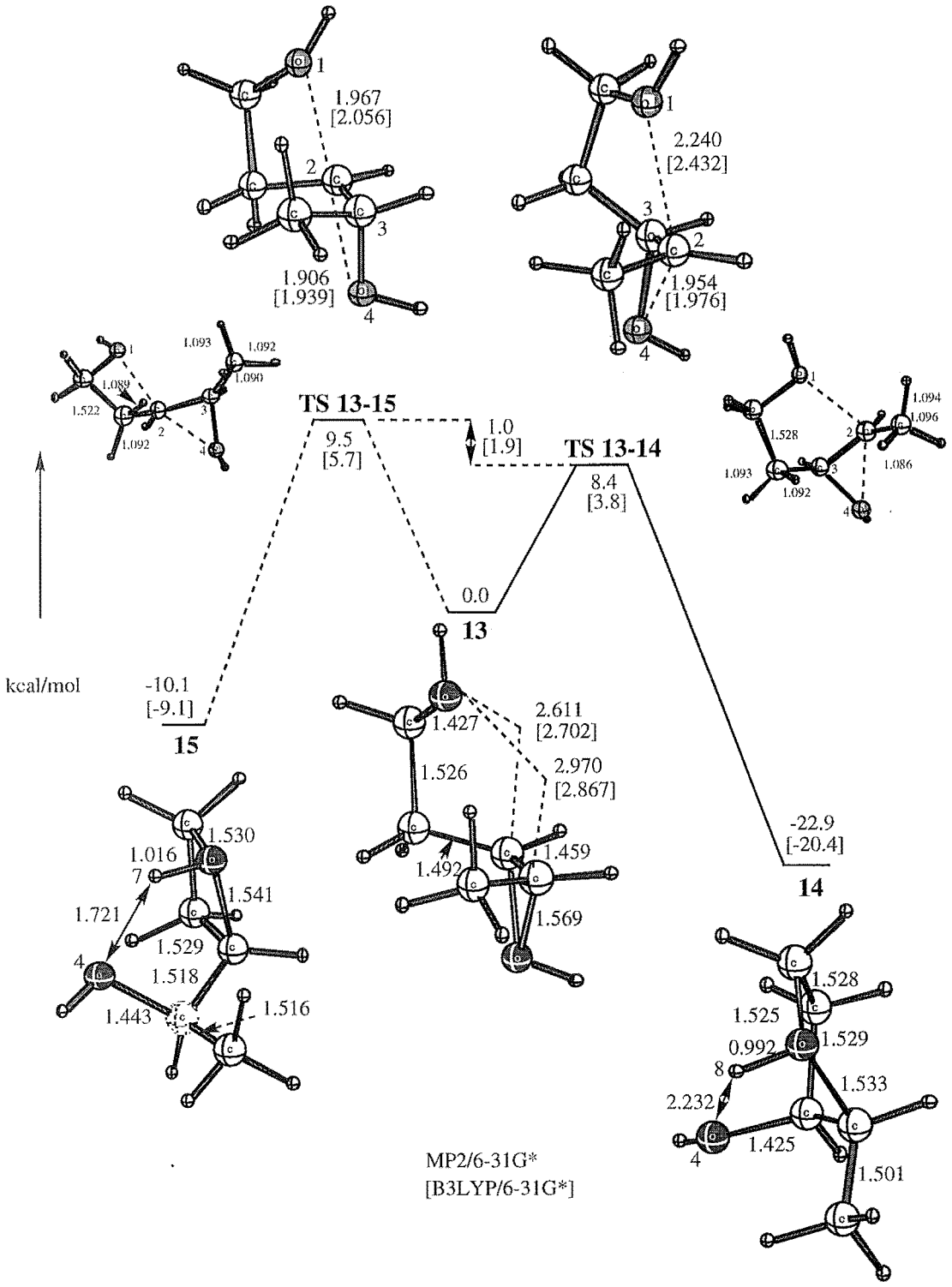

Figure 5. The potential energy profile for rearrangement of protonated *cis*-3,4-epoxypentan-1-ol (**13**) to **14** and **15**, both with inversion of configuration. Geometries (in Å and deg) at the MP2(full)/6-31G* level. Two perspectives of each transition structure are shown. The relative energies in two levels (MP2(full)/6-31G*, B3LYP/6-31G* in brackets) are in kcal/mol and include zero point corrections.

Transition structures for rearrangement of protonated *cis*-3,4-epoxypentan-1-ol, (13) and (17).

The rearrangement of *anti*-protonated *cis*-3,4-epoxypentan-1-ol **13** was investigated first. This protonated structure, was originally obtained at the completion of an IRC calculation at the MP2/6-31G* level from **TS 13-14** and shown to be in fact a global minima. The two transition structures for rearrangement with inversion of **13** to protonated 1-(oxacyclobutan-2'-yl)ethanol **15** and protonated *cis*-2-methylfuran-3-ol **14** are shown in Figure 5 with the corresponding energies with zero point corrections given in Tables 1 and 2 (see Appendix C1 and C2).

The five-membered transition structure **TS 13-14**[15] is favoured over the four-membered transition structure **TS 13-15** at all levels of theory studied. A notable difference between the four- and five-membered transition structures for inversion is that in the former the forming and the breaking C-O bonds are of comparable length (difference of 0.06Å at the MP2/6-31G* level) while in the latter the difference between the two is much larger (0.29Å). The C-O distances in **TS 13-15** are substantially longer than the corresponding distances in **TS 13-14**. One may say that **TS 13-14** is *earlier* and a substantially *looser* transition structure than **TS 13-15**. The larger exothermicity of the reaction **13→14** compared to **13→15** is consistent with the earlier transition structure for the former. The looseness of **TS 13-14** must be related to the distance that oxygen atom of the hydroxyl has to travel from the reactant **13** (a HO····C distance of 2.97Å at the MP2/6-31G* level, see Figure 5) to the reaction **TS 13-14** (2.24 Å), as compared with the corresponding distance from **13** (2.61 Å) to **TS 13-15** (1.97 Å). The path of reaction for **TS 13-14** is longer than that for **TS 13-15** and the forming O-C bond is still weak at **TS 13-14**. A selection of CC and CH bond

distances are given in Figure 5. There is no evidence for significant hyperconjugation from CH's of the methyl adjacent to the reaction centre for the five-membered transition structure or from analogous CH and CC bonds for the four-membered transition structure.

In order to be able to use calculations to predict the reaction regiochemistry, in this case the preference for five- over four-membered ring formation, the correct description of the energy difference between **TS 13-15** and **TS 13-14** is essential. This difference changes from 1.0 kcal/mol at MP2/6-31G*, 2.2 kcal/mol at MP3(frozen core), 1.7 kcal/mol at MP4SDQ(frozen core) to 1.0 kcal/mol at MP4SDTQ(frozen core). Although one has to also examine the effects of larger basis sets in order to obtain a fully converged results, there appears to be no doubt that **TS 13-14** is a few kcal/mol lower than **TS 13-15**. There is no experimental evidence for products of a four-membered transition structure. However, the calculated **TS 13-15** is only 1.0 kcal/mol (MP2/6-31G*) and 1.9 kcal/mol (B3LYP/6-31G*) higher than **TS 13-14** which suggests that the B3LYP result is more consistent with experiment.

The major product of reaction of **10** with boron trifluoride was **11**, a product that cannot be formed by a route involving inversion of configuration. A transition structure which retains the configuration was found. This transition structure **TS 17-18** results from reaction of the more stable *syn*-protonated epoxide diastereomer **17**. The energy of this transition structure (Figure 6), is 8.6 (MP2/6-31G*) and 5.7 kcal/mol (B3LYP/6-31G*) higher than **TS 13-14** resulting from inversion of configuration from the *anti*-protonated epoxide diastereomer **13**.[16]

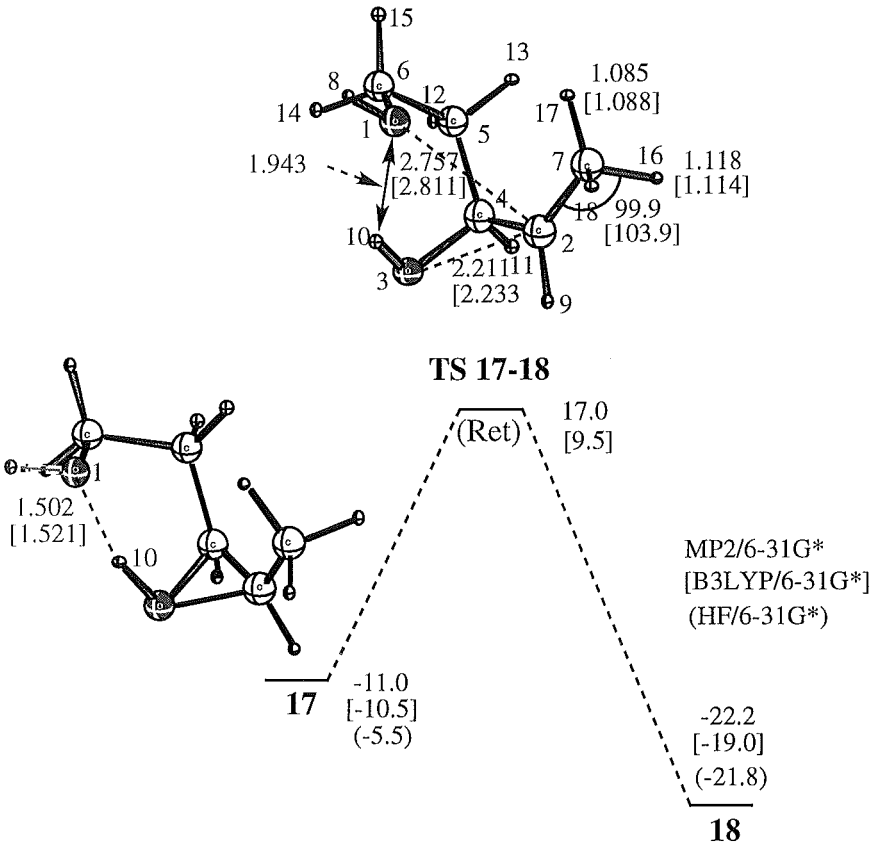

Figure 6. The potential energy profile for rearrangement of **17** to **18** with retention of configuration, compared with that of **13** to**14**. Geometries (in Å and deg) at the MP2(full)/6-31G* level. The relative energies in three levels (MP2(full)/6-31G*, B3LYP/6-31G* in bracket and HF/6-31G* in parentheses) are in kcal/mol and include zero point corrections.

The substantially higher energy of the transition structure **TS 17-18** compared to **TS 13-14** and the expected equilibrium between **13** and **17** suggests that the reaction with retention *via* **TS 17-18** to form **11** directly is not likely to occur. In the reaction with $BF_3{\cdot}Et_2O$, the isolation of **11** from **10**, a product of apparent retention of configuration at the site of nucleophilic attack most likely involves the intermediacy of fluorohydrin.

The transition structure for retention **TS 17-18** shows hyperconjugation between one of the methyl hydrogens and the carbocation centre exhibiting a reduced C2-C7-H16 angle of 100^0 and lengthening of one methyl C-H to 1.118Å. A comparison with corresponding bonds for the transition structure (**TS 19-20**, Figure 7) for rearrangement of protonated propene oxide (**19**) to protonated propanal (**20**) show that in the latter a suitably disposed CH adjacent to the developing site of electron deficiency increases to a maxima at the transition geometry of 1.13Å.[9] This bond length extension, indicative of hyperconjugative stabilization, is not observed for either the intramolecular four- or five-membered transition structures (Figure 5) for inversion of configuration which is consistent with intramolecular hydroxyl attack being earlier in the reaction coordinate that hydride migration in the propene oxide rearrangement. Furthermore, the rearrangement of propene oxide exhibits a reaction profile that could be described as asynchronous with two distinct and independent processes which are not linked by the formation of a discrete intermediate (Figure 7).

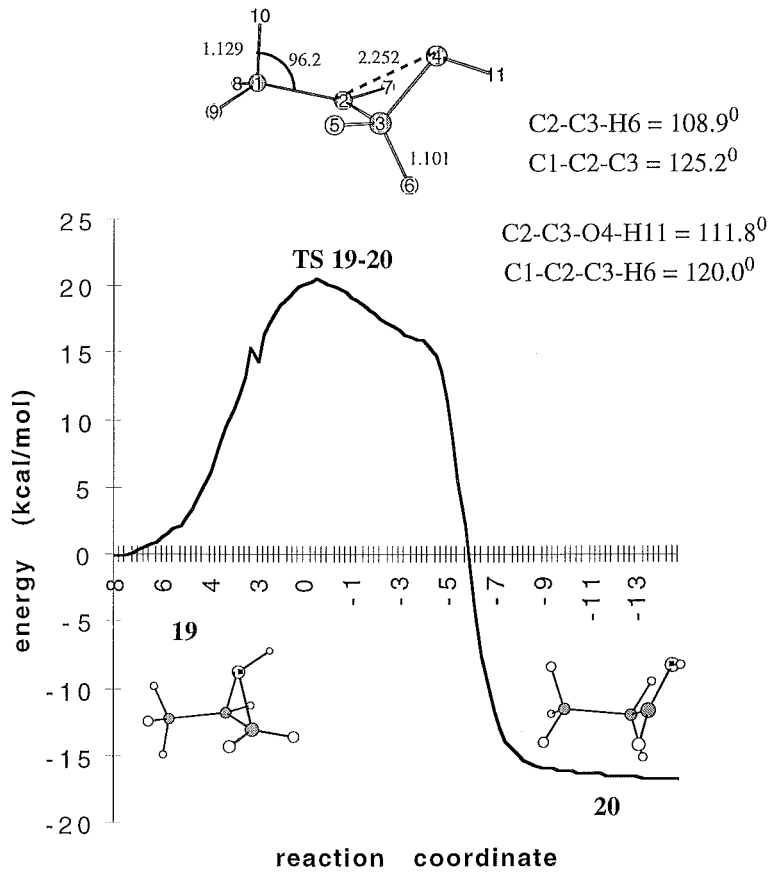

Figure 7. The potential energy profile for rearrangement of protonated propene oxide (**19**) to protonated propanal (**20**) at the MP2/6-31G* level.

The first process is rupture of the protonated epoxide and the second closely following process is hydride migration. These two sequential process are preceded by an initial rotation of the methyl to bring an adjacent CH of the methyl into alignment with the electron deficient centre that subsequently develops.[12] Rotation of the methyl group is not observed in the inversion transition structures for intramolecular ether formation for protonated *cis*-3,4-epoxypentan-1-ol **13** since the hydroxyl attack at carbon occurs early in the reaction and in concert with epoxide CO bond rupture. Carbonyl formation by hydride migration, does not compete with furan formation consistent with the higher calculated activation barrier for hydride migration.

The barrier to reaction for rearrangement of **13** to **14** (MP2/6-31G* ca 8.4 kcal/mol) is substantially lower (Figure 5) than for the lowest pathway found for rearrangement of protonated propene oxide to protonated propanal (17.7 MP2/6-31G* kcal/mol).[12] For the intramolecular nucleophilic attack of hydroxyl, the decrease in activation barrier compared with rearrangement of protonated propene oxide is a reflection of the facility of the hydroxyl to participate in concert with cleavage of the protonated epoxide. In contrast the migrating hydrogen in the rearrangement of protonated propene oxide occurs subsequent to epoxide cleavage with consequent charge development at carbon and hyperconjugative stabilization at the transition structure. This results in an asynchronous reaction pathway. In comparison with the reaction of propene oxide, the developing charge at the reaction carbon centre of **13** for both the four- and five-membered transition structures is offset by the close proximity of the nucleophile and does not require stabilization by hyperconjugation.

The intrinsic reaction coordinate (IRC) analysis of the rearrangement; 13 → TS 13-14 → 14.

The intrinsic reaction coordinate (IRC) is the minimum energy path or the path of the steepest decent from the transition state to both reactant and product directions with appropriate mass factor taken into account and provides a representative trajectory for the reaction.[17] An IRC calculation was performed at the MP2/6-31G* level for the more favored reaction pathway for **13** involving the five-membered transition structure **TS 13-14**. The energetics (without ZPE) and changes of important geometrical parameters along the IRC (stopped because of computational instability at 3.10 bohr.amu$^{1/2}$ on the reactant side and at -4.07 bohr.amu$^{1/2}$ on the product side are

shown in Figure 8. Analysis of the IRC reveals a number of interesting features of the course of the reaction.

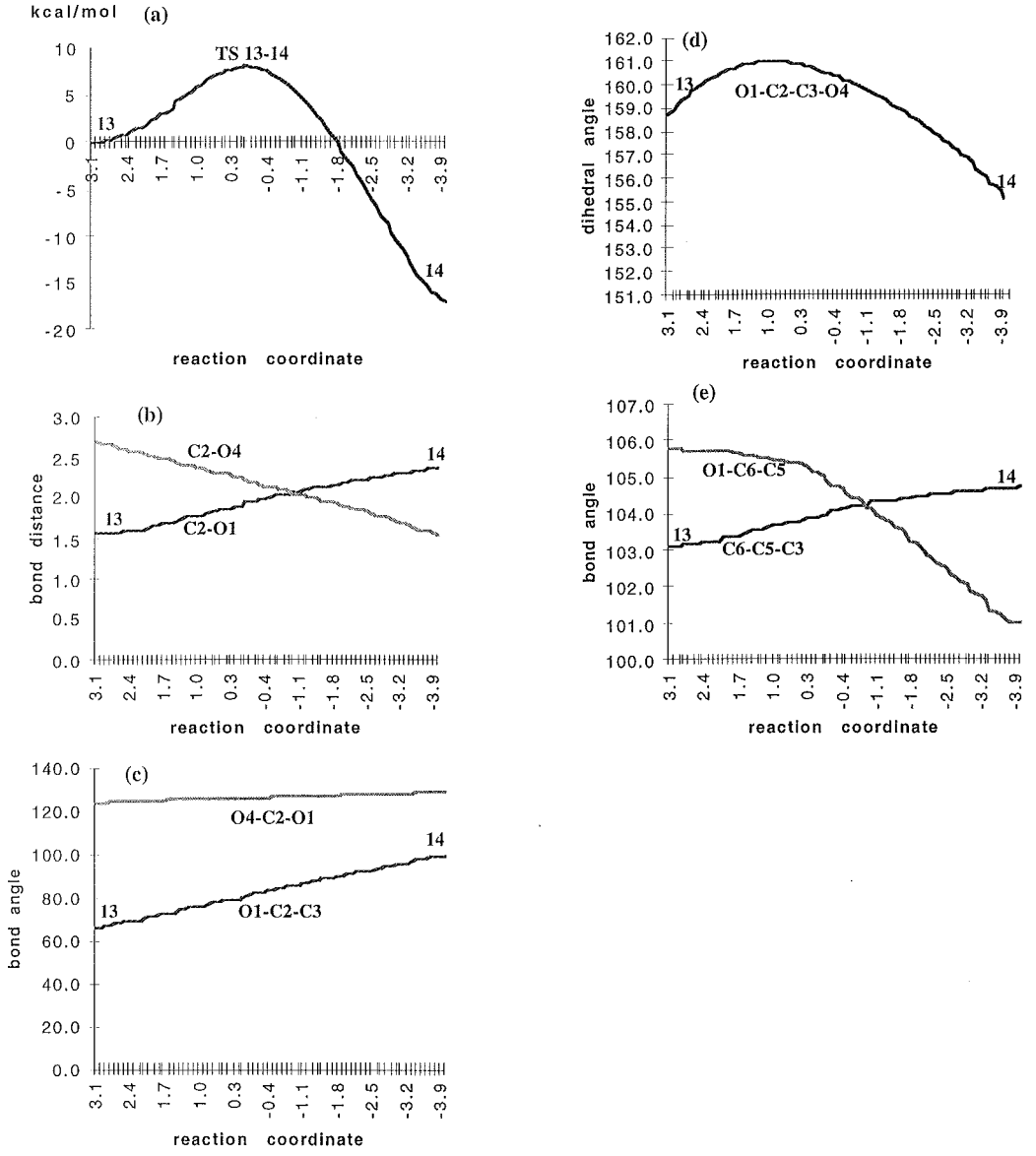

Figure 8. Intrinsic reaction coordinate (IRC) analysis for rearrangement of **13** to **14**. The abscissa in each figure is the reaction coordinate s in au.amu$^{1/2}$, with s=0 corresponding to the transition state. Distances are in Å and angles are in deg. (a) Energy. (b) C2-oxygen distances. (c) Bond angles and (d) torsional angle representing nucleophilic attack. (e) Internal bond angles.

The energy profile for the intramolecular rearrangement of **13** to **14** in Figure 8 (a) reflects a single concerted process. The increase in the C2-O4 bond distance for epoxide opening and the decrease in the O1-C2 distance for the attacking intramolecular nucleophile interaction occur at the same time and nearly linearly (Figure 8b). The O1-C2-C3 angle increases from 67^0 near structure **13** at the first point of the IRC to 81.7^0 at the transition structure and 100^0 approaching **14** at the end of the IRC (Figure 8c). The O1-C2-C3-O4 torsional angle increases from 158.8^0 and subsequently decreases at the transition structure (160.7^0) continuing to decrease to 155.2^0 near **14** (Figure 8d). The angles at the transition structure compare with the bond angle of 104.6^0 and torsional angle of 177.1^0 at the HF/6-31G* transition structure for attack of water on ethylene.[11]

The preference for the atoms most involved at the reaction centre to be in an anti periplanar conformation is compromised by the ring strain of the rupturing protonated epoxide and developing furan ring. The IRC trajectory shows that orbital overlap of the reacting centres for intramolecular attack is far from optimum. The change in the O1-C6-C5 and C6-C5-C3 bond angles are representative of internal bond angle variation as the reaction proceeds reflecting the compromise between optimizing the overlap of the reacting center and the conformational requirements associated with the development of the five-membered ring (Figure 8e). Overall, the IRC reveals clearly that the relief of the strain in the epoxide ring and the nucleophilic attack of the hydroxyl to the epoxide from the reverse face at the site of epoxide cleavage take place at the same time.

Potential energy surface for rearrangement of protonated *trans*-3,4-epoxypentan-1-ol (16).

Conformations of protonated *trans*-3,4-epoxypentan-1-ol (16), protonated *trans*-2-methylfuran-3-ol (18) and protonated 1-(oxacyclobutan-2'-yl)ethanol (21).

The lowest energy conformations of the reactant, protonated *trans*-3,4-epoxypentan-1-ol, and the two products, protonated *trans*-2-methylfuran-3-ol (**18**) and protonated 1-(oxacyclobutan-2'-yl)ethanol (**21**) are shown in figures 9 and 10. The lowest energy structure, **18**, optimised at the MP2/6-31G* level in Figure 9, shows intramolecular hydrogen bonding (2.155Å) between the ether proton and the hydroxyl oxygen.

Transition structures for rearrangement of protonated *trans*-3,4-epoxypentan-1-ol (16).

The transition structures for formation of **18** and **21** from protonated **16** are shown in Figure 9. For the inversion pathways, there is no evidence for hyperconjugation from CH's of the methyl adjacent to the reaction center for the five-membered transition structure or from analogous CH and CC bonds for the four-membered transition structure. The four-membered transition structure **TS 16-21**, analogous to **TS 13-15**, is tighter than the five-membered transition structure **TS 16-18**. For the former the bond distances from the reaction carbon centre to the two oxygens are comparable (1.961 and 1.907Å) while the corresponding values for the five-membered transition structure are larger and more asymmetric, with cleavage of the C-O bond of the epoxide more advanced than intramolecular hydroxyl attack. The **TS 16-18** is somewhat tighter than the corresponding **TS 13-14**.

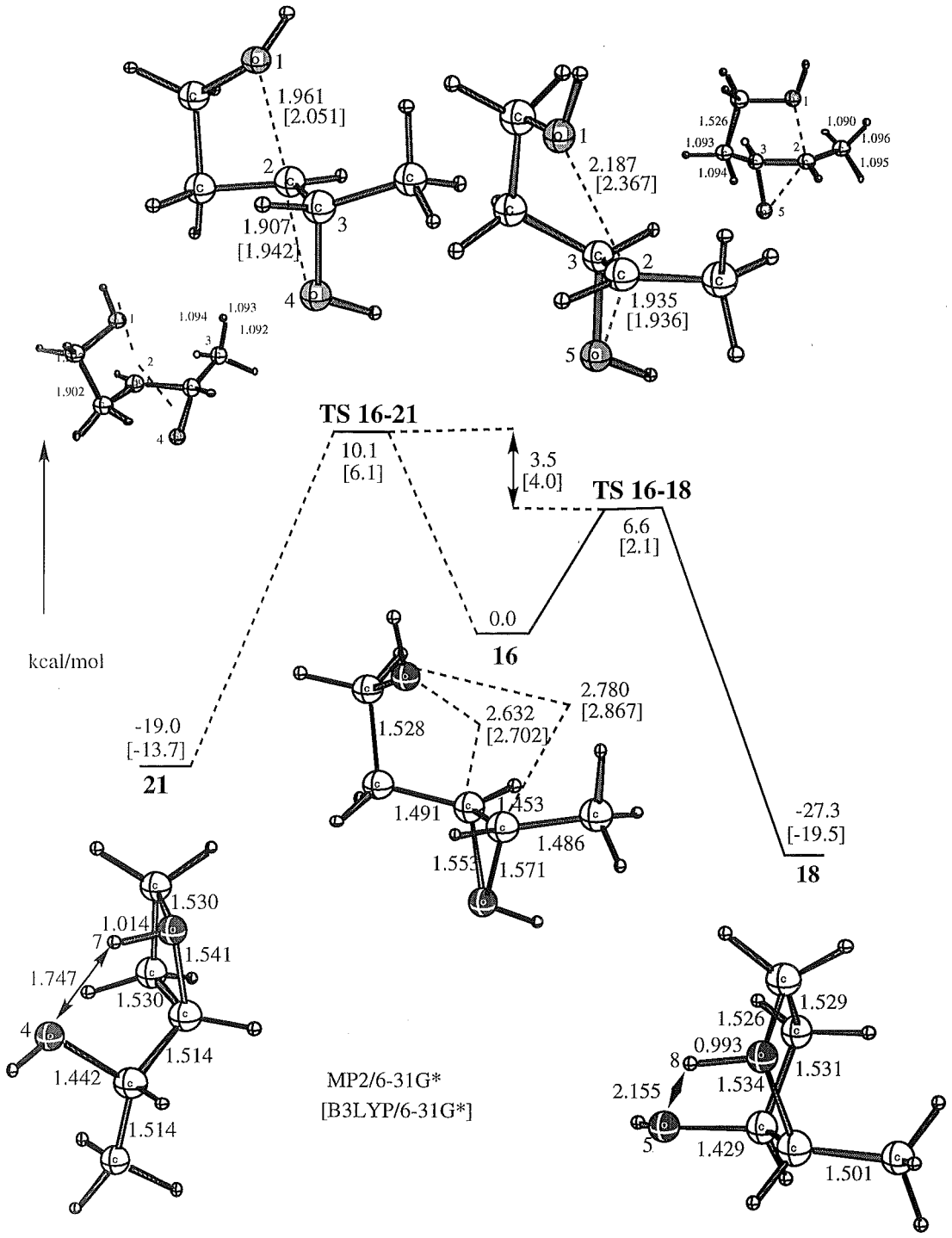

Figure 9. The potential energy profile for rearrangement of protonated *trans*-3,4-epoxypentan-1-ol (**16**) to **18** and **21**, both with inversion of configuration. Geometries (in Å and deg) at the MP2(full)/6-31G* level. Two perspectives of each transition structure are shown. The relative energies in two levels (MP2(full)/6-31G*, B3LYP/6-31G* in brackets) are in kcal/mol and include zero point corrections.

It is perhaps surprising that the difference in energy between the four- and five-membered transition structures is greater for **16** than **13**. For the latter both the four- and five-membered transition structures are congested by the methyl *cis* to the hydroxymethylene chain. For **16** the *trans* nature of the epoxide allows for some relief of this congestion, yet the difference in energy between the four- and five-membered ring transition structures becomes larger, 3.5 kcal/mol for **16** at the MP2/6-31G* level *vs* 1.0 kcal/mol for **13**.

The calculated barrier (6.6 kcal/mol at MP2/6-31G*) at **TS 16-18** is lower than that for the lowest asynchronous concerted pathway for rearrangement of protonated propene oxide to protonated propanal (17.7 kcal/mol). For the diastereomeric protonated epoxide **16**, the ability of the intramolecular hydroxyl to participate in concert with cleavage of the protonated epoxide would reduce the requirement for hyperconjugative stabilization of the developing charge at the carbon center where the reaction occurs. The experimental results for this reaction show no evidence for products that would arise from the four-membered transition structure and the yield of **11** is high (86%). The relative activation energy difference of four- to five-membered ring formation is calculated to be outside the energy window where such a process would be experimentally observed.

The minor product of the reaction of **9** with boron trifluoride was **12**, a product that cannot be formed by a route involving inversion of configuration. A search for a transition structure for retention of configuration from **16** to **14** was unsuccessful and it is not likely to exist. Only one transition structure with retention of configuration leading to **14** from the *trans* epoxide was found at the HF/6-31G*, B3LYP/6-31G*

and MP2/6-31G* levels. This transition structure **TS 22-14** results from reaction of the protonated epoxide diastereomer **22**, shown in Figure 10.

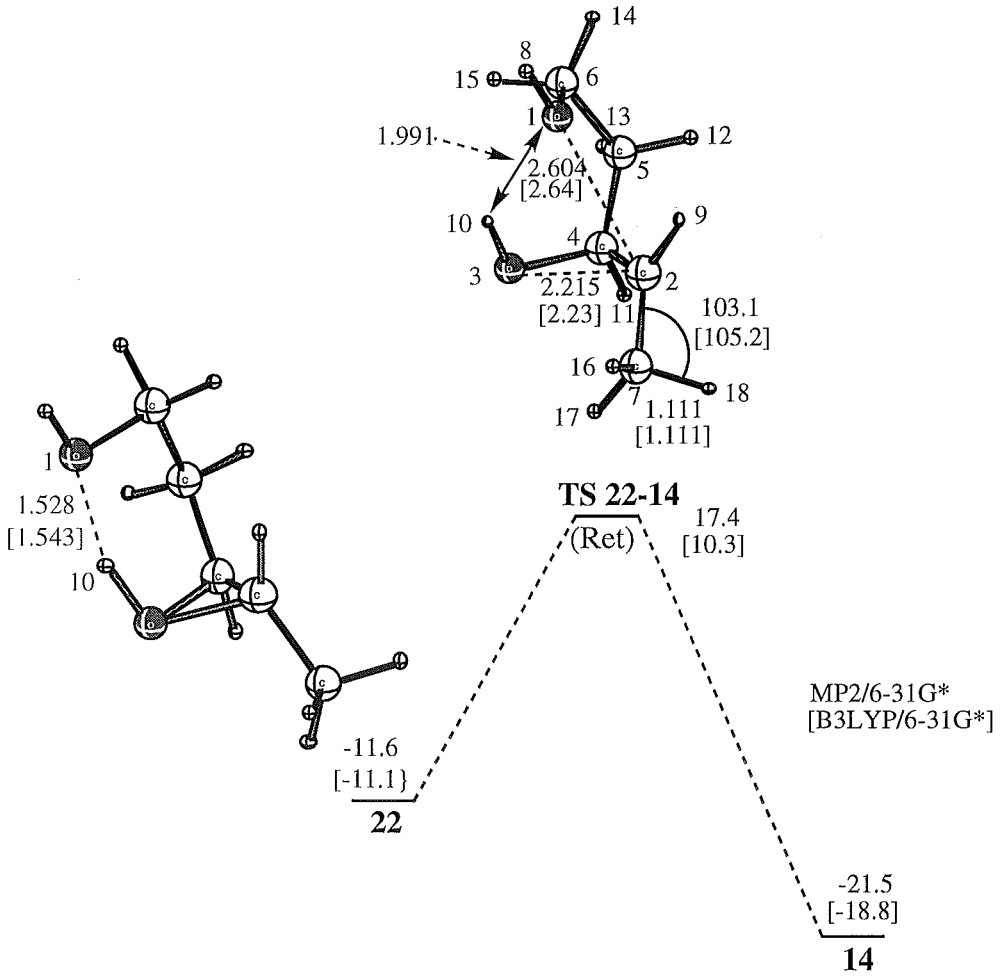

Figure 10. The potential energy profile for rearrangement of **22** to **14** with retention of configuration. Geometries (in Å and deg) at the MP2(full)/6-31G* level. The relative energies in two levels (MP2(full)/6-31G*, B3LYP/6-31G* in brackets) are in kcal/mol and include zero point corrections.

The energy of this transition structure is higher by 10.8 and 8.1 kcal/mol at the MP2/6-31G* and B3LYP/6-31G* levels respectively, than that of **TS 16-18** resulting from inversion of configuration from the protonated epoxide diastereomer **8**. This large energy difference suggests that **14** is formed not by a retention mechanism but

most likely *via* the intermediacy of fluorohydrin. For the reaction catalyzed with $BF_3 \cdot Et_2O$ **14** is the minor reaction product (8%). For the retention transition structure **TS 22-14**, hyperconjugation is observed between a methyl hydrogen and the carbocation, indicative of more pronounced development of charge at the reaction centre than for **TS 16 - 18**.

The intrinsic reaction coordinate (IRC) analysis of the rearrangement; 16 → TS 16-18 → 18.

An intrinsic reaction coordinate calculation (IRC) was performed at the MP2/6-31G* level for the more favoured reaction pathway **16 → TS 16-18 → 18** involving the five-membered transition structure. In this pathway, the intramolecular hydroxyl preferentially approaches the reaction centre from the reverse face at the site of epoxide cleavage to give the product of inversion of configuration, as seen in Figure 9. The IRC, shown in Figure 11, indicates that the transition structure **TS 16-18** is reached from the diastereomeric protonated epoxide **16** with the epoxide proton *syn* to the methyl and leads to the low energy diastereomer **18**, which exhibits intramolecular hydrogen bonding between the ether proton and the hydroxyl (2.155Å) with the proton on the ether oxygen *syn* to the hydroxyl.

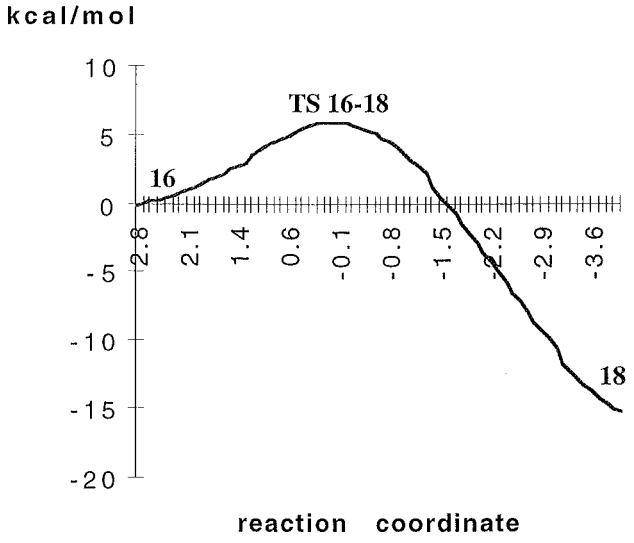

Figure 11. Intrinsic reaction coordinate (IRC) analysis for rearrangement of **16** to **18**. The abscissa is the reaction coordinate s in au.amu$^{1/2}$, with s=0 corresponding to the transition state.

The overall reaction profile in Figure 11, like that for **13** in Figure 8(a), is consistent with intramolecular nucleophilic attack occurring from the reverse face at the site of epoxide cleavage in concert with epoxide cleavage resulting in the product of inversion of configuration. The exothermic nature of the process reflects the driving force of the reaction, namely the relief of epoxide ring strain.

Conclusion.

The intramolecular inversion transition structures for the reaction of **13** and **16** at the B3LYP/6-31G* and MP2/6-31G* levels of theory reveal a preference for five-membered ring formation. Intrinsic reaction coordinate calculations for the formation of **14** from **13** and **18** from **16** show that intramolecular attack with inversion occurs in concert with ring opening. The retention transition structures **TS 17-18** and **TS 22-14** are calculated to be too high in energy to afford credible pathways in the formation

of **18** and **14** respectively and point to alternative pathways such as the intermediacy of fluorohydrin. The intrinsic reaction coordinates for inversion reaction of the nucleophile for the formation of **14** from **13** and **18** from **16** are far from optimum overlap and reflect the strained bicyclic nature of the transition structures.

References.

1 Baldwin, J. E. *J. Chem. Soc., Chem. Commun, **1976,** 734 see also Principles of Organic Synthesis'* by Sir Richard Norman and J.M. Coxon. Blackie Chapman and Hall, London and John Wiley and Sons, New York. **1993**, page 678.

2 Coxon, J.M.; Hartshorn, M.P.; Swallow, W.H. *Aust. J. Chem.* **1973**, *26*, 2521

3 Janda, K.D.; Shevlin, C.G.; Lerner, R.A. *Science* **1993**, *259*, 490.

4 Na, J. Houk, K.N. Shevlin, C.G.; Janda, K.D. Lerner, R.A. *J. Amer. Chem. Soc.* 1993, **115**, 8453.

5 Na, J.; Houk, K.N. *J. Amer. Chem. Soc.* 1996, **118**, 9204.

6 Methods defined herein: Coxon, J.M.; Houk, K.N.; Luibrand, R.T. *J. Org. Chem.* **1995**, *60*, 418-427.

7 AM1: Dewar, M. J. S.; Zoebisch, E. G.; Healy, E. F.; Stewart, J. J. P. *J. Am. Chem. Soc.* **1985**, *107*, 3902.

8 (a) Becke, A. D. *Phys. Rev. A* **1988**, *38*, 3098. (b) Becke, A. D. *J. Chem. Phys.* **1993**, *98,* 1372. (c) Lee, C.; Yang, W.; Parr, R. G. *Phys. Rev. B* **1988**, *37*, 785.

9 c.f. Schreiner, P. R. ; Schleyer, P. von R.; Schaefer, H.F. *J. Org. Chem.* **1997**, *62*, 4216.

10 Gaussian 94, Revision B.1. Frisch, M.J.; Trucks, G. W.; Schlegel, H. B.; Gill, P.

M. W.; Johnson, B. G.; Robb, M. A.; Cheeseman, J. R.; Keith, T.; Petersson, G. A.; Montgomery, J. A.; Raghavachari, K.; Al-Laham, M. A.; Zakrzewski, V. G.; Ortiz, J. V.; Foresman, J. B.; Cioslowski, J.; Stefanov, B. B.; Nanayakkara, A.; Challacombe, M.; Peng, C. Y.; Ayala, P. Y.; Chen, W.; Wong, M. W.; Andres, J. L.; Replogle, E. S.; . Gomperts, R.; Martin, R. L.; Fox, D. J.; Binkley, J. S.; Defrees, D. J.; Baker, J.; Stewart, J.; P.; Head-Gordon, M.; Gonzalez, C.; and Pople, J. A. Gaussian, Inc., Pittsburgh PA, 1995.

[11] Ford, G.P.; Smith, C.T. *J. Am. Chem. Soc.* **1987**, *109*, 1325.

[12] Coxon, J. M.; Maclagan, R. G. A. R.; Rauk, A.; Thorpe, A. J.; Whalen, D. *J. Am. Chem. Soc.* **1997,** *119,* 4712-4718.

[13] The direct rearrangement between the diastereomers **13** and **17** is unlikely, as suggested by a high transition state energy (ca 17 kcal/mol at MP2/6-31G*) between the invertomers of protonated propene oxide.[12] Therefore, these two protonated diastereomers are likely to be in equilibrium *via* reversible protonation/deprotonation, and **17** is the most abundant protonated form of the *cis*-epoxide.

[14] The lowest energy conformer **14** with the ether proton *syn* to the hydroxyl was 5.4 kcal/mol lower in energy than the lowest energy structure protonated *anti* to the hydroxyl and has a hydrogen bond between O4 and H8 (2.232Å at MP2/6-31G*). The O1-H8 bond (0.992Å) is somewhat longer than it would be in the absence of this H-bonding.

[15] **TS 13-14** was calculated to be lower in energy by 1.0 kcal/mol (HF/6-31G* + ZPC) than when the proton was positioned *syn* to the epoxide substituent groups therefore the IRC was conducted from the anti protonated structure (**TS 13-14**)

even though **17** (Figure 6) is lower than **13**.

[16] Another transition structure involving retention of configuration for the conversion of **13** to **18** was found at the HF/3-21G* level with a high barrier of 14.3 kcal/mol (HF/3-21G* + ZPC). However, this structure does not exist at higher levels of theory.

[17] Fukui, K; Kato, S.; Fujimoto, H. *J. Am. Chem. Soc.* **1975**, *97*, 1. Ishida, K.; Morokuma, K.; Komornicki, A. *J. Chem. Phys.* 1977, *66*, 2153.

Chapter 5.

Theozymes for intramolecular ring cyclisation reactions.

Summary.

A complex of the 5-membered transition structure **9** with the Houk theozyme 3.5 kcal/mol lower in energy than the complex previously reported as a model for the antibody IgG26D9 catalysed intramolecular cyclisation of *trans*-4,5-epoxyhexan-1-ol reverses the preference of that theozyme to favour furan formation. This negates the theozyme as a model for the antibody reaction. A new theozyme is reported which favours pyran formation over furan formation consistent with the antibody result.

Introduction.

Lerner and Janda[1] demonstrated that the catalytic antibody IgG26D9, elicited from a tertiary amine oxide antigen (hapten) **1**, catalyses the intramolecular rearrangement of

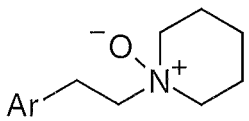

1

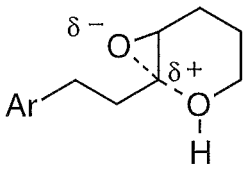

2

one of the enantiomers **3** stereospecifically to the tetrahydropyran **5**. This product is the result of intramolecular nucleophilic cyclisation with inversion of configuration and is formed in preference to tetrahydrofuran **4** (Figure 1) the chemically favoured reaction.[2] The tetrahydropyran **5** is considered to arise because the transition structure to its formation has similarities (c.f. **2**) to the hapten **1**.

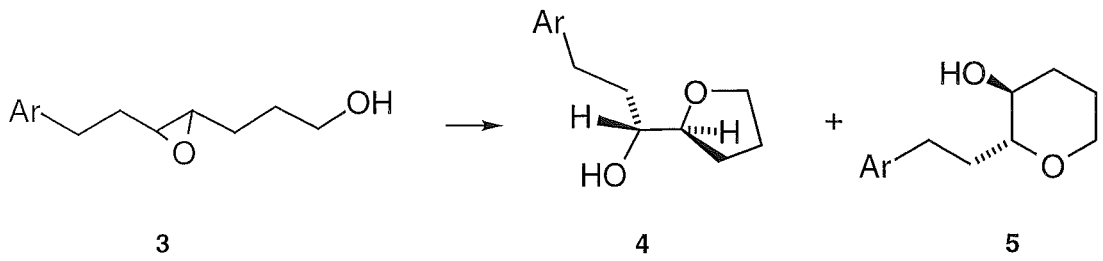

3 4 5

Figure 1. Intramolecular rearrangement of *trans*-7-aryl-4,5-epoxyheptan-1-ol **3** to 6-*endo-tet* product **5** and tetrahydropyran **4**.

The Lewis acid catalysed rearrangement of the analogue of **3**, namely **6**, to result in formation of the tetrahydrofuran ring **7**, a 5-*exo-tet* process, in preference to the 6-*endo-tet* tetrahydropyran product **8**[3] (figure 2) has previously been reported[4]. *Ab initio* calculations[5] at the HF/6-31G* level of the transition structures **9** and **10** from protonated **6** to the tetrahydrofuran **7** and tetrahydropyran **8** (figure 2) are consistent with these experimental results since the transition structure to the former product **7** is 1.9 kcal/mol lower.[6,7,8] Partition of the reaction of **3** by antibody IgG26D9 to pyran product **5**, (>99%) is considered a result of antibody transition structure stabilisation estimated to be ca 3.6 kcal/mol.[9]

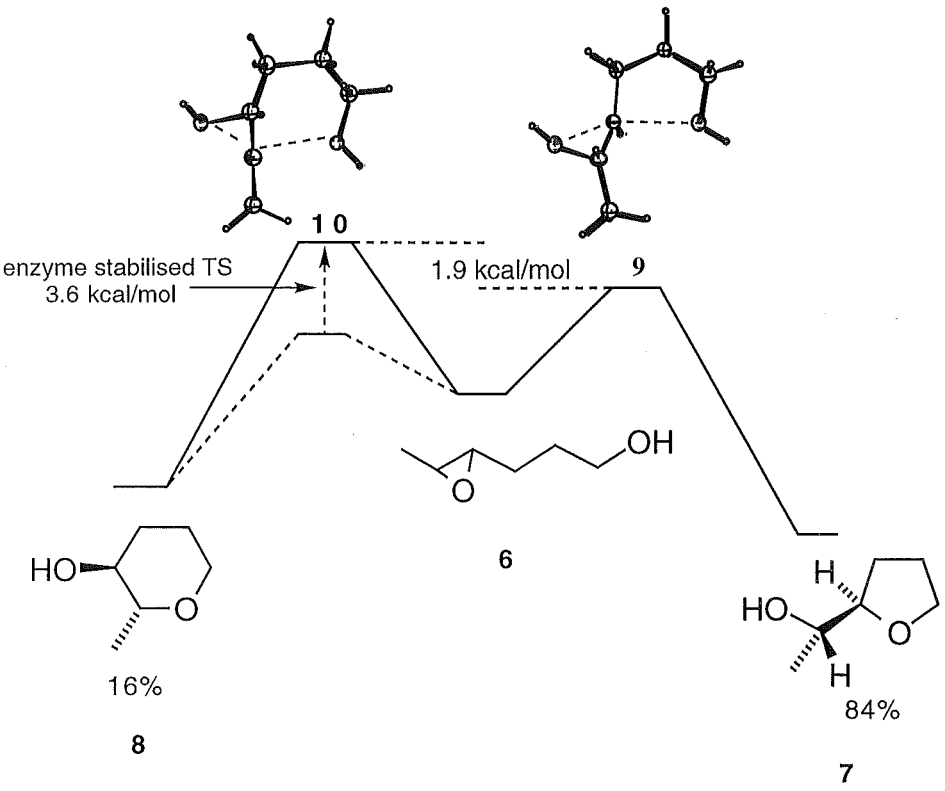

Figure 2. Reaction coordinate diagram of the acid catalysed rearrangement of *trans*-4,5-epoxyhexan-1-ol.

Houk[5] developed a theoretical model for antibody transition state catalysis based on optimising electrostatic stabilisation of the N-oxide hapten dipole with an acid and a base, produced by positioning a molecule of methanol (or formic acid) to stabilise the electronegative oxygen of the hapten and a formate ion near the electropositive nitrogen. Constraints were placed on the positions of the acid and base stabilising groups relative to each other. Removing the hapten creates a theoretical catalytic cavity of the enzyme. It is this model for which the term "*theozyme*" is coined.[5]

The 5- and 6-membered transitions structures **9** and **10** for formation of furan and pyran, with the epoxide proton removed, were positioned by trial and error within this fixed theozyme cavity. The internal coordinates of the transition structures with the epoxide proton deleted were fixed, with the exception the hydroxyl OH bond length which was

allowed to vary. The complex was optimised specifically allowing the epoxide oxygen...H...OMe hydrogen bond lengths to optimise along with the orientation of the transition structure with respect to the formate anion.[10] The calculations were reported[5] to show the *methanol/formate model* to stabilise the six-membered transition structure **10** over the five-membered transition structure **9** by 1.2 kcal/mol at the HF/6-31G* level. Houk argued the 6-membered transition structure was more stabilised relative to the 5-membered transition structure since in the former the developing carbocation centre was closer to the formate anion. If these complexes are global minima then the relative energy of the complexes gives support for the hypothesis that electrostatic stabilisation from the antibody IgG26D9 occurs to a greater extent when bound to the six-membered transition structure **10** than for the five-membered transition structure **9**.

Computational methods.

Initial conformations of the methanol/formate stabilised N-oxide hapten were determined through extended grid calculations at the AM1 level. *Ab initio* calculations at the HF/6-31G* level using the *Gaussian94* program[11] were performed on the lowest energy hapten stabilised conformations. Five- and six-membered transition structures optimised at the HF/6-31G* level[6] were used in conjunction with the various methanol/formate models.[6] The transition structures, with the epoxide proton removed, and with constraints applied to all internal bond lengths, angles and torsions (except the alkyl oxygen-proton bond length) were optimised with respect to methanol and formate ion, whose positions relative to each other were also constrained. The energies of the optimised theozyme complexes are presented in Table 1 (Appendix D).

Results and discussion.

The validity of the specific methanol-formate theozyme model reported earlier (by Houk) is in question. A complex of the five membered transition structure with his theozyme is reported which is 3.5 kcal/mol lower in energy than his analogous complex thereby reversing the preference and favouring furan formation.[12] Secondly, an alternative theozyme is reported for which the 6-membered transition structure is more stabilised than the 5-membered transition structure. In attempting to reproduce the Houk theozyme, and in the absence of published coordinates, a structure of the hapten stabilised by methanol and formate anion **12** was produced which has coincidently the same energy as the Houk theozyme/hapten complex **11** but with a different orientation of methanol relative to the formate ion (see Figure 3).

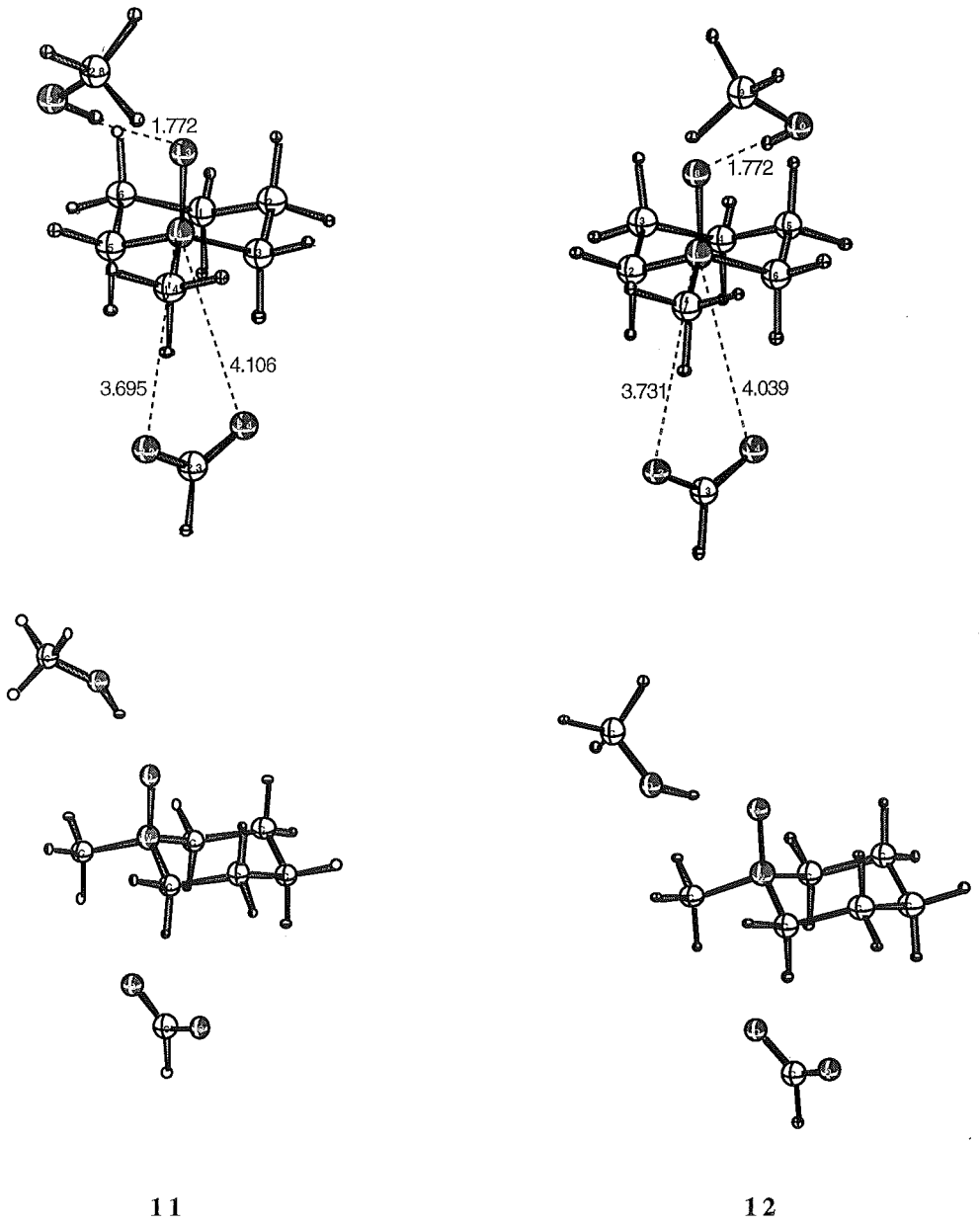

Figure 3. Hapten model bound to the theozymes as generated by Houk[6] and the present work. Two views of each complex are given.

Knowing that theozyme **12** was different from Houk's theozyme **11**, the positioning of the 5- and 6- membered transition structures within the cavities of both theozymes was examined. In attempting to reproduce his complexes, a complex was

located for the 5-membered transition structure **15**, 3.5 kcal/mol lower in energy than his reported analogous 5-membered transition structure complex **14** (Figure 4) and thereby 2.3 kcal/mol lower than his 6-membered transition state complex **13**.[13] This result negates his methanol/formate theozyme as a model supporting the catalytic antibody experiment.[14] Closer inspection of the 5-membered transition structure complex with the Houk theozyme **14** shows the methanol methyl and transition structure alkyl chain to be sterically crowded. This crowding in not present in the lower energy 5-membered transition structure complex **15**.

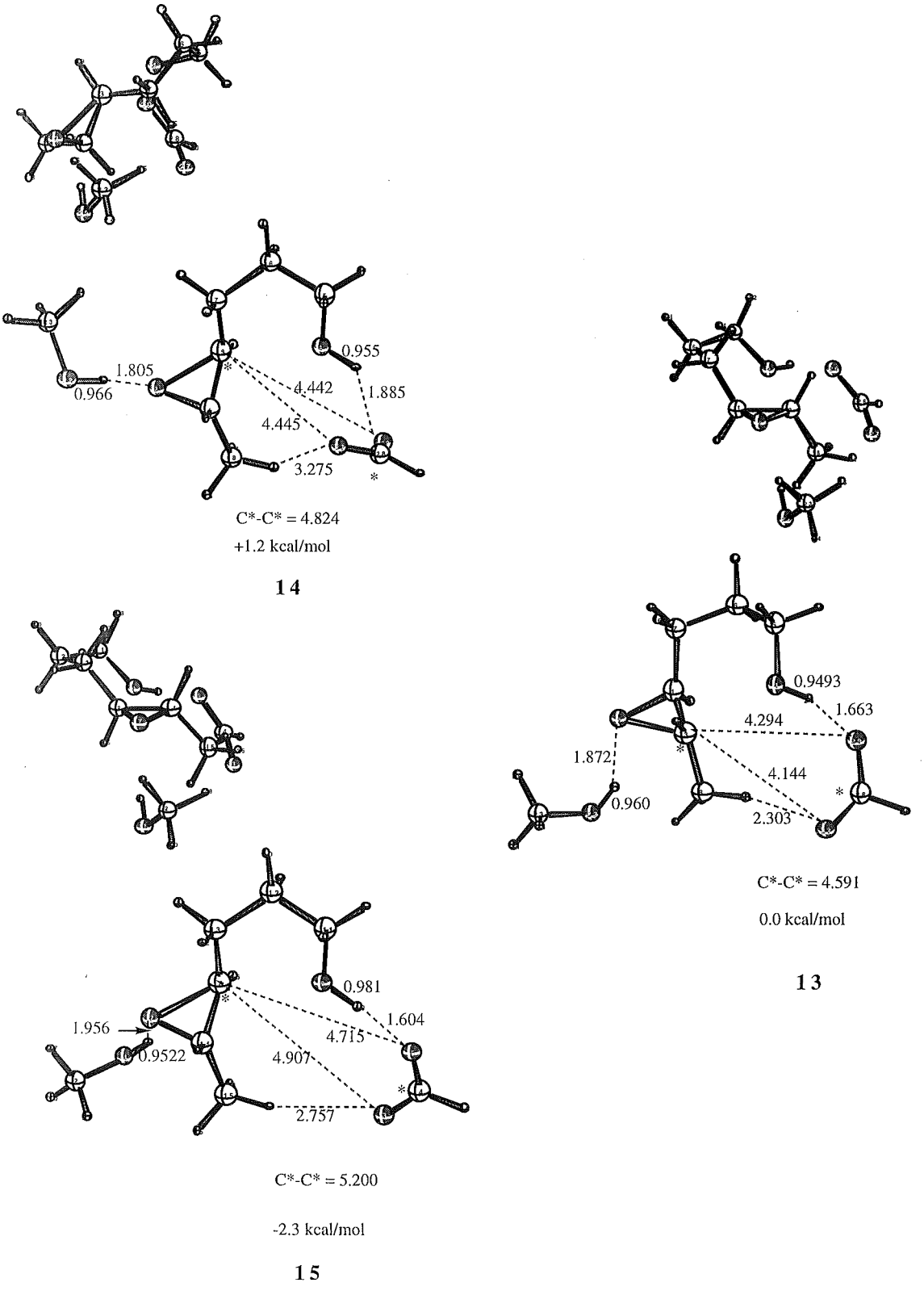

Figure 4. Complexes of 5- and 6-membered transitions states with the Houk theozyme. Two orientations of each complex are given.

The stabilisation of the new lower energy 5-membered transition structure complex **15** relative to the 6-membered transition structure complex **13** is not due to a more favourable electrostatic stabilisation of the carbocation with the formate ion (see figure 4) since the carbocation centre is positioned further from the formate ion in the former complex. The methanol hydrogen bond length to the epoxide oxygen is longer in **15** than in **13** however the hydrogen bond between the formate anion and the alkyl hydroxy proton of the transition structure in the former is shorter (1.604Å) than in **13** (1.663Å).

Lowest energy complexes of the 5- and 6-membered transition structures positioned within the theozyme cavity of **12** were determined. The lowest energy 6-membered transition structure complex **17** was found to be 1.4 kcal/mol lower in energy than the lowest energy 5-membered transition structure complex **16** (Figure 5). Both complexes **16** and **17** are lower in energy than the corresponding complexes **13** and **14**. In each of **16** and **17**, the transition structures are inserted between the methanol/formate complex in a similar relative position (see Figure 5) in contrast to **13** and **14** where this is not the case. The greater stabilisation of **17** over **16** is manifested by the closer proximity of the carbocation of the 6-membered transition structure to the formate anion and by a shorter bond length between the formate anion and the alkyl hydroxy proton (1.624Å for **17** and 1.682Å for **16**).

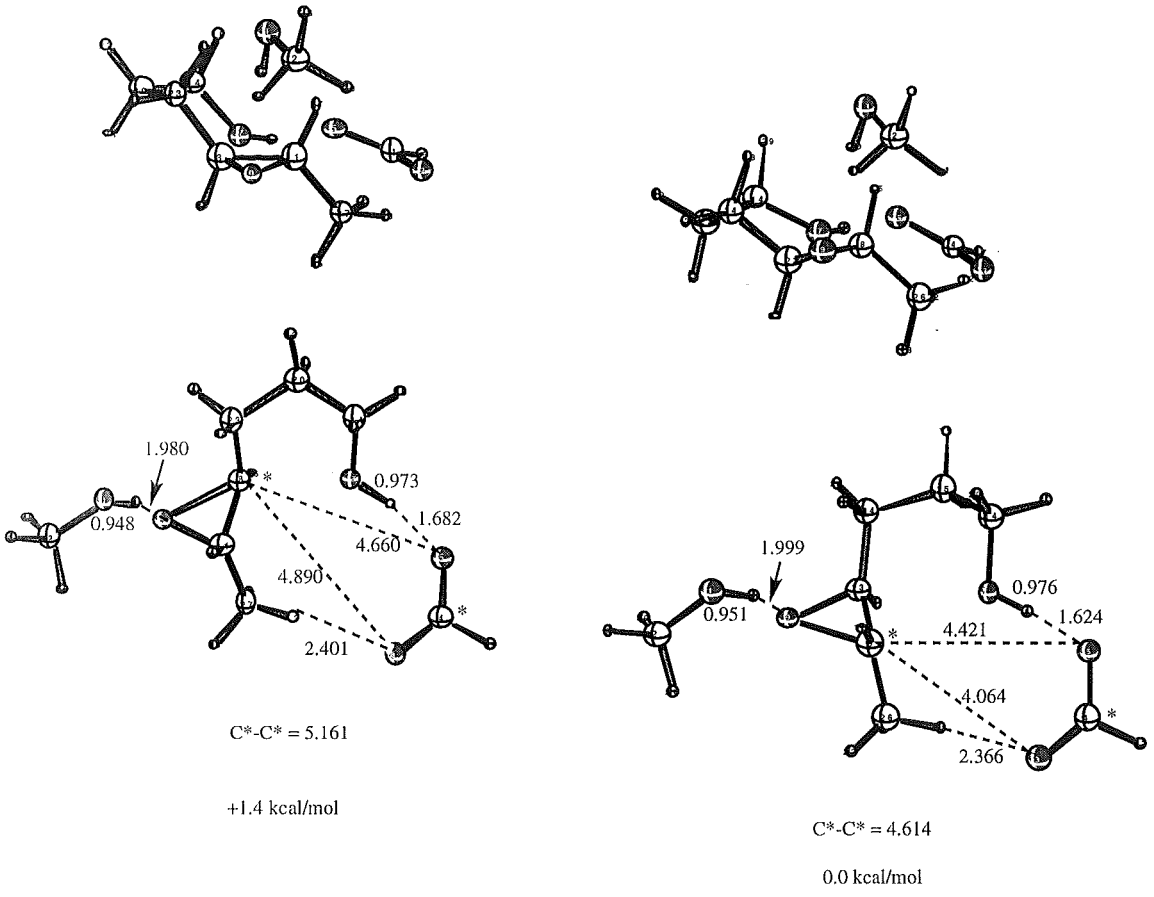

16 **17**

Figure 5. Complexes of 5- and 6-membered transitions structures stabilised within the theozyme cavity of **12**. Two orientations of each complex are given.

This result supports the experimental antibody results of Lerner and Janda but suggests the need for caution in predicting the structure of theozymes since conformational space needs to be fully explored. The possibility of transition structure stabilisation by more than two substituents of a theozyme cannot be ruled out in order to define an appropriate transition structure complex.

References.

[1] Janda, K. D.; Shelvin, C. G.; Lerner, R. A. *Science* **1993**, *259*, 490-493. Janda, K. D.; Shelvin, C. G.; Lerner, R. A. *J. Am. Chem. Soc.* **1995**, *117*, 2659-2660.

[2] No tetrahydrofuran could be detected in the product.

[3] This preference was subsequently encapsulated in the rules for ring closure enunciated by Baldwin, J. E. *J. Chem. Soc., Chem. Commun.* **1976**, 734. *see also Principles of Organic Synthesis*' by Sir Richard Norman and J.M. Coxon. Blackie Chapman and Hall, London and John Wiley and Sons, New York. **1993**, page 678. Baldwin, J. E.; Lusch, M. J. *Tetrahedron* **1982**, *19*, 2939.

[4] Coxon, J. M.; Hartshorn, M. P.; Swallow, W. H. *Aust. J. Chem.* **1973**, *26*, 2521-2526.

[5] Na, J.; Houk, K. N.; Shelvin, C. G.; Janda, K. D.; Lerner, R. A. *J. Am. Chem. Soc.* **1993**, *115*, 8453-8454. see also C and E News, 1996, Sept 30th, 35 "Using the theozyme technique, Houk has explained and experimentally verified why the reactions of a hydroxy epoxide catalysed by an antibody yields a tetrahydropyran rather than the tetrahydrofuran largely produced with acid or base catalysis."

[6] Thank you to Professor Ken Houk an Dr Jim Na for supplying their coordinates.

[7] Coxon, J. M.; Maclagan, R. G. A. R.; Rauk, A.; Thorpe, A. J.; Whalen, D. *J. Am. Chem. Soc.* **1997**, *119*, 4712-4718.

[8] The preferential formation of furan **7** via **9** reflects a more favourable co-linear trajectory of the approaching alkyl hydroxyl and the lesser strain necessary to form the five-membered ring.

[9] Na, J.; Houk, K. N. *J. Am. Soc.* **1996**, *118*, 9204-9205. "Formation of the 5-*exo*-product is predicted to be favored by about 1.8 kcal/mol in aqueous solution. This should produce a 96:4 5-*exo*:6-*endo* ratio. To favor the 6-*endo* product by a similar amount, the

catalytic antibody must lower the 6-*endo* activation energy 3.6 kcal/mol more than it lowers the 5-exo activation energy."

[10] It was envisaged that hydrogen bonding between the methanol proton and the epoxide oxygen, and between the hydroxyl proton of the deprotonated transition structures **9** and **10** and the formate anion are the important features of the catalytic stabilisation. In addition the carbocation would be stabilised by the formate anion.

[11] Gaussian 94, Revision D.2. Frisch, M. J.; Trucks, G. W.; Schlegel, H. B.; Gill, P. M. W.; Johnson, B. G.; Robb, M. A.; Cheeseman, J. R.; Keith, T.; Petersson, G. A.; Montgomery, J. A.; Raghavachari, K.; Al-Laham, M. A.; Zakrzewski, V. G.; Ortiz, J. V.; Foresman, J. B.; Cioslowski, J.; Stefanov, B. B.; Nanayakkara, A.; Challacombe, M.; Peng, C. Y.; Ayala, P. Y.; Chen, W.; Wong, M. W.; Andres, J. L.; Replogle, E. S.; Gomperts, R.; Martin, R. L.; Fox, D. J.; Binkley, J. S.; Defrees, D. J.; Baker, J.; Stewart, J. P.; Head-Gordon, M.; Gonzalez, C.; Pople, J. A. Gaussian, Inc., Pittsburgh PA, **1995**.

[12] Houk noted that "calculations on both five-membered complexes for more than 200 optcycles produce the complexes shown. After the first 100 steps, the optimisations showed an oscillating pattern between optcycles, but no real change in energy occurs. Both six-membered complexes are energy-minimised structures."[11]

[13] The important contribution by Houk in support of electrostatic catalytic stabilisation from a theozyme is acknowledged, however an alternate positioning of the methanol/formate ion is required to support the experimental result.[1]

[14] The reported model[5] is not a global minimum complex.

Chapter 6.

An *ab initio* study of intramolecular ring cyclisation of protonated and BF_3 coordinated *trans*- and *cis*-4,5-epoxyhexan-1-ol.

Summary.

The potential energy surface for the rearrangement of *cis*- and *trans*-4,5-epoxyhexan-1-ol with acid and the Lewis acid, BF_3, to 5- and 6-membered cyclic ethers has been investigated by *ab initio* methods. The transition structures involving both inversion and retention of configuration at the reaction centre at the HF/6-31G* and B3LYP/6-31G* levels are characterised. The preference for furan formation over pyran is attributed to the more favourable O-C_{ep}-O bond angles at the transition structures for furan formation. The torsional O-C_{ep}-C_{ep}-O angles associated with tetrahydrofuran and tetrahydropyran formation vary with structure and do not directly correlate with the preferred pathway.

Introduction.

Ring opening of epoxides with a proton or Lewis acid is an important method in chemical synthesis of initiating intramolecular ring closure. Catalytic antibodies (eg. 26D9) elicited to an antigen, N-[2-arylethyl]piperidine-N-oxide, have been developed by Janda and Lerner[1] to effect rearrangement of *trans*-8-aryl-4,5-epoxyheptan-1-ols enantioselectively to 6-*endo*-*tet*-tetrahydropyrans[2,3,4] rather than to the chemically favoured tetrahydrofurans (Figure 1). The catalytic antibodies effect chiral selection and overcome the stereoelectronic preference for 5- over 6-membered ring formation.

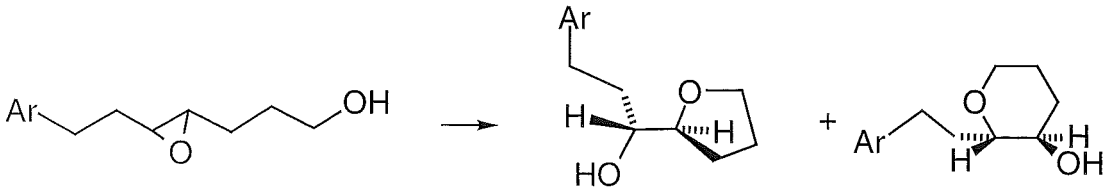

Figure 1. Intramolecular rearrangement of *trans*-7-aryl-4,5-epoxyheptan-1-ol to 5-*exo-tet* and 6-*endo-tet* products.

The reaction in the presence of the catalytic antibody is considered to arise because the transition structure to the tetrahydropyran has similarities to the hapten. The catalytic effect reflects an interplay between electronic stabilisation (the hapten carrying a positive nitrogen) and general acid base catalysis. Houk has carried out single point MP2/6-31G* calculations on the HF/6-31G* optimised geometries for the transition structure of a model system, *trans*-4,5-epoxyhexan-1-ol, lacking the aryl group and estimated[5] that the catalytic antibody must lower the 6-*endo* activation energy 3.6 kcal/mol more than it lowers the 5-*exo* activation barrier. Calculations have been used to show the effect of a proximate acid source and counterion in influencing transition state structure thereby mimicking the regiochemistry dictated by the catalytic antibody.[6] However, a complex[7] of the 5-membered transition structure with the Houk theozyme 3.5 kcal/mol lower in energy than the complex previously reported[6] as a model for the antibody reverses the preference of that theozyme to favor furan formation. This negates the theozyme as a model for the antibody reaction.[7] An alternative theozyme has been determined which favours pyran formation over furan formation consistent with the antibody result.[7]

The rearrangement of *trans*-4,5-epoxyhexan-1-ol (**1**) with BF_3-Et_2O has previously been reported to give *trans*-(1RS,2'RS)-1-(tetrahydrofuran-2'-yl)ethanol (**2**) (84%) and tetrahydropyran **3** (16%) (Figure 2). Under the same conditions *cis*-4,5-epoxyhexan-1-ol (**4**) rearranges to give *cis*-(1SR,2'RS)-1-(tetrahydrofuran-2'-yl)ethanol (**5**) (97%).[8] The stereochemistry of the products is the result of

intramolecular nucleophilic attack of the hydroxy oxygen at either C4 or C5 with inversion of configuration.

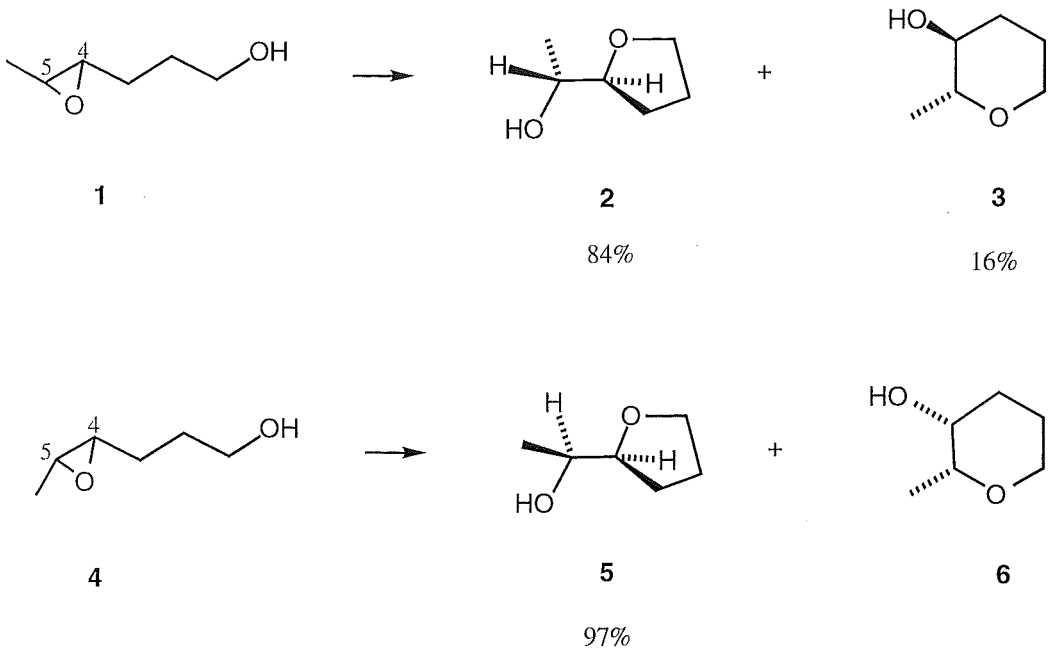

Figure 2. BF_3-catalysed rearrangement of *cis* and *trans*-4,5-epoxyhexan-1-ol.

The preferential formation of the furan products **2** and **5** from **1** and **4** (*5-exo-tet* process) over the pyran products **3** and **6** (*6-endo-tet* process) is thought[8] to reflect a more favourable trajectory of the S_N2 attack of the hydroxy oxygen to C4 and concomitant reduction in transition structure ring strain. The present study seeks to define these parameters along with the bond and torsional angles associated with the transition structures. Baldwin[9] defined rules for ring closure, based on the perceived stereochemical requirements of the transition states leading to ring formation. What is of particular interest in the present study is that the departing nucleophile as well as the incoming nucleophile are both connected to the system and the transition structures are bicyclic (Figure 3).

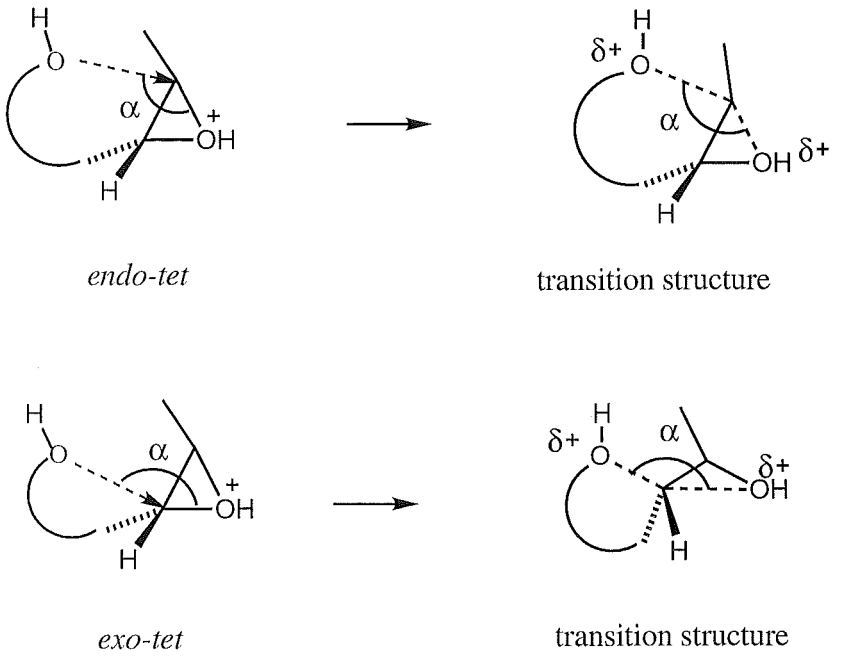

Figure 3. Schematic representation of acid initiated epoxide ring opening in conjunction with intramolecular nucleophilic attack *via exo-tet* and *endo-tet* processes.

The optimum value of the O-C_{ep}-O angle (α) (154.9^0) and O-C_{ep}-C_{ep}-O torsional angle (177.1^0) for nucleophilic attack at protonated epoxide (Figure 3) follow from a computational study[10] of the reaction of water with protonated ethylene oxide. These values reflect frontier orbital overlap of the HOMO of the nucleophile and the LUMO of protonated ethylene oxide.[11] *Ab initio* calculations have previously been reported on the acid catalysed rearrangement of *cis*- and *trans*-3,4-epoxypentan-1-ol.[12] The calculations were in agreement with the experimental results showing furan formation to be favoured in preference to oxetane *via* 5- and 4-membered transition structures respectively. The lower energy 5-membered transition structures were found to be earlier and substantially looser than the 4-membered transition structures. The O-C_{ep}-C_{ep}-O torsional angles in the 5-membered transition structures, which are in the range 155^0-161^0, show that optimum antiperiplanar orbital overlap at the reaction centre was not achieved. The transition structures reflect a compromise between conformational ring strain and attaining an optimum trajectory angle and antiperiplanar O-C_{ep}-C_{ep}-O transition geometry. The activation barriers from the lowest energy conformation of the protonated epoxides to the *trans*- and *cis*-5-membered transition structures were low

(1.6 - 2.9 kcal/mol, HF/6-31G*) consistent with only a minor change in geometry between the reactant epoxide and the transition structures for the ring opening process.

Computational methods.

Exploratory calculations on the potential energy surface were carried out with the semi-empirical AM1[13] model. The low energy conformations of the protonated furan and pyran products were initially determined by conformational searches at the AM1 level using the Osawa method encapsulated in Spartan.[14] All stationary points presented were obtained at the *ab initio* HF/6-31G* level using the GAUSSIAN 94[15] suite of programs. A selection of 6-membered transition structures were optimised at the gradient-corrected hybrid density functional B3LYP/6-31G*[16] level of theory, however difficulties were encountered locating optimised geometries for the 5-membered transition structures by this method. The nature of all stationary points were confirmed through vibrational frequency analysis with transition structures characterised by the presence of one and only one imaginary frequency. Zero-point corrections (ZPC) are included in the relative energies reported with the HF/6-31G* zero point vibrational energies scaled by 0.893. The absolute and relative energies of the optimised minima and transition structures are shown in Tables 1 and 2 (Appendix E1 and E2).

Results and discussion

Ab initio molecular orbital calculations are presented on the transition structures for inversion of configuration and related stationary points on the potential energy surface for the proton and BF_3 assisted ring opening of *cis*- and *trans*-4,5-epoxyhexan-1-ol. For comparison transition structures involving retention of configuration for protonated *cis*- and *trans*- 4,5-epoxyhexan-1-ol are presented.

Houk has reported calculations at the HF/6-31G* level on the rearrangement of *trans*-4,5-epoxyhexan-1-ol with acid.[17] The epoxide was protonated on the face *cis* to the hydroxyalkyl chain. The term "invertomer" has been coined[18] to describe the

diastereomers resulting from positioning of the proton on either face of an epoxide. The protonated epoxide in an extended conformation **7** (Figure 4)[19] was reported by Houk to be 10.4 and 11.3 kcal/mol lower in energy than the 5- and 6-membered transition structures **8** and **9** leading to the formation of furan and pyran respectively. Protonated epoxide **7** is however the invertomer of the transition structures **8** and **9** and not directly on the pathway to **8** and **9**.

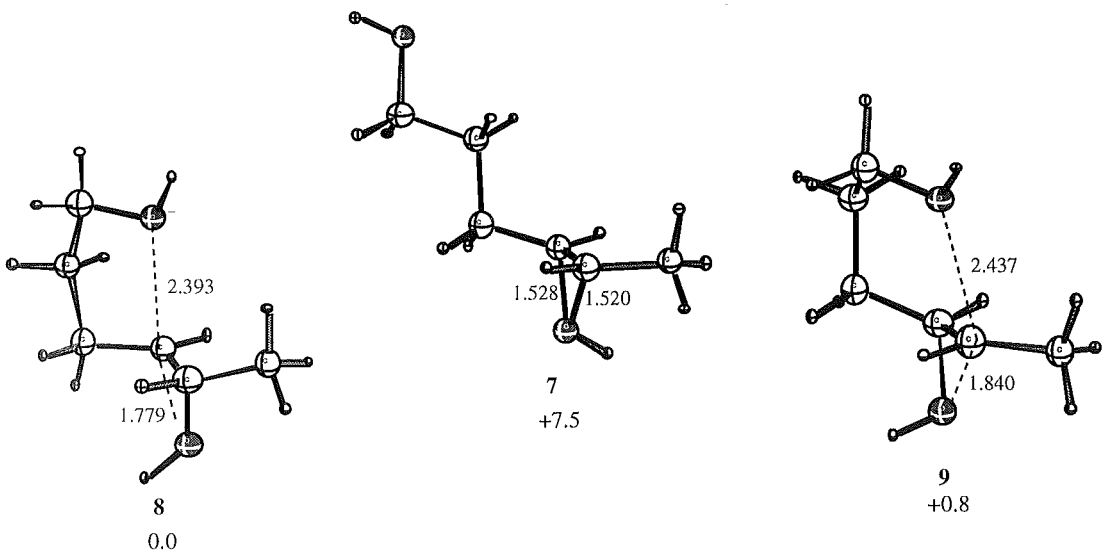

Figure 4. Transition structures **8** and **9** for ring opening of epoxide **7** as determined by Houk. The stationary points are optimised at the HF/6-31G* level and the relative energies (kcal/mol) include zero point corrections. Bond distances are in (Å).

It is somewhat surprising that the extended conformation of the protonated epoxide **7** is a global minimum, since, for the protonated 3,4-epoxypentan-1-ols, the extended conformations were not the global minimum.[12] As well as seeking the global minima of protonated *trans*-4,5-epoxyhexan-1-ol, the extended conformation of the protonated epoxide **7** was reoptimised at the HF/6-31G* level. While the geometry did not change, the energy was not as reported 10.4 and 11.3 kcal/mol lower in energy than transition structures **8** and **9** respectively, but 7.5 and 6.7 kcal/mol higher (see Figure 4). The extended conformation of epoxide **7** (though the wrong invertomer) is therefore not as reported on the immediate reaction path to the transition structures for furan and pyran formation.

To determine the lowest energy conformations of protonated *trans*-4,5-epoxyhexan-1-ol, extensive AM1 grid search calculations involving rotation about the torsional angles of the hydroxyalkyl side chain were performed. Selected low energy conformers were optimised at the HF/6-31G* level and the lowest energy conformer found is **10** (Figure 5). The large difference in energy between the protonated epoxide conformers **7** and **10** (8.3 kcal/mol) is an indication of the importance of charge stabilisation of the C4 and C5 centres by the hydroxyl oxygen for the latter conformer. It should be noted that these are gas phase calculations and in solution hydrogen bonding may be of lesser importance. The C_{ep}-O bonds in **10** are longer than in **7** facilitating ring opening. A schematic representation of the potential energy surface for the rearrangement of protonated *trans*-4,5-epoxyhexan-1-ol (**10**) (same invertomer as published by Houk)[17] with the transition structures (invertomers of those reported by Houk) to protonated *trans*-2-methyltetrahydrofuran-3-ol **11** and protonated *trans*-2-methyltetrahydropyran-3-ol **12** is shown in Figure 5. All stationary points are fully optimised at the HF/6-31G* level.

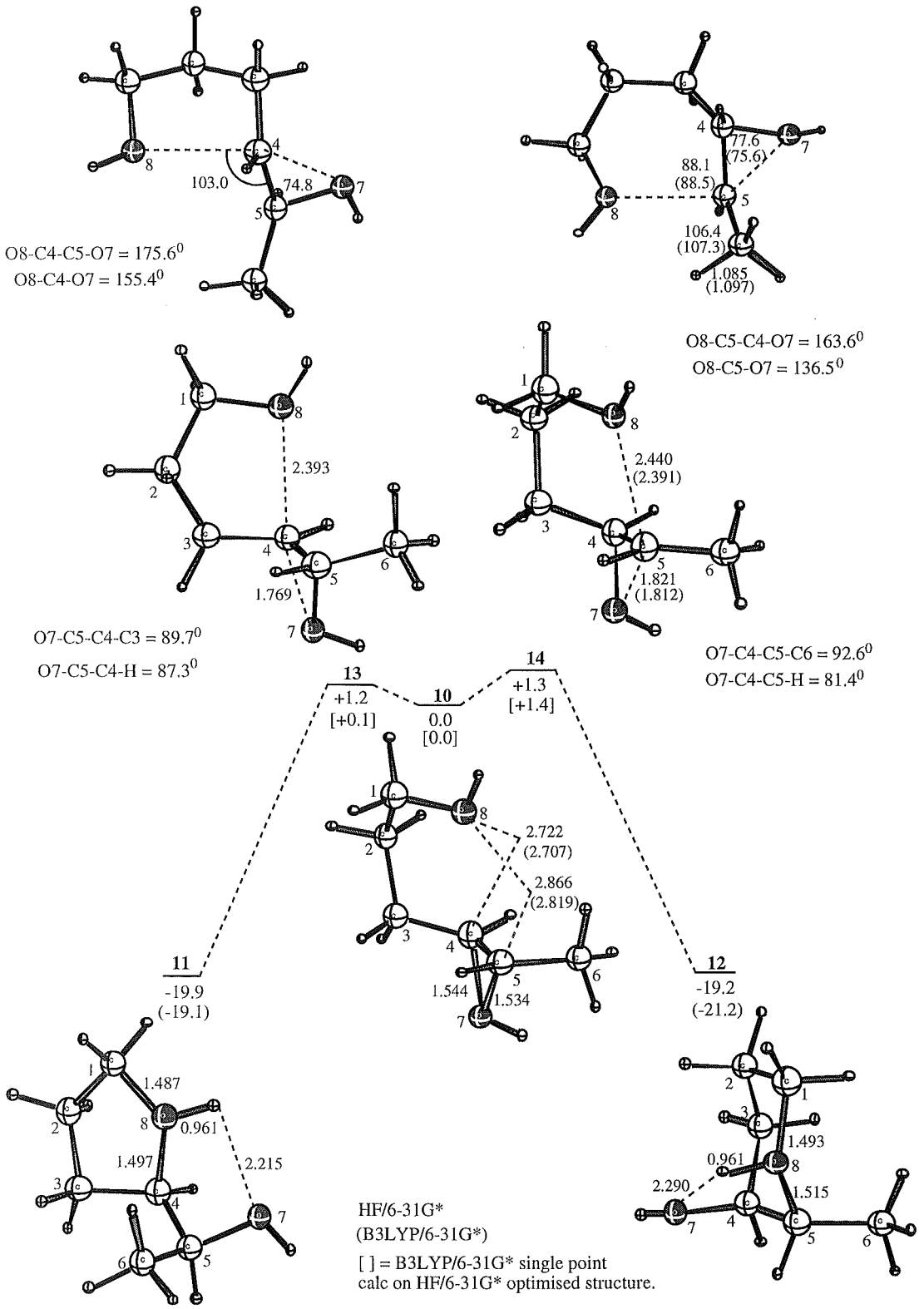

Figure 5. The potential energy surface for the rearrangement of **10** to **11** and **12**. Geometries are optimised at the HF/6-31G* level. Two perspectives of each transition structure are shown. The relative energies (kcal/mol) include zero point corrections. Bond lengths are in Å and bond angles are in degrees.

The lowest energy conformer **10** resembles a pre-chair with the hydroxyl oxygen positioned closer to C4 (2.722Å) than to C5 (2.866). In this conformation the hydroxyl oxygen p-orbital is positioned for orbital overlap with the developing cationic centre at C4 as cleavage of the C4-O7 bond occurs. The energy of **10** is close to the transition structures **13** and **14** with activation barriers of only 1.2 and 1.3 kcal/mol respectively. The lowest energy conformations of the protonated furan and pyran rings **11** and **12** optimised at the HF/6-31G* level both exhibit hydrogen bonding between the hydroxyl proton and protonated ether oxygen. The rearrangement of **10** is highly exothermic and reflects the relief of epoxide ring strain. The transition structures **13** and **14** to furan and pyran are reactant-like with a geometry closely resembling epoxide **10**. The transition structure **13** is marginally favoured (0.1 kcal/mol) over the 6-membered transition structure **14** and the forming O8-C4 and breaking C4-O7 bond lengths of the former differ by less than 0.05Å from the analogous bond lengths in **14**. The internal O8-C4-O7 bond angle (155.4°) in **13** is close to the O-C_{ep}-O bond angle for the addition of water to protonated oxirane (154.9°) however for **14**, the O8-C5-O7 bond angle (136.5°) is less than optimum reflecting poorer orbital overlap and the greater strain required to form the 6-membered ring.

The O8-C4-C5-O7 torsional angle (175.6°) in the forming bicyclic spiro structure **13** is close to antiperiplanar and more favourable than the analogous O8-C5-C4-O7 torsional angle (163.6°) in **14**. The latter is more constrained reflecting bicyclic ring strain of the transition structure. It is therefore surprising that the difference in energy between **13** and **14** is as little as 0.1 kcal/mol (HF/6-31G*) favouring the former. The energy and skeletal geometry of the transition structures are almost insensitive to which face of the epoxide is protonated. The transition structure invertomers of **13** and **14** (Figure 5) namely **8** and **9** (Figure 4) are 0.4 kcal/mol higher and 0.3 kcal/mol lower in energy respectively. The difference in energy between the 5- and 6-membered transition structures **8** and **9** is 0.8 kcal/mol favouring the former, a difference moderately larger than between **13** and **14**. A B3LYP/6-31G* optimised geometry was obtained for transition structure **14** but not **13**. For **14** the optimised

geometry at the HF/6-31G* and B3LPY/6-31G* levels is similar with a minor contraction in the O8-C5+ (2.391Å) and C5+-O7 (1.812Å) bond lengths observed at the latter level of theory.

Nucleophilic attack of the intramolecular hydroxy oxygen in **10** occurs in concert with the opening of the epoxide but without any substantial twisting of the cleaving C-O bond about the epoxide C-C bond. For transition structure **13** the O7-C5-C4-C3 and O7-C5-C4-H torsional angles are 89.7° and 87.3° and for **14** the corresponding O7-C4-C5-C6 and O7-C4-C5-H torsional angles are 92.6° and 81.4° respectively. These values and the dihedrals O8-C4-C5-O7 (175.6°) for **13** and O8-C5-C4-O7 (163.6°) for **14** define the orientation of the nucleophile with respect to the epoxide plane with the former showing a more planar interaction at the reaction centre. In contrast, ring opening of protonated propene oxide occurs with substantial rotation about the epoxide C-C bond, and in concert with, but before hydride migration is initiated[20] (Figure 6). For this reaction, intramolecular hydride attack is late on the reaction coordinate.

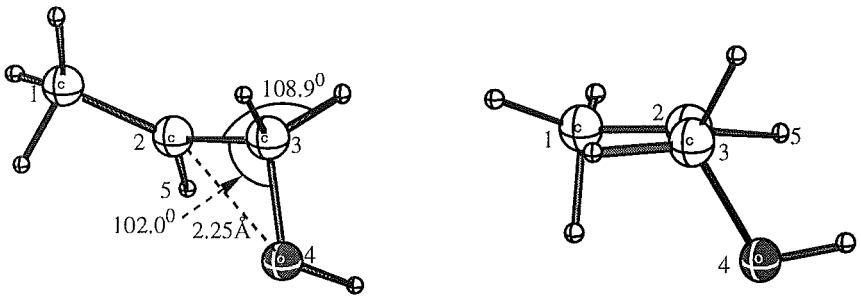

Figure 6. Two perspectives of the MP2/6-31G* optimised lowest energy transition structure for epoxide ring opening.[20]

Transition structures for retention of configuration.

A 6-membered transition structure for both the reaction of **10** and its invertomer to a tetrahydropyran involving retention of configuration at the site of epoxide ring opening have been determined at the HF/6-31G* level (Figure 7). The transition

structures are too high in energy for these pathways to be competitive with the reaction of the epoxide occurring with inversion of configuration. For both structures the O8-C5-O7 bond angles (75.2^0 and 66.8°) reflect poor overlap of the nucleophile with the epoxide bond undergoing cleavage. The transition structure from the invertomer of **10** is the lower in energy because of an intramolecular H-O8 bond (2.007Å, HF/6-31G* and 1.847Å, B3LYP/6-31G*).

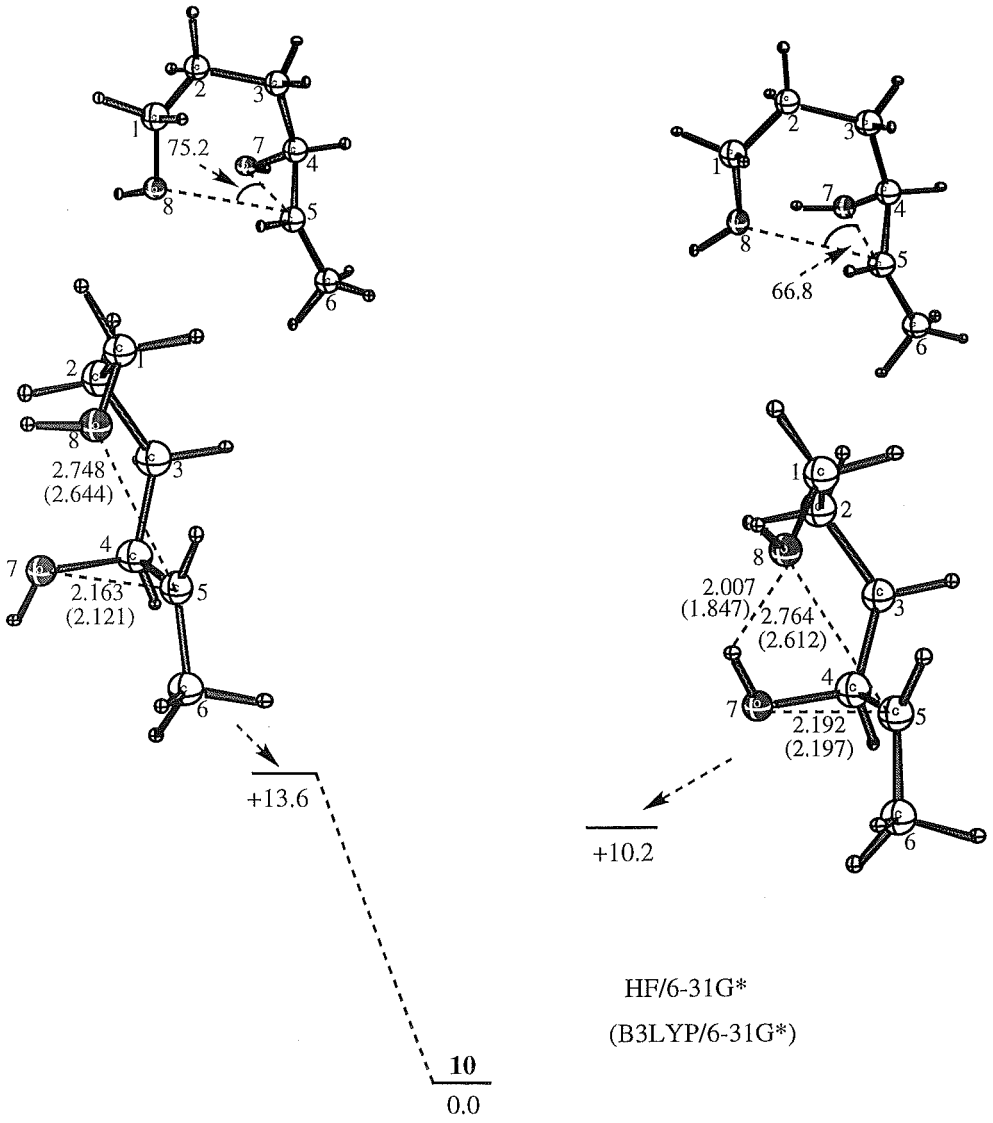

Figure 7. 6-membered transition structures involving retention of configuration for ring opening of epoxide **10** and its invertomer. Energies in kcal/mol are relative to epoxide **10**. Bond lengths are in Å and bond angles in degrees. Two perspectives of each structure are shown.

Potential energy surface for the rearrangement of protonated *cis*-4,5-epoxyhexan-1-ol (15).

The potential energy surface for the rearrangement of protonated *cis*-4,5-epoxyhexan-1-ol (**15**) to protonated *cis*-2-methyltetrahydrofuran-3-ol (**16**) and protonated *cis*-2-methyltetrahydropyran-3-ol (**17**) is shown in Figure 8 for the lowest energy conformers. The rearrangement proceeds by competing pathways involving the 5- and 6-membered transition structures **18** and **19** with inversion of configuration at the epoxide carbons. All structures are fully optimised at the HF/6-31G* level.

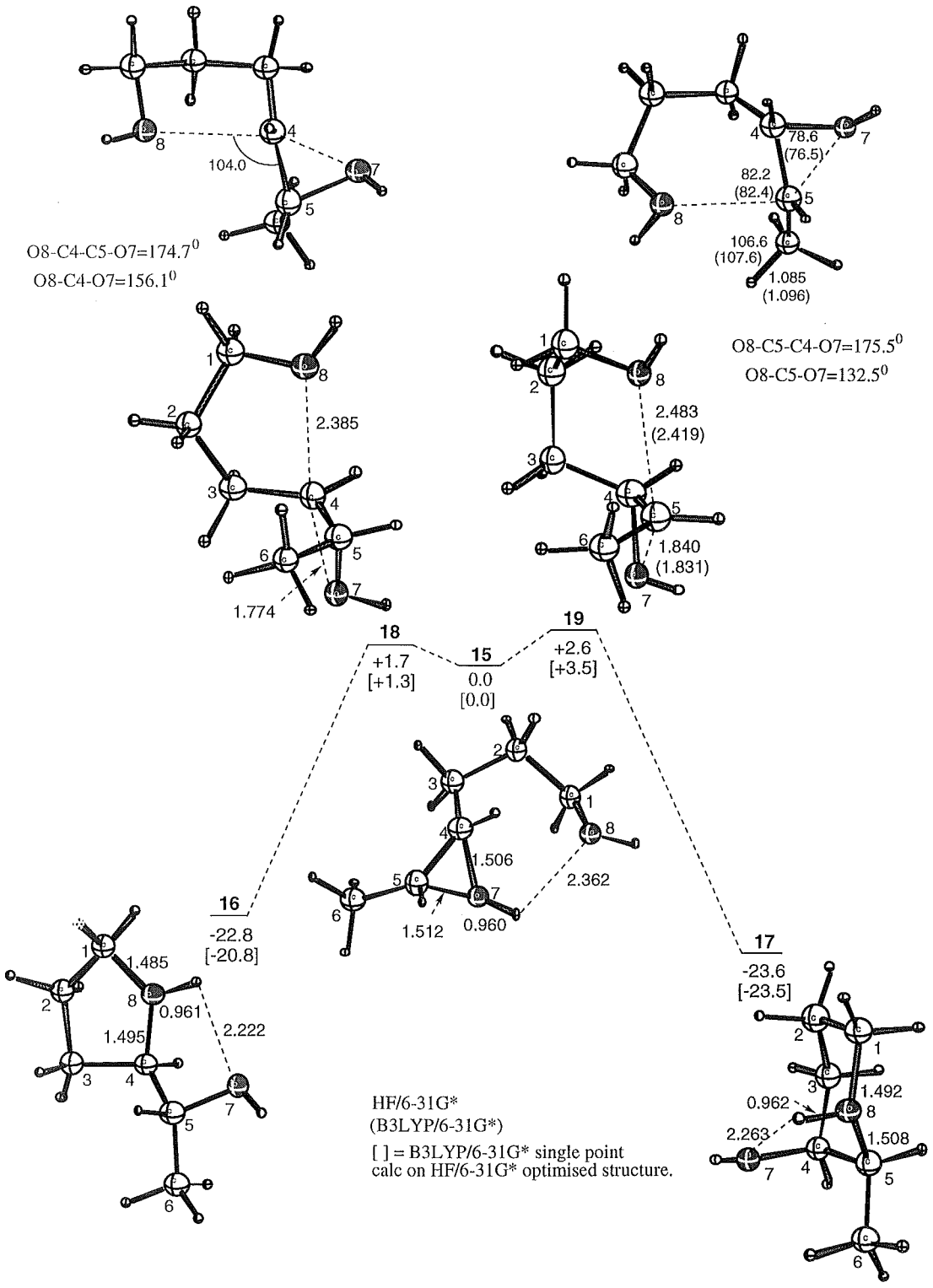

Figure 8. The potential energy surface for the rearrangement of **15** to **16** and **17** with relative energies (kcal/mol), bond distances (Å) and bond angles (degrees) at the HF/6-31G* level. Two perspectives of each transition structure are shown.

The lowest energy conformation of the reactant protonated epoxide **15** is different in geometry to the isomeric protonated epoxide **10**. In the former the hydoxyalkyl group is hydrogen bonded with the epoxide proton[21] while in the latter the hydroxyalkyl group is in close proximity to the epoxide carbons and *anti* to the epoxide oxygen. The lowest energy product conformers **16** and **17** both exhibit intramolecular hydrogen bonding between the ether proton and the hydroxyl oxygen with the latter adopting a chair structure. The activation barriers for furan and pyran formation from **15** *via* transition structures **18** and **19** (1.7 and 2.6 kcal/mol) are marginally greater than the analogous barriers for the rearrangement of the *trans*-epoxide **10** (1.2 and 1.3 kcal/mol, Figure 5). The calculations show that the pathway involving a 5-membered transition structure **18** leading to a furan is favoured over pyran by 0.9 kcal/mol however the latter product is not observed experimentally. A geometry of **19** was optimised at the B3LYP/6-31G* level which is structurally similar to the HF/6-31G* optimised geometry. The C5-O7 bond length is almost identical in both geometries (1.831Å (B3LYP/6-31G*) and 1.840Å (HF/6-31G*)) with only a minor reduction observed in the O8-C5 bond length (2.419Å) in the B3LYP/6-31G* transition structure (2.483Å, HF/6-31G*). The transition structure **18** could not be found at the B3LYP/6-31G* level.

The O-C_{ep}-O bond and O-C_{ep}-C_{ep}-O torsional angles of the transition structures examined in this study are important parameters in defining reaction trajectory (Table 3). The O8-C4-O7 bond angle in transition structure **18** of 156.1^0 is close to the value for addition of water to protonated oxirane (154.9^0) and comparable to the analogous angle (155.4^0) for the transition structure **13** for formation of furan from **10** (Figure 5). The O8-C4-C5-O7 (174.7^0) and O8-C5-C4-O7 (175.7^0) torsional angles for the transition structures **18** and **13** are close to antiperiplanar and further reflect favourable orbital overlap for both structures. For both the reaction of **10** and **15** the transition structures **13** and **18** respectively represent the favoured pathway, and for the latter reaction the exclusive pathway.

Table 3. Bond and torsional angles of the H^+ and BF_3 coordinated 5- and 6-membered transition structures involving inversion of configuration at the reaction centre.

Transition structure	Bond angle O8-C5-O7	Bond angle O8-C4-O7	Torsional angle O8-C5-C4-O7	Torsional angle O8-C4-C5-O7	Δ energy (5TS-6TS) (kcal/mol)
H^+					
13 (5TS)		155.4^0		175.6^0	-0.1
14 (6TS)	136.5^0		163.6^0		
18 (5TS)		156.1^0		174.7^0	-0.9
19 (6TS)	132.5^0		175.5^0		
BF_3					
24 (5TS)		149.1^0		175.5^0	-0.3
25 (6TS)	137.1^0		173.3^0		
29 (5TS)		147.1^0		174.4^0	+0.6
30 (6TS)	141.8^0		171.3^0		
32 (5TS)		148.6^0		177.8^0	+3.4
33 (6TS)	139.3^0		164.5^0		

For the *trans*-6-membered transition structure **14** the O8-C5-O7 bond angle (136.5^0) is more favourable and the O8-C5-C4-O7 torsional angle less favourable (163.6^0) than in the *cis*-6-membered transition structure **19** (132.5^0 and 175.5^0 respectively). Since **14** is close in energy to **13** (0.1 kcal/mol) c.f **19** and **18** (0.9 kcal/mol), the more favourable O8-C5-O7 bond angle in **14** (136.5^0) is the dominating feature determining the lower energy difference.

Transition structures for retention of configuration.

Five and six membered transition structures **20** and **21** for reaction with retention of configuration at the site of epoxide ring cleavage in epoxide **15** have been determined at the HF/6-31G* level (Figure 9).

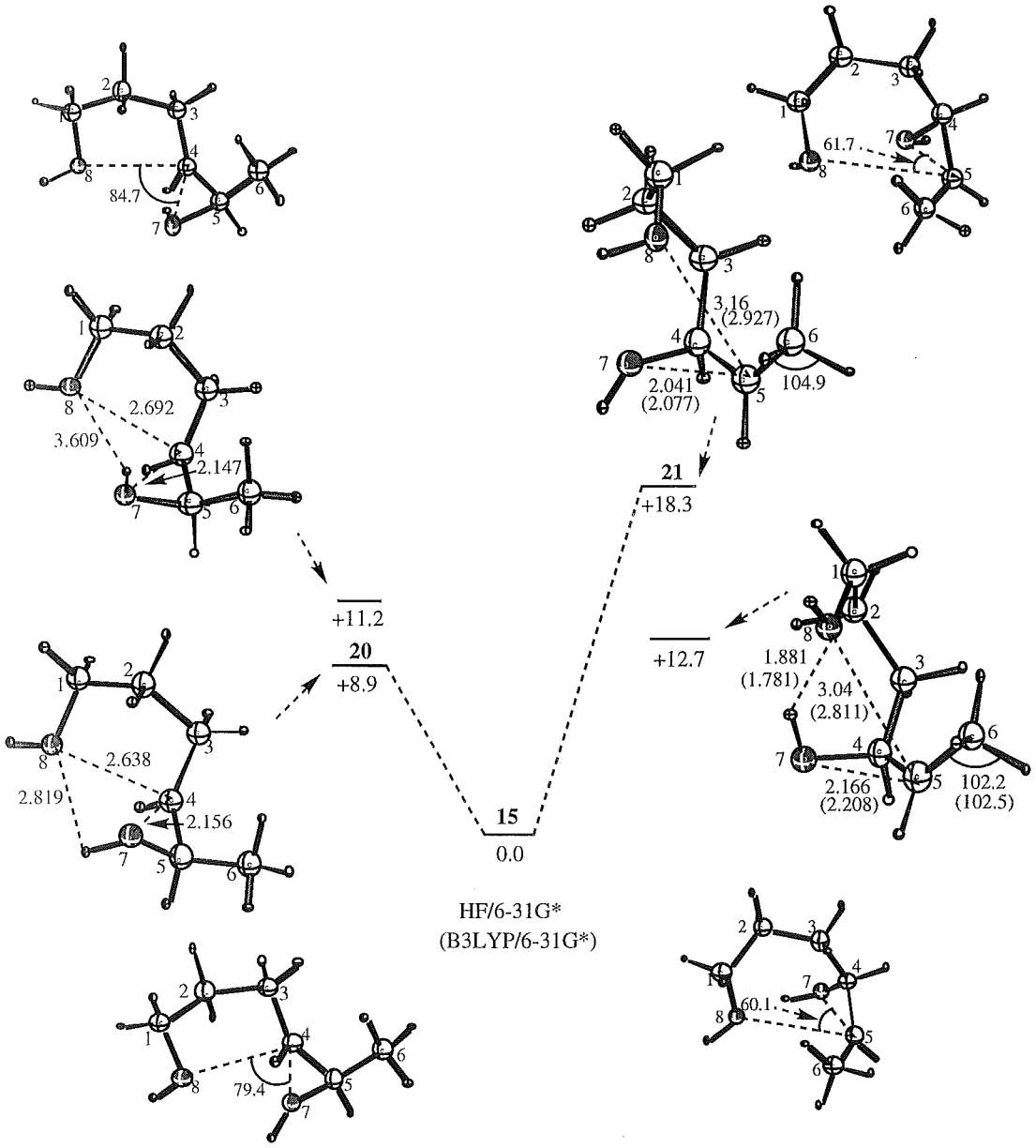

Figure 9. HF/6-31G* calculated stationary point structures (distances in Å, angles in degrees) for the rearrangement of **15** *via* transition structures **20** and **21** with retention of configuration. Also shown are the transition structure invertomers of **20** and **21**. Two perspectives of each transition structure are shown. The relative energies (kcal/mol) include zero point corrections.

The activation barriers leading to **20** and **21** from epoxide **15** are large (8.9 and 18.3 kcal/mol) in comparison with the pathways involving inversion of configuration for the *cis*-transition structures **18** and **19** (1.7 and 2.6 kcal/mol, Figure 8). Consequently furan and pyran ring formation *via* the transition structures **20** and **21** is

not expected. The retention transition structures are congested and the epoxide C_{ep}-O7 ring opening and O8-C_{ep} ring forming bond lengths are both longer than in the inversion transition structures. The O8-C_{ep}-O7 bond angles are highly strained in both **20** (79.4^0) and **21** (61.7^0) and the large difference in energy between **20** and **21** favouring the former by 9.4 kcal/mol is a consequence of the lesser bicyclic ring strain in **20**. Two further transition structures for retention of configuration for the invertomer of **15** are shown in Figure 9. These are also high in energy and will not compete with the inversion pathways.

Potential energy surface of the rearrangement of *cis*- and *trans*- 4,5-epoxyhexan-1-ol with BF_3.

For the BF_3-catalysed rearrangement of the *cis*-4,5-epoxyhexan-1-ol, the potential energy surface was examined with the Lewis acid coordinated to the least hindered face *trans* to both substituents while for the *trans* epoxide, the potential energy surfaces were examined with the BF_3 coordinated to each face.

(i) *cis*-4,5-Epoxyhexan-1-ol coordinated to BF_3 (21).

The stationary points on the potential energy surface for the rearrangement of BF_3 coordinated *cis*-4,5-epoxyhexan-1-ol **21** to the furan **22** and pyran **23** are shown in Figure 10. The activation barriers from the epoxide **21** to the 5- and 6-membered transition structures **24** and **25** (25.6 and 25.9 kcal/mol) are noticeably larger than the analogous activation barriers for the proton-catalysed rearrangement (1.7 and 2.6 kcal/mol, Figure 8). The transition structures **24** and **25** are positioned near midway on the potential energy surface between the reactant epoxide **21** and the respective furan **22** and pyran **23** products and represent later transition structures in comparison with the analogous protonated transition structures **18** and **19**.

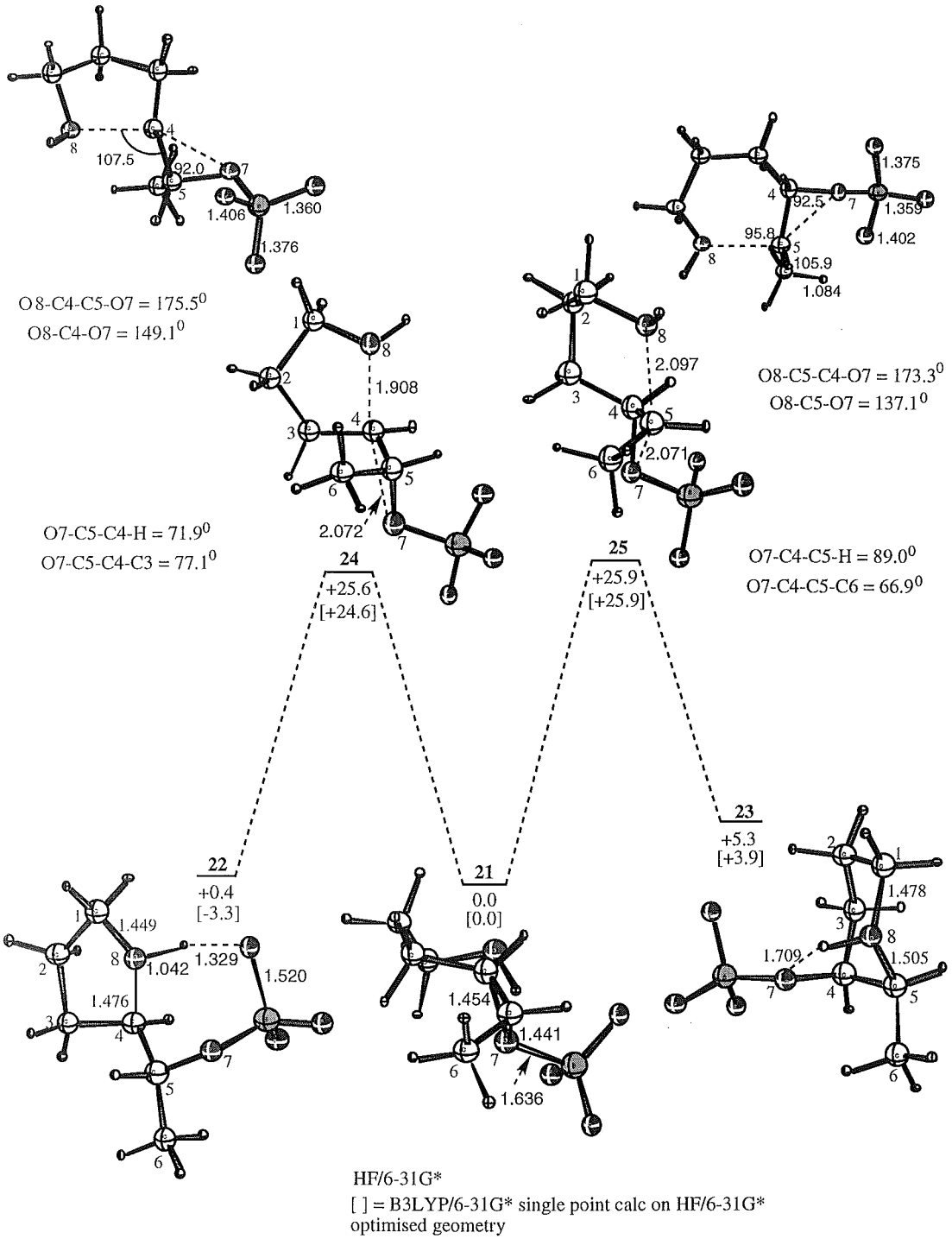

Figure 10. The potential energy surface for the rearrangement of **21** to **22** and **23**. Stationary points displayed are optimised at the HF/6-31G* level. Two perspectives of each transition structure are shown. The relative energies (kcal/mol) include zero point corrections. Bond distances are in Å and bond angles in degrees.

The 5-membered transition structure **24** is marginally lower in energy (0.3 kcal/mol) than the 6-membered transition structure **25** with the epoxide C-O7 bonds undergoing cleavage in each being of similar length (2.072Å and 2.071Å respectively) and significantly longer than for the protonated transition structures **13, 14, 18** and **19** (1.76-1.84Å). Intramolecular nucleophilic attack is also more advanced in both pathways than for the proton-catalysed rearrangements (2.39-2.48Å). The bond length between the oxygen of the nucleophile and the epoxide carbon (C4-O8) is 1.908Å in **24** and longer in **25** (O8-C5 = 2.097Å) and since the difference between the O8-C_{ep} bond lengths in each of the furan **22** (1.476Å) and pyran **23** (1.505Å) products is small, **24** can be considered to be a later, more product-like transition structure than **25**. This result is in contradiction of the Hammond principle[22] since the relative energies of the products is such that **23** is 4.9 kcal/mol higher in energy than **22**. Removal of BF_3 from **22** and **23** is reversible and accordingly the uncoordinated furan and pyran products are expected to be substantially lower in energy relative to the uncoordinated epoxide mirroring the rearrangement of the protonated epoxides **10** (Figure 5) and **15** (Figure 8).

The O8-C4-C5-O7 and O8-C5-C4-O7 torsional angles in **24** (175.5^0) and **25** (173.3^0) are similar reflecting near antiperiplanar orbital overlap between the nucleophile and the epoxide. The O8-C4-O7 bond angle (149.1^0) in **24** is more favourable than the corresponding O8-C5-O7 bond angle in **25** (137.1^0) and the energy difference between **24** and **25** (0.3 kcal/mol) is smaller than that between the protonated transition structures **18** and **19** (0.9 kcal/mol, Figure 8) where there is a larger difference between the O8-C_{ep}-O7 bond angles (156.1^0 for **18** and 132.5^0 for **19**) (see Table 5.3). For the 5-membered transition structure **24**, C4 is pyramidalised away from the incoming nucleophile as evidenced by the torsional angles O7-C5-C4-H of 71.9^0 and O7-C5-C4-C3 of 77.1^0 which reflect the lateness of the transition structure. In the same way C5 is pyramidalised in **25** (O7-C4-C5-H (89.0) and O7-C4-C5-C6 (66.9)) but the transition structure is marginally less advanced along the reaction coordinate.

(ii) *trans*-4,5-Epoxyhexan-1-ol coordinated to BF_3 (*trans* to methyl) (26).

For *trans*-4,5-epoxyhexan-1-ol, both faces of the epoxide can be coordinated with BF_3 and stationary points on the potential energy surface for reaction of both invertomers are examined. The stationary points on the potential energy surface for the rearrangement of *trans*-4,5-epoxyhexan-1-ol (**26**) with BF_3 coordinated to the epoxide *cis* to the hydroxyalkyl chain, which is the lower energy invertomer (by 2.1 kcal/mol), are shown in Figure 11.

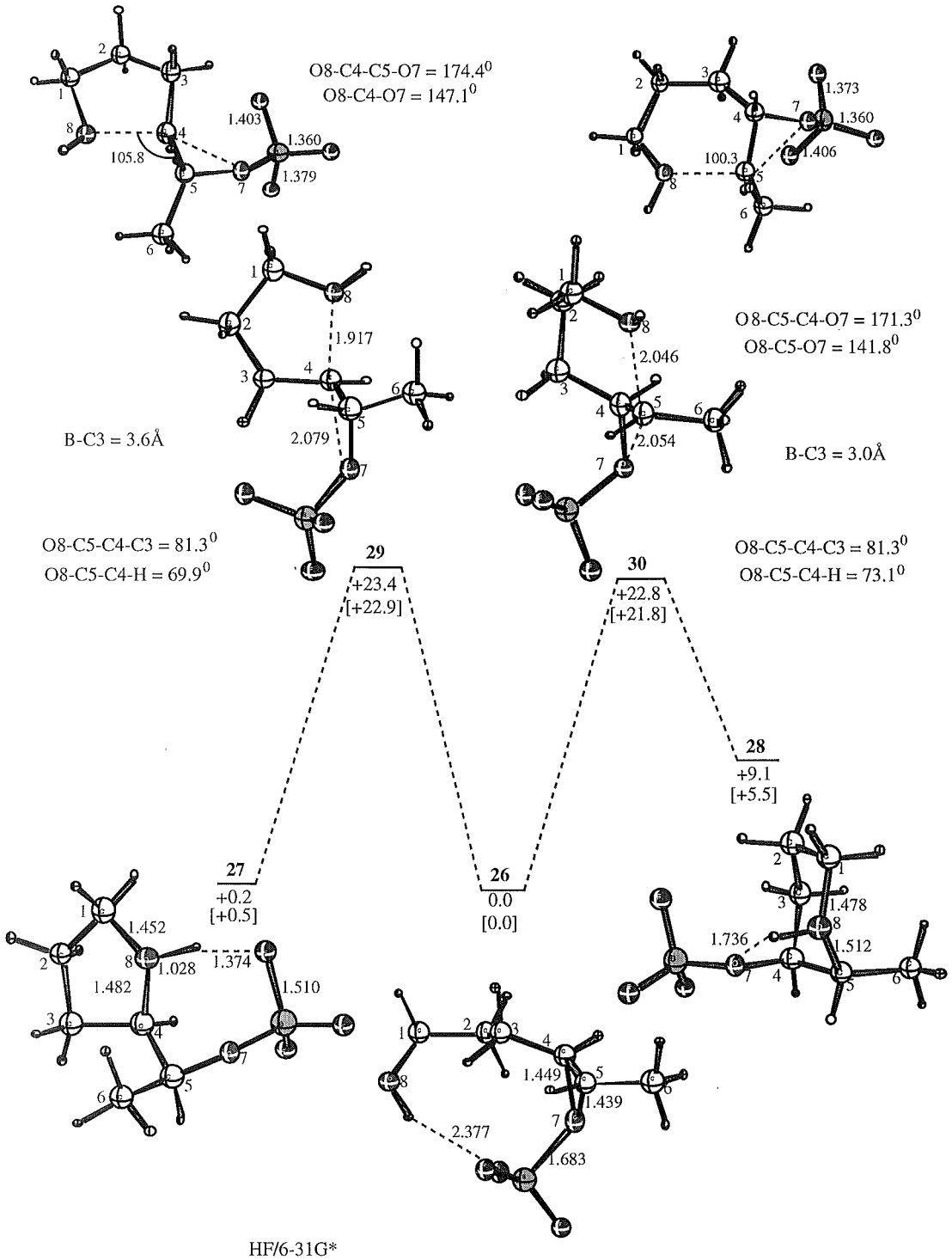

Figure 11. The potential energy surface for the rearrangement of **26** to **27** and **28** optimised at the HF/6-31G* level. The relative energies (kcal/mol) include zero point corrections. Two perspectives of each transition structure are shown with bond lengths in Å and bond angles in degrees.

Calculations at the HF/6-31G* level show that ring opening at the C4 position and nucleophilic attack of the hydroxyl to give the 5-membered transition structure **29** is less favoured (by 0.6 kcal/mol) over nucleophilic attack at C5 to give pyran by way of transition structure **30**. This result contrasts to the proton-catalysed rearrangement of *trans*-4,5-epoxyhexan-1-ol **10** (Figure 5) where the pathway involving a 5-membered transition structure is favoured over pyran formation. The experimental results with BF_3 as catalyst show a furan:pyran ratio of 84:16. It is somewhat surprising that **30** is lower in energy than **29** given that the BF_3 group in the former is in closer proximity with the hydroxyalkyl side chain (B-C3 = 3.0Å) than in **29** (B-C3 = 3.6Å) while in the latter, the BF_3 is near eclipsed with the C5-H (B-O7-C5-H = 7.9°).

The potential energy surfaces in Figures 5, 8 and 10 have shown that the energy difference between the 5- and 6-membered transition structures decreases as the O8-C5-O7 bond angle of the 6-membered transition structure becomes closer to the O8-C4-O7 bond angle of the 5-membered transition structure (see Table 3). The O8-C5-O7 bond angle of **30** (141.8^0) is more favourable than the corresponding bond angle in the 6-membered transition structures **14** (136.5^0), **19** (132.5^0) and **25** (137.1^0) and is only 5.3^0 smaller than the O8-C4-O7 bond angle in **29** (147.1^0). The ring forming and ring opening bond lengths of the *trans*- 5- and 6-membered transition structures **29** and **30** are similar to the corresponding bond lengths in the *cis*- 5- and 6- membered transition structures **24** and **25** (Figure 10). The only notable difference is the moderately tighter O8-C5 (2.046Å) and C5-O7 (2.054Å) bond lengths in **30** in comparison to **25** (O8-C5 = 2.097Å and C5-O7 = 2.071Å).

Transition structure **29** can be considered to be more product-like in geometry than transition structure **30** by comparison of the O8-C_{ep} bond lengths in each relative to the O8-C_{ep} bond lengths in the respective furan **27** and pyran **28** products. The difference between the O8-C4 bond lengths in **29** (1.917Å) and in furan **27** (1.482Å) is 0.435Å, moderately smaller than the difference between the O8-C5 bond lengths in **30** (2.046Å) and in pyran **28** (1.512Å) of 0.534Å. For the 5-membered transition structure **29**, C4 is pyramidalised away from the incoming nucleophile as evidenced by

the torsional angles O7-C5-C4-H of 69.9° and O7-C5-C4-C3 of 81.3° reflecting the lateness of the transition structure. In the same way C5 is similarly pyramidalised in **30** (O7-C4-C5-H (73.1) and O7-C4-C5-C6 (81.3)) but the transition structure is marginally less advanced along the reaction coordinate.

(iii) *trans*-4,5-Epoxyhexan-1-ol coordinated to BF_3 (*cis* to methyl) (31).

The optimised stationary points on the HF/6-31G* potential energy surface for the BF_3-catalysed rearrangement of epoxide **31** to furan **27** and pyran **28** are displayed in Figure 12. The transition structures **29** and **30** for the rearrangement of the invertomer **26** are included on the potential energy surface for comparison. Intramolecular nucleophilic attack and epoxide ring opening at C4 in **31** leading to transition structure **32** is 3.4 kcal/mol higher in energy than the pathway *via* transition structure **33** leading to pyran formation. This result is in contrast to the experimental results where furan is preferentially formed. The BF_3 group is eclipsed with an adjacent proton (B-O7-C4-H = 4.2^0, B-C4H = 3.6Å) in **33** and is in a sterically less crowded position than in **32** where the BF_3 group is close to the methyl (B-O7-C5-C6 = 31.2^0, B-C6 = 2.99 Å).

The ring forming and ring breaking bond lengths in **33** (O8-C5 (2.031Å) and C5-O7 (2.069Å)) and **32** (O8-C4 (1.916 Å) and C4-O7 (2.085 Å)) are similar to the corresponding bond lengths of the 5- and 6-membered transition structures **29** and **30** (Figure 11) and more advanced than the proton catalysed transition structures. A B3LYP/6-31G* optimised geometry of **33** was determined and shown to have similar O8-C5-O7 bond and O8-C5-C4-O7 torsional angles (142.2^0 and 164.8^0) respectively to the analogous angles in the HF/6-31G* optimised geometry (139.3^0 and 164.5^0). Intramolecular nucleophilic attack and epoxide ring opening is more advanced in the B3LYP/6-31G* optimised geometry of **33** as defined by the O8-C5 (1.902Å) and C5-O7 (2.127Å) bond lengths. An optimised geometry of **32** at the B3LYP/6-31G* level was not found.

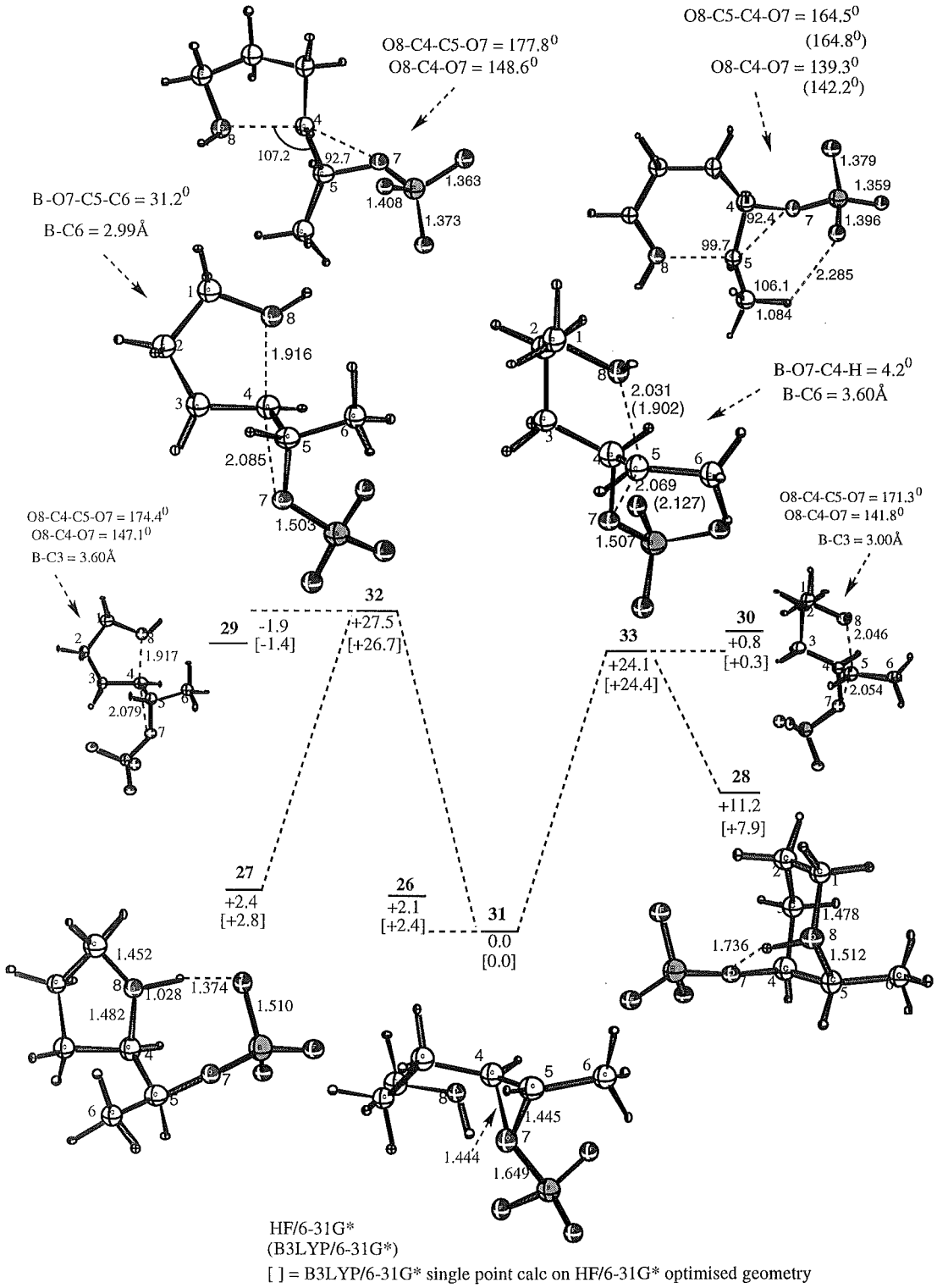

Figure 12. The potential energy surface for the rearrangement of **31** to **27** and **28**. Structures presented are optimised at the HF/6-31G* level. Two perspectives of the transition structures **32** and **33** are shown. The relative energies (kcal/mol) include zero point corrections. Bond lengths in Å and bond angles in degrees.

The O8-C4-O7 bond angle (148.6^0) and the O8-C4-C5-O7 torsional angle (177.8^0) in **32** show that more favourable orbital overlap is achieved at the reaction centre than in transition structure **33** (O8-C5-O7 (139.3^0) and O8-C5-C4-O7 (164.5^0)). Intramolecular nucleophilic attack is more advanced in the former as evidenced by the shorter O8-C4 (1.916Å) bond length in comparison with the O8-C5 bond length in **33** (2.031Å) relative to the O8-C_{ep} bond lengths in the furan **27** (1.482Å) and pyran **28** (1.512Å) products. The difference in energy between the 5-membered transition structures **29** and **32** favouring the former by 1.9 kcal/mol is attributed to the sterically less crowded position of the BF_3 group in **29** (B-C3 = 3.60Å) than in **32** (B-C6 = 2.99Å). Both structures show favourable orbital overlap at the C4 reaction centre with little variation observed between the O8-C4-O7 bond and O8-C4-C5-O7 torsional angles for each (see Figure 12). The positioning of the BF_3 group in the 6-membered transition structures **33** and **30** is also an important geometrical feature affecting the relative energy of each. Transition structure **33** is 0.8 kcal/mol lower in energy than transition structure **30** due to the more favoured position of the BF_3 group in the former (B-C6 = 3.60Å) than in the latter (B-C3 = 3.0Å). The smaller energy difference between **33** and **30** (0.8 kcal/mol) compared with the energy difference between **29** and **32** (1.9 kcal/mol) is most likely due to the poorer orbital overlap associated with transition structure **33** (O8-C4-O7 (139.3^0) and O8-C5-C4-O7 (164.5^0)) than in **30** (O8-C5-O7 (141.8^0) and O8-C5-C4-O7 (171.3^0)).

The BF_3 coordinated *cis*- and *trans*- 5-membered transition structures **24**, **29** and 32 show similar values for the O8-C4-O7 bond angles (see Table 3) and are 6-9^0 less than in the *cis*- and *trans*- protonated 5-membered transition structures **13** and **18**. The O8-C4-C5-O7 torsional angles for **24**, **29** and **32** are comparable to those for **13** and **18** and are close to ideal for maximum orbital overlap. For the BF_3 coordinated 6-membered transition structures **25**, **30** and **33**, the O8-C5-O7 bond angles are more favourable than for the protonated transition structures **14** and **19** and reflect a more advanced degree of bond formation at the transition structure. The O8-C_{ep}-C_{ep}-O7

torsional angles for all the 6-membered transition structures examined in this study vary somewhat with the torsional angles for the *trans*-6-membered transition structures **14** (163.6^0) and **33** (164.5^0) poorer than in the *cis*-6-membered transition structures **19** (175.5^0) and **25** (173.3^0).

Conclusion.

For rearrangement of protonated *cis*- and *trans*-4,5-epoxyhexan-1-ol, the pathway involving a 5-membered transition structure in each case is marginally favoured over pyran formation. The energy difference between the 5- and 6-membered transition structures is more sensitive to change in the O-C_{ep}-O bond angle than in the O-C_{ep}-C_{ep}-O torsional angle. The transition structures are reactant like with minimal epoxide ring opening at the transition structure. The transition structures for furan and pyran formation for the BF_3 catalysed rearrangement of *cis*- and *trans*-4,5-epoxyhexan-1-ol are more advanced than for the corresponding protonated transition structures. The main structural variation between the 5- and 6-membered transition structures is the extent of intramolecular nucleophilic attack, which is more advanced in the 5-membered transition structures. For the BF_3 catalysed rearrangement of *cis*-4,5-epoxyhexan-1-ol, the calculations show a pathway involving a 5-membered transition structure is favoured and is in agreement with the experimental result where furan is formed exclusively. The potential energy surface for rearrangement of each invertomer of protonated *trans*-4,5-epoxyhexan-1-ol is in contrast to the experimental results and favours pyran formation in preference to furan.

References

1 Janda, K.D.; Shevlin, C.G.; Lerner, R.A. *Science* **1993**, *259*, 490.

2 Na, J. Houk, K.N. Shevlin, C.G.; Janda, K.D. Lerner, R.A. *J. Am. Chem. Soc.* **1993**, *115*, 8453.

3 Janda, K. D.; Shelvin, C. G.; Lerner, R. A. *Science* **1993**, *259*, 490-493. Janda, K. D.; Shelvin, C. G.; Lerner, R. A. *J. Am. Chem. Soc.* **1995**, *117*, 2659-2660.

4 No tetrahydrofuran could be detected in the product.

5 In the absence of the catalytic antibody the 5-*exo* process is calculated to be favored by 1.8 kcal/mol (single point solvent calculation, HF/6-31G* (SCRF)).[2] Assuming a negligible entropic difference in the two transition structures this translates to a 96:4 product ratio at 25 °C "To favor the 6-*endo* product to a similar amount, the catalytic antibody must lower the 6-endo activation energy 3.6 kcal/mol more than it lowers the 5-exo activation barrier."[2]

6 Na, J.; Houk, K.N. *J. Am. Chem. Soc.* **1996**, *118*, 9204.

7 Thorpe, A. PhD Thesis, University of Canterbury, **1999**. Unpublished results.

8 Coxon, J. M.; Hartshorn, M. P.; Swallow, W. H. *Aust. J. Chem.* **1973**, *26*, 2521.

9 This preference was subsequently encapsulated in the rules for ring closure enunciated by Baldwin, J. E. *J. Chem. Soc., Chem. Commun.* **1976**, *734*. see also Principles of Organic Synthesis' by Sir Richard Norman and J. M. Coxon. Blackie Chapman and Hall, London and John Wiley and Sons, New York. **1993**, page 678. Baldwin, J. E.; Lusch, M. J. *Tetrahedron* **1982**, *19*, 2939.

10 Ford, G. P.; Smith, C. T. *J. Am. Chem. Soc.* **1987**, *109*, 1325.

11 M. A. Battiste and J. M. Coxon. *The Chemistry of the Cyclopropyl Group*, Ed,; Zhi Rappoport, John Wiley and Sons: New York, **1987**, page 255-305.

12 Coxon, J. M.; Morokuma, K.; Thorpe, A. J.; Whalen, D. *J. Org. Chem.* **1998**, *63*, 3875-3883.

13 Dewar, M. J. S.; Zoebisch, E. G.; Healy, E. F.; Stewart, J. J. P. *J. Am. Chem. Soc.* **1985**, *107*, 3902.

14 SPARTAN Version 4.1, Wavefunction, Inc., 18401 Von Karman, Irvine, CA 92715.

15 Gaussian 94, Revision D.2. Frisch, M. J.; Trucks, G. W.; Schlegel, H. B.; Gill, P. M. W.; Johnson, B. G.; Robb, M. A.; Cheeseman, J. R.; Keith, T.; Petersson, G. A.; Montgomery, J. A.; Raghavachari, K.; Al-Laham, M. A.; Zakrzewski, V. G.; Ortiz, J. V.; Foresman, J. B.; Cioslowski, J.; Stefanov, B. B.; Nanayakkara, A.;

Challacombe, M.; Peng, C. Y.; Ayala, P. Y.; Chen, W.; Wong, M. W.; Andres, J. L.; Replogle, E. S.; Gomperts, R.; Martin, R. L.; Fox, D. J.; Binkley, J. S.; Defrees, D. J.; Baker, J.; Stewart, J. P.; Head-Gordon, M.; Gonzalez, C.; Pople, J. A. Gaussian, Inc., Pittsburgh PA, **1995**.

16 Becke, A. D. Phys. Rev. A **1988**, *38*, 3098. Becke, A. D. *J. Chem. Phys.* **1993**, *98*, 1372. Lee, C.; Yang, W.; Parr, R. G. *Phys. Rev.* B **1988**, *37*, 785.

17 Na, J.; Houk, K. N.; Shelvin, C. G.; Janda, K. D.; Lerner, R. A. *J. Am. Chem. Soc.* **1993**, *115*, 8453-8454.

18 George, P.; Bock, C. W.; Glusker, J. P. *J. Phys. Chem.* **1990**, *94*, 8161-8168.

19 Thank you to Professor Ken Houk an Dr Jim Na for supplying the coordinates of their published structures.

20 Coxon, J. M.; Maclagan, R. G. A. R.; Rauk, A.; Thorpe, A. J.; Whalen, D. *J. Am. Chem. Soc.* **1997**, *119*, 4712-4718.

21 The intramolecular hydrogen bond in **15** may reflect the gas phase nature of the calculations.

22 Hammond, G. S. *J. Am. Chem. Soc.* **1955**, *77*, 334.

Appendix A

(Tabulated structures are from Chapter 2.)

Table 1. MP2/6-31G*//MP2/6-31G* calculations. (ZPVE scaled by 0.95)

Structure	Energy (au)	ZPVE (au)	Energy+ scaled ZPVE (kcal/mol)		E-E(**21**) (kcal/mol)
19	-192.8046084	0.100498	-120926.9095		0.2
21	-192.8048585	0.100445	-120927.0980		0.0
28	-192.784743	0.094906	-120917.7773		9.3
26	-192.8313888	0.100143	-120943.9261		-16.8
27	-192.8323146	0.099633	-120944.8111		-17.7
TS				Imag freq (icm^{-1})	
20	-192.7757563	0.098068	-120910.2531	971	16.8
22	-192.7675821	0.096066	-120906.3172	380	20.8
23	-192.7700047	0.095411	-120908.2279	240	18.9
24	-192.7689419	0.095523	-120907.4942	346	19.6
25	-192.7720926	0.095633	-120909.4057	202	17.7
29	-192.7790352	0.094600	-120914.3781	96	12.7

Appendix B1

(Tabulated structures are from Chapter 3.)

Table 1. Energies of stationary points. (ZPVE scaled by 0.961 (B3LYP) and 0.893 (HF))

Transition structure.		Energy (au)	ZPVE (au)	Energy + scaled ZPVE (au)	Imag freq (icm^{-1})	E-E(**16**) (Kcal/mol)
H^+						
17	Optimized					
	B3LYP/6-31G*	-232.74694	0.12246	-232.62926	158.8	+2.7
		-232.79896[a]				+5.0
18	Optimized					
	B3LYP/6-31G*	-232.74642	0.12234	-232.62886	142.3	+3.0
		-232.79860[a]				+5.2
20	Optimized					
	HF/6-31G*	-231.27333	0.13039	-231.15680	760.8	+0.3
	B3LYP/6-31G*	-232.75119	0.12168	-232.63426	637.9	-0.4
		-232.80322[a]				+2.3
Minima						
H^+						
16	Optimized					
	HF/6-31G*	-231.27756	0.13468	-231.15730		0.0
	B3LYP/6-31G*	-232.75432	0.12559	-232.63363		0.0
		-232.80693[a]				0.0
19	Optimized					
	HF/6-31G*	-231.28822	0.13079	-231.17143		-8.9
	B3LYP/6-31G*	-232.75956	0.12192	-232.64240		-5.5
		-232.81078[a]				-2.4
21	Optimized					
	HF/6-31G*	-231.30390	0.14147	-231.17757		-12.7
	B3LYP/6-31G*	-232.77439	0.12631	-232.65301		-12.2
		-232.82970[a]				-14.3

[a] B3LYP/6-31G* (SCI-PCM) single point calculations. A dielectric constant of 2.23 (CCl_4) was used at 298.15K.

Appendix B2

(Tabulated structures are from Chapter 3.)

Table 2. Energies of stationary points. (ZPVE scaled by 0.961 (B3LYP) and 0.893 (HF))

Transition structure.		Energy (au)	ZPVE (au)	Energy + scaled ZPVE (au)	Imag Freq (icm^{-1})	E-E(**22**) (kcal/mol)
BF_3						
23	Optimized					
	HF/6-31G*	-554.12414	0.13573	-554.00294	188.2	+23.2
	B3LYP/6-31G*	-556.96517	0.12692	-556.84320	231.0	+22.4
		-556.97626[a]				+20.8
25	Optimized					
	HF/6-31G*	-554.11428	0.13471	-553.99398	115.1	+28.8
	B3LYP/6-31G*	-556.95532	0.12521	-556.83499	139.7	+27.6
		-554.97200[a]				+23.5
26	Optimized					
	HF/6-31G*	-554.11408	0.13454	-553.99394	129.7	+28.9
	B3LYP/6-31G*	-556.95462	0.12526	-556.83425	128.5	+28.0
		-556.96928[a]				+25.2
28	Optimized					
	HF/6-31G*	-554.11823	0.13282	-553.99962	635.8	+25.3
	B3LYP/6-31G*	-556.96058	0.12372	-556.84169	333.3	+23.4
		-556.97709[a]				+20.3
29	Optimized					
	HF/6-31G*	-554.11914	0.13284	-554.00051	763.6	+24.7
	B3LYP/6-31G*	-556.95969	0.12365	-556.84086	615.5	+23.9
		-556.97528[a]				+21.5
31	Optimized					
	HF/6-31G*	-554.11632	0.13300	-553.99755	30.9	+26.6
	B3LYP/6-31G*	-556.95742	0.12352	-556.83872	55.8	+25.2
		-556.97909[a]				+19.1
Minima						
BF_3						
22	Optimized					
	HF/6-31G*	-554.16294	0.13776	-554.03992		0.0
	B3LYP/6-31G*	-557.00282	0.12890	-556.87895		0.0
		-557.00948[a]				0.0
27	Optimized					
	B3LYP/6-31G*	-556.96335	0.12439	-556.84382		+22.0
		-556.97772[a]				+19.9

30	Optimized				
	HF/6-31G*	-554.19794	0.13697	-554.07563	-22.4
	B3LYP/6-31G*	-557.03104	0.12827	-556.90777	-18.1
		-557.03710[a]			-17.3
24	Optimised				
	HF/6-31G*	-554.18654	0.13953	-554.06194	-13.8
	B3LYP/6-31G*	-557.02071	0.13055	-556.89526	-10.2

[a] B3LYP/6-31G* (SCI-PCM) single point calculations. A dielectric constant of 2.23 (CCl_4) was used at 298.15K.

Appendix C1

(Tabulated structures are from Chapter 4.)

Table 1. Energies of transition structures.
(ZPVE scaled by 0.95 (MP2), 0.961 (B3LYP) and 0.8929 (HF))

Transition structures.		Energy (au)	ZPVE (au)	Energy + scaled ZPVE (au)	Difference 4m-5m TS (kcal/mol)	Imag Freq (icm^{-1})
TS 13-14	Optimized					
	HF/6-31G*	-345.16148	0.17011	-345.00959	3.53	249
	MP2 (full)/6-31G*	-346.18167	0.16206	-346.02771	1.04	438
	B3LYP/6-31G*	-347.27163	0.15869	-347.11913	1.94	300
	Single point at MP2 geom					
	HF	-345.15514	0.16206	-345.00118	4.74	
	MP2 (fc)	-346.15208	0.16206	-345.99812	1.01	
	MP3	-346.19787	0.16206	-346.04391	2.23	
	MP4D	-346.22135	0.16206	-346.06740	1.91	
	MP4DQ	-346.20549	0.16206	-346.05153	2.12	
	MP4SDQ	-346.21733	0.16206	-346.06337	1.71	
	MP4SDTQ	-346.24880	0.16206	-346.09484	0.99	
TS 13-15	Optimized					
	HF/6-31G*	-345.15620	0.17049	-345.00397		252
	MP2 (full) /6-31G*	-346.18064	0.16273	-346.02605		483
	B3LYP/6-31G*	-347.26930	0.15948	-347.11604		310
	Single point at MP2 geom					
	HF	-345.14823	0.16273	-344.99364		
	MP2 (fc)	-346.15112	0.16273	-345.99652		
	MP3	-346.19496	0.16273	-346.04036		
	MP4D	-346.21895	0.16273	-346.06436		
	MP4DQ	-346.20275	0.16273	-346.04816		
	MP4SDQ	-346.21525	0.16273	-346.06065		
	MP4SDTQ	-346.24786	0.16273	-346.09327		
TS 16-18	Optimized					
	HF/6-31G*	-345.16605	0.17028	-345.01401	5.19	208
	MP2 (full) /6-31G*	-346.18699	0.16200	-346.03309	3.54	393
	B3LYP/6-31G*	-347.27694	0.15884	-347.12429	3.97	233
	Single point at MP2 geom					
	HF	-345.16015	0.16200	-345.00625	6.76	
	MP2 (fc)	-346.15737	0.16200	-346.00348	3.48	
	MP3	-346.20300	0.16200	-346.04911	4.52	
	MP4D	-346.22646	0.16200	-346.07257	4.21	
	MP4DQ	-346.21055	0.16200	-346.05666	4.42	
	MP4SDQ	-346.22236	0.16200	-346.06847	3.99	
	MP4SDTQ	-346.25382	0.16200	-346.09993	3.28	

TS 16-21	Optimized				
	HF/6-31G*	-345.15786	0.17038	-345.00574	258
	MP2 (full)/6-31G*	-346.18190	0.16258	-346.02745	485
	B3LYP/6-31G*	-347.27112	0.15937	-347.11797	312
	Single point at MP2 geom				
	HF	-345.14993	0.16258	-344.99548	
	MP2 (fc)	-346.15238	0.16258	-345.99793	
	MP3	-346.19635	0.16258	-346.04190	
	MP4D	-346.22031	0.16258	-346.06586	
	MP4DQ	-346.20407	0.16258	-346.04962	
	MP4SDQ	-346.21656	0.16258	-346.06211	
	MP4SDTQ	-346.24915	0.16258	-346.09470	
TS 17-18	Optimized				
	HF/6-31G*	-345.15095	0.16999	-344.99917	174
	MP2 (full)/6-31G*	-346.16688	0.16108	-346.01385	248
	B3LYP/6-31G*	-347.26176	0.15792	-347.11000	209
TS 22-14	Optimized				
	HF/6-31G*	-345.15416	0.16945	-345.00286	223
	MP2 (full)/6-31G*	-346.16843	0.16092	-346.01556	308
	B3LYP/6-31G*	-347.26295	0.1578	-347.11130	257

Appendix C2

(Tabulated structures are from Chapter 4.)

Table 2. Energies of minima. (ZPVE scaled by 0.95 (MP2), 0.961 (B3LYP) and 0.8929 (HF))

Minima		Energy (au)	ZPVE (au)	Energy + scaled ZPVE (au)
13	Optimized			
	HF/6-31G*	-345.16772	0.17225	-345.01392
	MP2 (full) /6-31G*	-346.19631	0.16357	-346.04092
	B3LYP/6-31G*	-347.27909	0.16012	-347.12521
14	Optimized			
	HF/6-31G*	-345.20557	0.17442	-345.04983
	MP2 (full)/6-31G*	-346.23515	0.16597	-346.07748
	B3LYP/6-31G*	-347.31366	0.16229	-347.15770
15	Optimized			
	HF/6-31G*	-345.18299	0.17399	-345.02763
	MP2 (full)/6-31G*	-346.21387	0.16507	-346.05705
	B3LYP/6-31G*	-347.29531	0.16196	-347.13967
16	Optimized			
	HF/6-31G*	-345.17016	0.17027	-345.01813
	MP2 (full)/6-31G*	-346.19855	0.16343	-346.04329
	B3LYP/6-31G*	-347.28152	0.16008	-347.12768
17	Optimized			
	HF/6-31G*	-345.17764	0.17346	-345.02276
	MP2 (full)/6-31G*	-346.21433	0.16403	-346.05850
	B3LYP/6-31G*	-347.29665	0.16105	-347.14188
18	Optimized			
	HF/6-31G*	-345.20438	0.17434	-345.04871
	MP2 (full)/6-31G*	-346.23419	0.16614	-346.07636
	B3LYP/6-31G*	-347.31201	0.16281	-347.15555
23	Optimized			
	HF/6-31G*	-345.18344	0.17407	-345.02801
	MP2 (full)/6-31G*	-346.21441	0.16520	-346.05747
	B3LYP/6-31G*	-347.29568	0.16210	-347.13990
24	Optimized			
	HF/6-31G*	-345.18224	0.17306	-345.02771
	MP2 (full)/6-31G*	-346.21734	0.16369	-346.06183
	B3LYP/6-31G*	-347.29970	0.16055	-347.14541

Appendix D

(Tabulated structures are from Chapter 5.)

Table 1.

Structure	HF/6-31G* optimised Energy (au).
11	-667.27638
12	-667.27737
13	-687.08810
14	-687.08618
15	-687.09178
16	-687.08792
17	-687.09011

Appendix E1

(Tabulated structures are from Chapter 6.)

Table 1. Energies of transition structures. (ZPVE scaled by 0.961 (B3LYP) and 0.893 (HF))

Transition structures.		Energy (au)	ZPVE (au)	Energy + scaled ZPVE (au)	Imag freq (icm^{-1})
H^+					
TS 8 (inv)	Optimized				
5TS *trans*	HF/6-31G*	-384.20882	0.20165	-384.02875	266
TS 9 (inv)	Optimized				
6TS *trans*	HF/6-31G*	-384.20739	0.20142	-384.02752	255
TS 13 (inv)	Optimized				
5TS *trans*	HF/6-31G*	-384.20853	0.20202	-384.02813	259
		-386.59807[a]			
TS 14 (inv)	Optimized				
6TS *trans*	HF/6-31G*	-384.20786	0.20156	-384.02787	261
	B3LYP/6-31G*	-386.60009	0.18817	-386.41926	246
		-386.59597[a]			
TS 18 (inv)	Optimized				
5TS *cis*	HF/6-31G*	-384.20613	0.20233	-384.02545	255
		-386.59544[a]			
TS 19 (inv)	Optimized				
6TS *cis*	HF/6-31G*	-384.20384	0.20155	-384.02386	298
	B3LYP/6-31G*	-386.59599	0.18821	-386.41512	282
		-386.59187[a]			
TS 20 (ret)	Optimized				
5TS *cis*	HF/6-31G*	-384.19334	0.20088	-384.01396	219
TS 21 (ret)	Optimized				
6TS *cis*	HF/6-31G*	-384.17792	0.20044	-383.99893	171
	B3LYP/6-31G*	-386.56960	0.18670	-386.38990	216
BF_3					
TS 24 (inv)	Optimized				
5TS *trans*	HF/6-31G*	-707.04466	0.20569	-706.86098	306

		-710.79941[a]			
TS 25 (inv) 6TS *trans*	Optimized HF/6-31G*	-707.04423 -710.79730[a]	0.20476	-706.86138	309
TS 29 (inv) 5TS *cis*	Optimized HF/6-31G*	-707.04549 -710.80007[a]	0.20515	-706.8623	296
TS 30 (inv) 6TS *cis*	Optimized HF/6-31G*	-707.04638 -710.80192[a]	0.20501	-706.86331	302
TS 32 (inv) 5TS *trans*	Optimized HF/6-31G*	-707.04267 -710.79783[a]	0.20545	-706.8592	307
TS 33 (inv) 6TS *trans*	Optimized HF/6-31G* B3LYP/6-31G*	-707.04746 -710.80608 -710.80144[a]	0.20472	-706.86465	262

[a] B3LYP/6-31G* single point calculation on HF/6-31G* optimised structures.

Appendix E2

(Tabulated structures are from Chapter 6.)

Table 2. Energies of minimum structures. (ZPVE scaled by 0.961 (B3LYP) 0.893 (HF))

minima structures.		Energy (au)	ZPVE (au)	Energy + scaled ZPVE (au)
H^+				
Epoxide 7	Optimized			
trans	HF/6-31G*	-384.19751	0.20229	-384.01687
Epoxide 10	Optimized			
trans	HF/6-31G*	-384.21100 -386.59816[a]	0.20266	-384.03005
Furan 11	Optimized			
trans	HF/6-31G*	-384.24521 -386.62860[a]	0.20539	-384.06180
Pyran 12	Optimized			
trans	HF/6-31G*	-384.24664 -386.63194[a]	0.20662	-384.06070
Epoxide 15	Optimized			
cis	HF/6-31G*	-384.20920 -386.59750[a]	0.20282	-384.02808
Furan 16	Optimized			
cis	HF/6-31G*	-384.24754 -386.63062[a]	0.20507	-384.06442
Pyran 17	Optimized			
cis	HF/6-31G*	-384.25000 -386.63489[a]	0.20634	-384.06574
BF_3				
Epoxide 21	Optimized			
cis	HF/6-31G*	-707.08587	0.20605	-706.90187

		-710.83864[a]		
Furan 22 *cis*	Optimized HF/6-31G*	-707.08579 -710.84396[a]	0.20666	-706.90125
Pyran 23 *cis*	Optimized HF/6-31G*	-707.07737 -710.83246[a]	0.20912	-706.89063
Epoxide 26 *trans*	Optimized HF/6-31G*	-707.08333 -710.83659[a]	0.20575	-706.89960
Furan 27 *trans*	Optimized HF/6-31G*	-707.08459 -710.83583[a]	0.20752	-706.89928
Pyran 28 *trans*	Optimized HF/6-31G*	-707.07223 -710.82775[a]	0.20948	-706.88517
Epoxide 31 *trans*	Optimized HF/6-31G*	-707.08725 -710.84034[a]	0.20632	-706.90301

[a] B3LYP/6-31G* single point calculation on HF/6-31G* optimised structures.

The work in this thesis follows from my M.Sc thesis titled *"Modelling studies on the epoxide-carbonyl rearrangement."* During the early period of my Ph.D studies, when computer facilities were inadequate for the level of calculation required in this work, I spent 12 months as a teaching assistant at the University of Maryland at Baltimore County. I am grateful to Professor Dale Whalen for his facilities and advice. Calculations were performed in conjunction with Professor Jim Coxon, Professor Arvi Rauk, University of Calgary and Professor Keiji Morokuma, Cherry L. Emerson Centre for Scientific Computing, Emory University using the high level computing facilities at Calgary and Atlanta. For the remaining time of my Ph.D the computer facilities were funded by a Marsden grant. I acknowledge financial support from a Marsden funded Fellowship.